Identification of Non-local Force Interactions in Self-Adhesive Polymeric Films

D I S S E R T A T I O N
zur Erlangung des akademischen Grades

Doktoringenieur
(Dr.-Ing.)

von M.E. Behnaz Bagheri
geboren am 19.04.1991 in Zanjan

genehmigt durch die Fakultät für Maschinenbau
der Otto-von-Guericke-Universität Magdeburg

Gutachter:
1. apl. Prof. Dr.-Ing. habil. Konstantin Naumenko
2. Prof. Dr. Victor A. Eremeev

Promotionskolloquium am 14.09.2022

Kurzfassung

Kunststoffe werden im täglichen Leben der Menschen in großem Umfang verwendet, entweder privat oder industriell. Eines der größten Probleme in diesem Zusammenhang ist die Umweltverschmutzung, die durch diese Materialien verursacht wird. Deshalb versucht die Industrie, z. B. die Verpackungsindustrie, den Kunststoffverbrauch jeden Tag mehr zu reduzieren. Die Herstellung dünner Kunststofffolien ist daher eine der Möglichkeiten, den Kunststoffverbrauch zu reduzieren. Je nach Verwendungszweck sind Probleme mit der Haftung oder der Leistung eine der Herausforderungen. Um die Haftfähigkeit der Folien zu gewährleisten, gibt es eine Vielzahl von Herstellungsverfahren, wie z. B. die Koextrusion von Polymeren, die üblicherweise zur Herstellung selbstklebender Polymerfolien verwendet wird.

Die Klebeleistung der Folien wird in der Regel anhand geeigneter Peel-Test Ergebnisse beurteilt, obwohl ein Peel-Test allein keine ausreichenden Daten liefert, um die Produktleistung darauf zu stützen. Zu diesem Zweck wird in der vorliegenden Arbeit eine neuartige Idee zur Modellierung der Delaminierung von dünnen, flexiblen Polyethylenfolien mit Selbstklebefähigkeit untersucht. Die allgemeine Idee dieses Modells besteht darin, einen inversen Weg einzuschlagen, indem man die Delaminationskonfigurationen aus den Peel-Test entnimmt und daraus die traction-separation Kurve erstellt. Danach werden diese traction-separation Kurven eingesetzt, um sie in den nicht-lokalen Modellierungsverfahren anzuwenden und die unbekannten Materialparameter zu ermitteln.

Zu diesem Zweck wurden T-Peel-Tests an verschiedenen PE-Folienproben durchgeführt, die aus zwei Schichten identischer Folie bestanden, die durch die Haftflächen miteinander verbunden waren, gemäß der Norm ASTM 1876. Der Peel-Test wurde mit einer mikroskopischen Kamera aufgezeichnet, um die digitalen Bilder der Folienkonfiguration aus einer Transversalebene zu extrahieren. Es wurden verschiedene Digitalisierungsmethoden verwendet, um die beste Methode zur mathematischen Definition der Folienkonfiguration zu finden. Diese Daten, die in Form von Koordinaten oder Winkeln vorlagen, dienten als Grundlage für die Ermittlung der Wechselwirkungskräfte zwischen den Filmen. Der Identifizierungsschritt wurde aus Gründen der Genauigkeit und zur Validierung mit drei verschiedenen Ansätzen durchgeführt. Zwei der Ansätze wurden auf der Grundlage direkter Verfahren und einer auf der Grundlage des Prinzips der komplementären Energie entwickelt, die in dieser Studie als direkter, exponentieller bzw. komplementärer Energieansatz bezeichnet wurden. Die Ansätze brachten korrekte Ergebnisse und waren auch in der Lage, Charakteristika der adhäsiven Interaktion wie die Adhäsionsenergie, die maximale Kraft und die kritische Öffnungsverschiebung zu liefern. Zusätzlich zu den individuell validierten Ergebnissen der Ansätze zeigten alle drei Ansätze ein qualitativ ähnliches traction-separation verhalten, das der untersuchten Probe entsprach.

Der letzte Schritt dieser Arbeit beinhaltete die Modellierung der Wechselwirkungen zwischen den Filmen, die vom nichtlokalen Typ waren. Die Modellierung wurde unter Verwendung der Ideen der auf peridynamischen Bindungen basierenden Theorie erstellt. Die erforderlichen Eingabedaten für diesen Schritt waren die identifizierten traction-separation Kurven, um die unbekannten Materialparameter zu berechnen. Auf diese Weise wird das gesamte Delaminationsverhalten anhand der Delaminationskonfiguration und der Materialeigenschaften modelliert.

Abstract

Plastic materials are used vastly in people's daily life, either personally or industrially. One of the major concerns in this regard is the environmental pollution caused by these materials. Therefore, industries, such as packaging, are trying to reduce plastic consumption more and more every day. Hence, going in the direction of thin plastic films production is one of the ways of plastic usage reduction. However, like any other product, these films face some challenges as well. According to their usage, adhesion problems or performance is one of the challenges. In order to provide the adhesion ability in the films, plenty of manufacturing methods are available such as polymer cling material coextrusion, which is commonly used to produce self-adhesive polymer films.

The adhesion performance of the films is usually judged based on suitable peel test results, although a peel test alone does not provide sufficient data to rely on the product performance on it. To this end, the thesis at hand studies a novel idea to model the delamination of thin, flexible polyethylene films with self-adhesive ability. The general idea of this model is to go from a reverse path of taking the delamination configurations from the peel test specimens then provide the traction-separation curve from them, which is the specific traction-separation curve to this material. Then take those traction-separation curves into account, to apply in the non-local modeling procedures and define the unknown material parameters.

Towards this goal, T-peel tests were performed on different PE film specimens, provided from two layers of identical film, attached to one another by the cling surfaces, according to the standard ASTM 1876. The peel test procedure was recorded with a microscopic camera, in order to extract the digital images of the film configuration from a transverse view. Different methods of digitization were used to find the best way of mathematically defining the film configuration. These data, which were in a coordinate or angle form, were the input to identify interaction forces between the films. The identification step was done by three different approaches for accuracy and validation purposes. Two of the approaches were developed from direct procedures and one from the complementary energy principles, they were called in this study the direct, exponential, and complementary energy approaches respectively. The approaches performed correctly and were also able to provide characteristics of the adhesive interaction such as the energy of adhesion, maximum force, and critical opening displacement. In addition to the approaches individually validated results, all three of the approaches showed qualitatively similar traction-separation behavior, corresponding to the evaluated specimen.

The final step of this framework contained modeling the interactions between the films, which were from non-local type. The modeling was created using the ideas of peridynamic bond-based theory. The required input data for this step was the identified traction-separation curves, in order to calculate the unknown material parameters which completed the non-local model performance. This way, the whole delamination behavior is modeled by taking the delamination configuration and the material characteristics.

Erklärung

Ich versichere hiermit, dass ich die vorliegende Arbeit ohne unzulässige Hilfe Dritter und ohne Benutzung anderer als der angegebenen Hilfsmittel angefertigt habe. Die Hilfe eines kommerziellen Promotionsberaters habe ich nicht in Anspruch genommen. Dritte haben von mir weder unmittelbar noch mittelbar geldwerte Leistungen für Arbeiten erhalten, die im Zusammenhang mit dem Inhalt der vorgelegten Dissertation stehen. Verwendete fremde und eigene Quellen sind als solche kenntlich gemacht. Ich habe insbesondere nicht wissentlich:

- Ergebnisse erfunden oder widersprüchliche Ergebnisse verschwiegen,
- statistische Verfahren absichtlich missbraucht, um Daten in ungerechtfertigter Weise zu interpretieren,
- fremde Ergebnisse oder Veröffentlichungen plagiiert,
- fremde Forschungsergebnisse verzerrt wiedergegeben

Mir ist bekannt, dass Verstöße gegen das Urheberrecht Unterlassungs- und Schadensersatzansprüche des Urhebers sowie eine strafrechtliche Ahndung durch die Strafverfolgungsbehörden begründen kann.

Ich erkläre mich damit einverstanden, dass die Dissertation ggf. mit Mitteln der elektronischen Datenverarbeitung auf Plagiate überprüft werden kann.

Die Arbeit wurde bisher weder im Inland noch im Ausland in gleicher oder ähnlicher Form als Dissertation eingereicht und ist als Ganzes auch noch nicht veröffentlicht.

Magdeburg, 04.02.2022   Behnaz Bagheri

Contents

Notation

Latin Symbols

A	area	m	mass
A	integration constant	$\mathbf{m}$	knot multiplicity
a	material parameter	N	normal force
B	area	$N_{i,p}$	B-spline basis function
B	Integration constant	n	upper limit
$\mathbf{B}$	bending stiffness	$\mathbf{n}$	normal vector
B_i	control points	P	area
b	diameter	p	B-spline degree
b	material parameter	$\tilde{Q}$	area
C_2H_4	ethylene	Q	shear force
C_T	tensile stiffness	q	adhesive force distribution
$C^{p-\mathbf{m}}$	NURBS continuity factor	$\mathbb{R}$	set of real numbers
C	constant	$R_{i,k}$	auxiliary matrix
c	constant	r	position vector amplitude
c_s	constant	$\hat{\mathbf{r}}$	connecting vector
Δc	diameter	r_a	material parameter
D_i	coefficient	r_b	material parameter
D_s	distance	r_s	position vector
d	diameter	$\tilde{r}_s$	position vector
$\mathrm{d}s_0$	line element reference state	r_{vw}	atomic distance
$\mathrm{d}\tilde{s}$	element	s	diameter
E	YOUNG's modulus	s_1	coordinate
$\mathbf{e}_y$	vertical unit vector	s_2	coordinate
F_{peel}	peel force	$\mathbf{t}$	tangential vector
$\tilde{F}_{\mathrm{peel}}$	peel force	U_E	strain energy
F_s	long-range force	$U_{\mathbf{f}}$	force density potential
F_{vw}	inter-atomic force	U_l	thermal energy
f_i	auxiliary matrix	U_{m}	weight potential energy
$\mathbf{f}$	force vector	U_p	load potential
$\mathbf{f}_R$	bond force density	U_q	adhesive force potential
g	gravitational constant	U_T	total energy
H	horizontal force component	u	experimental displacement value
h	diameter		
i	index	V	vertical force component
j	index	v	atom 1
k	index	w	atom 2
l	diameter	W	strain energy density
M	bending moment	$\mathcal{W}\mathrm{adh}$	work of adhesion
m	upper limit	x	coordinate

x_c	coordinate	y_c	coordinate
x_l	coordinate	Z	knot vector
y	coordinate		

Greek Symbols

α	experimental material parameter	λ	local stretch
β	experimental material parameter	ξ	scalar variable
γ	transverse shear strain	σ_{max}	maximum traction
δ_n	normal separation	Υ	adhesive energy
δ_t	tangential separation	φ	angle
ε_l	engineering strain	χ	local curvature
ζ_i	knots	Ψ	elliptic function
ζ	scalar variable	ψ	angle
θ	angle magnitude	Ω	complementary energy
Λ	cosine function		

Indices and Accents

$\Box_*$	critical opening value	$\Box_i$	w.r.t. the ith iteration step
$\Box'$	derivative	$\Box_j$	w.r.t. the jth iteration step
$\Box_{eq}$	equilibrium value	$\Box_n$	w.r.t. the nth time step
$\Box^{-1}$	inverse value	$\Box_m$	w.r.t. the mth time step
$\Box_{max}$	maximum	$\Box_k$	w.r.t. the kth time step
$\Box_{min}$	minimum	$\dot{\Box}$	1st derivative w.r.t. the time
$\tilde{\Box}$	normalized variable	$\ddot{\Box}$	2nd derivative w.r.t. the time
$\Box_0$	reference boundary state	$\dddot{\Box}$	3rd derivative w.r.t. the time
$\times\Box$	times of multiplication	$\ddddot{\Box}$	4th derivative w.r.t. the time
$\hat{\Box}$	vector		

Operators

$\Delta\Box$	difference value	$\sin(\Box)$	sine function
$d\Box$	infinitesimal value	$\tan(\Box)$	tangent function
$\exp(\Box)$	exponential function	$\partial\Box$	partial differentiation
$\cos(\Box)$	cosine function		

Abbreviations

BoPA	biaxially-oriented polyamide	DVC	digital volume correlations
BoPE	biaxially-oriented polyethylene	EA	exponential approach
CAD	computer-aided design	ENF	end-notch flexure
CAM	computer-aided manufacturing	ESPI	electronic speckle pattern interferometry
CAE	computer-aided engineering		
CEA	complementary energy approach	LDPE	Low density polyethylene
		LEFM	linear elastic fracture mechanics
CZM	cohesive zone model	LLDPE	linear low density polyethylene
DA	direct approach	LVDTs	Linear variable displacement transducers
DCB	double cantilever beam		
DIC	digital image correlation	MMF	mixed-mode flexure

NURBS	Non Uniform Rational B-Splines	PVC	polyvinyl chloride
PE	polyethylene	SEM	scanning electron microscope
PET	polyethylene terephthalate	VCM	vinyl chloride monomer
PP	polypropylene		

1 Introduction

1.1 Plastic Films

Plastic film is referred to a material which consists of a thin continuous polymeric substances. The existence of a wide variety for these films created from either different manufacturing methods or different polymer types, provided a vast range of application for such films. Thereby, this variety provides also a wide range of properties compatible with many products. These are the main reasons of why polymers are getting more and more popular for the producers day by day. However, the impact of such plastic production and consumption growth on the environment is one of the major concerns in the world. Therefore, utilizing kind of polymers that have the potential to be produced as a considerably thin layer film in order to reduce the plastic usage on one hand and finding the polymer type that can also be recycled on the other hand will be a middle ground solution to satisfy the protecting environment as well as using polymer products. Some of the primary polymers that are capable of being used to produce plastic films are briefly mentioned as following:

- **Polypropylene** This polymer is produced by chain-growth polymerization of the monomer propylene and was first demonstrated by two chemists called J. Paul Hogan and Robert Banks in 1951. The crystallization temperature for PP long molecules is when the molecules of propylene associate to one another since the point that temperature goes below the melting point. At this temperature the molecules start to gather into a crystal order and thereby the regions of ordered crystalline are created. For PP typically, the onset of crystallization starts at ca. $110 - 120°C$ at a cooling rate of $10 \,\mathrm{K/min}$. Based on the usage and processing technology applied, sheets and films can be produced from PP in the thickness rage of 5 to $2000 \,\mu\mathrm{m}$. The most common processing type in these films is casting with extrusion from a slit die onto a relatively cold roll. PP is a thermoplastic polymer which is also the second-most widely produced plastic commodity after polyethylene. Its properties are similar to polyethylene, but it is slightly harder and more heat resistant with high chemical resistance [1, 2].

- **Polyester-BoPE** or in longer terms is called biaxially-oriented polyethylene tereph-thalate. As it can be realized also from the naming it is a polyester film made from stretched polyethylene terephthalate in bi-axial directions. Additionally, polyester it-self is defined as all polymers that contain units of the ester group repeating in the polymer chain. BoPE films were created for the first time in mid-1950s and they were utilized because of their specific properties such as high tensile strength, chemical and dimensional stability, transparency, reflectivity, gas and aroma barrier properties, and electrical insulation. These properties come from the ability of its molecules that not only the monomers can be added to the growing chains, but also single chains can react with each other. The manufacturing procedures for this film begins with the extrusion of a film of molten polyethylene terephthalate (PET) onto a chill roll, that suppresses it into the formless state, then it is biaxially oriented by drawing [3–5].

- **Nylon** is the general form of the synthetic polymers produced from polyamides, mean-

ing it contains repeating units linked by amide links, which provides thermoplastic properties and therefore, can be processed by melting and shaped into fibers or films. Nylon is the first commercially popular synthetic polymer. It was produced within a project research of DuPont research facility in 1935 by Wallace Hume Carothers. There is plenty of Nylon types available now but the first nylon was referred to as type 6,6. This numbers is chosen because each of the two chemicals used in making this type of nylon has six carbon atoms. Polyamide/Nylons can be processed as both blown or cast film, and can be used for extrusion coating and the procution of biaxially oriented film (BOPA). They melt at a relatively high temperatures, the melting temperature for blown and cast film is $250°C$ and $265°C$. Since nylon is also a semicrystalline material, processes that rapidly cool the polyamide film will result in lower crystallinity and therefore provide more transparent, flexible, thermoformable film. Such films are able to be mixed wtih a wide variety of additives. Regarding the environmental aspects, many types of Nylons can be broken down in fire although by doing so they form hazardous smoke, and toxic fumes or ash which usually contains hydrogen cyanide. Besides, burning such materials need a high value of energy which makes it expensive. Typically a discarded Nylon garbage takes approximately 30 - 40 years to break down and this means polluting the nature such as the fishing nets left in the waters that contribute debris in the ocean. Since the recycling process faces some challenges and is also expensive, very few companies care to do it, and they mostly prefer to use cheaper and newer plastics [6–10].

- **Polyvinyl chloride** also known as PVC, is the third most used polymer in the world, the absolute value of PVC production annually is about 40 million tons which is potential for many usages and shapes. This polymer is produced from polymerization of the vinyl chloride monomer (VCM) and was discovered in 1872 by German chemist called Eugen Baumann. It was produced inside a flask full of vinyl chloride that was left shelf protected from sunlight for four weeks and appeared as a solid. Flexible PVC films have decent sealant capability to oily substances but oxygen can pass through them. It is not an expensive material to make products with and it has such wide variety of usage that its versatility is almost unlimited. Typically, three types of processing are used to make PVC products such as: suspension that provides 80% of world production, emulsion 12% and mass 8%. If we compare PVC to other polymer, we can find out that it needs less energy per unit weight to be produced. Moreover, the plastic products are criticized for their long-lasting waste but in PVC only 12% of its products are used for consumables and at least 64% are used for products with an expected useful life of minimum 15 years. Therefore, they are not disposed immediately. Recycling PVC materials are also not as challenging as the other polymers, they break down into small chips and after removing the impurities the product can be refined to make pure PVC one more time. PVC can be recycled roughly seven times and has a lifespan of approximately 140 years [11–13].

- **Polyethylene**, abbreviated as PE, is the most popular polymer nowadays. According to the statistics, since 2017 approximately 100 million tones of PE is produced annually, which is around 34% of the total polymer production market. This polymer was synthesized for the first time by a German Chemist called Hans von Pechmann out of his intentions in 1998. He discovered PE during the investigation of another material and after his colleagues characterized the white and waxy substance that was created. They realized it is made of long $(C_2H_4)_n$ chains, and it was the origin of Polyethylene terminology. Until the present, Many types of PE materials are produced, that posses

different types of density because of their internal chain bonds and orientations. It can start from low-density and reach to high-density with manufacturing adjustments such as the pressure od temperature during the extrusion. Mechanically, PE materials show high ductility and low friction behavior. Most PEs, regardless of their density, similar to most polymers, provide excellent resistance against chemicals such as strong acids, or bases. This polymer as well as the others is not a biodegradable material and managing PE waste is challenging if they are not recycled since, the absolute value of PE products is significantly higher than the other polymers. But, it has two advantages over the other ones in this regard, first, it's life span is not as long as the others in the nature and second, according to some new research achievements in 2017, polyethylene garbage can be eaten by some specific types of caterpillars so they can be used to remove the polyethylene waste. Moreover, based a recent discovery the polyethylene plastic bags can get degraded up to 40% within six weeks by Pseudomonas fluorescens with the help of Sphingomonas bacterias [14–16]. Hence, according to the mentioned advantages and many other features, flexible polyethylene films are widely used in different fields. For instance, in packaging industry like food or pharmaceutical packaging [17, 18], in protection and transportation [19, 20], in glass panels and photovoltaic modules as the laminating layer [18, 21–24], in devices with flexible OLED and PLED like electronic health care patches for vital information monitoring or drug delivery systems [25–29], etc. Among all these usages packaging industry is considered as the major usage and more specifically flexible packaging that in its variety of forms, has been the fastest growing direction of the packaging industry since the 1970s. An important feature which is required in flexible packaging is the ability to form thin, light, heat-seal ability and compact packages. Thereby, Low density polyethylene, LDPE's, good chemical and oil resistance, along with its low cost and all other features mentioned above, makes it excellent for many flexible packaging applications. LDPE and linear low density polyethylene (LLDPE) account for the majority of plastics used in flexible packaging. For example, LDPE was the first plastic to come into common commercial use in packaging, in the late 1940s [30].

Beside all the segments of a flexible film one of the useful and popular improvements is to provide the film with adhesion ability to full fill the packaging purpose independent from any other material being involved. Such segment can be created by different manufacturing methods, some of those methods are explained briefly in the following subsection, which also include the procedures of producing self-adhesive polymer films.

1.1.1 Design

Plastic films can be divided into two categories: monolithic structures, and those containing two or more layers of other materials combined in one film. Multilayer film structure can consist layers of single plastic only or different materials. In general, two major manufacturing methods are used to produce either types of such films: they are called casting or blowing. These methods are both continuous processes that start with extrusion. Choosing between blown and cast film begins with examination of the unique needs of the product and process. If the **cast** film production method is chosen, it starts by small plastic pellets called resin getting melted by a heated screw barrel until they become molten, then it is continuously fed to the extruder through a narrow slot die horizontally, creating a sheet of the fed substance. The thickness and width of the stretch wrap is actually determined by the dimension of the slot in the die. Afterwards, the resin is getting pinned to a highly polished chilled roller using

an air curtain or vacuum box. This step solidifies and cools the film quickly before trimming and rolling process, then with the help of tension rollers the film is minimally pre-stretched to draw the wrap to the winding and trimming stations.
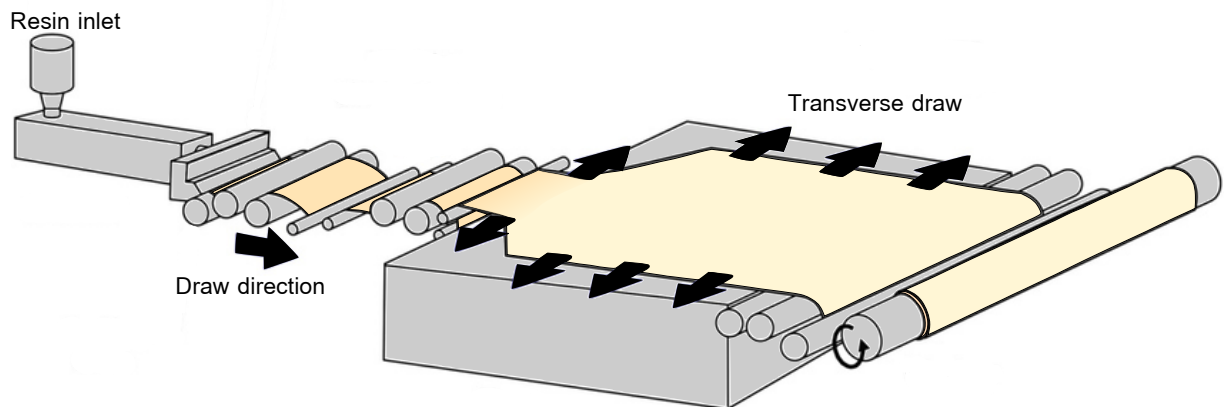

Figure 1.1: Cast film production schematic, after [31]

The **blown** film production method starts similar to the casting process until the molten plastic preparation then it is fed to a circular and vertical extruder facing upward, and exits in a continuous tubular form, therefore such films are sometimes also referred to as tubular films. Afterwards, an air pressure is introduced through the center of the hot resin and expands it, producing a tubular bubble.This way the resin is vertically blown upward and outward to the desired diameter and meanwhile also slowly cools and solidifies the plastic before it is flattened. Such slow cooling process is one of the reasons the wraps usually look hazy and dull. The thickness of the film is controlled by the speed at which it is pulled from the die. The width of the film is controlled by the amount of air inserted in the bubble. Once it reaches to the very top of the tower the nip rollers flatten the material into a tube that can be reeled for creating bags and pouches, or slit and then reeled as a flat sheet of film [30, 32, 33].

The differences of these two methods regarding the resulting films properties are shown briefly in the following table:

Table 1.1: Blown film vs. Cast film properties [33]

	Blown Film	Cast Film
Cooling	Slow	Rapid
Resin Molecule Alignment	Random (in all directions)	Linear (in one direction)
Clarity	Potentially Hazy	Very clear
Puncture Resistance	Very good	Good
Stretch Resistance	Higher	Lower

Regardless of polymer film manufacturing process, the self adhesion feature can be provided by some follow up procedures for the films. Such procedures are also chosen based on the product usage. Nowadays, preparing adhesion ability for plastic films are in the interest of plenty of industrial companies and scientific studies, therefore new methods are developing day by day. Some recent studies called the investigation on gecko effect imply the state of the art in self-adhesive plastic films production. The main idea behind this study is inspired by
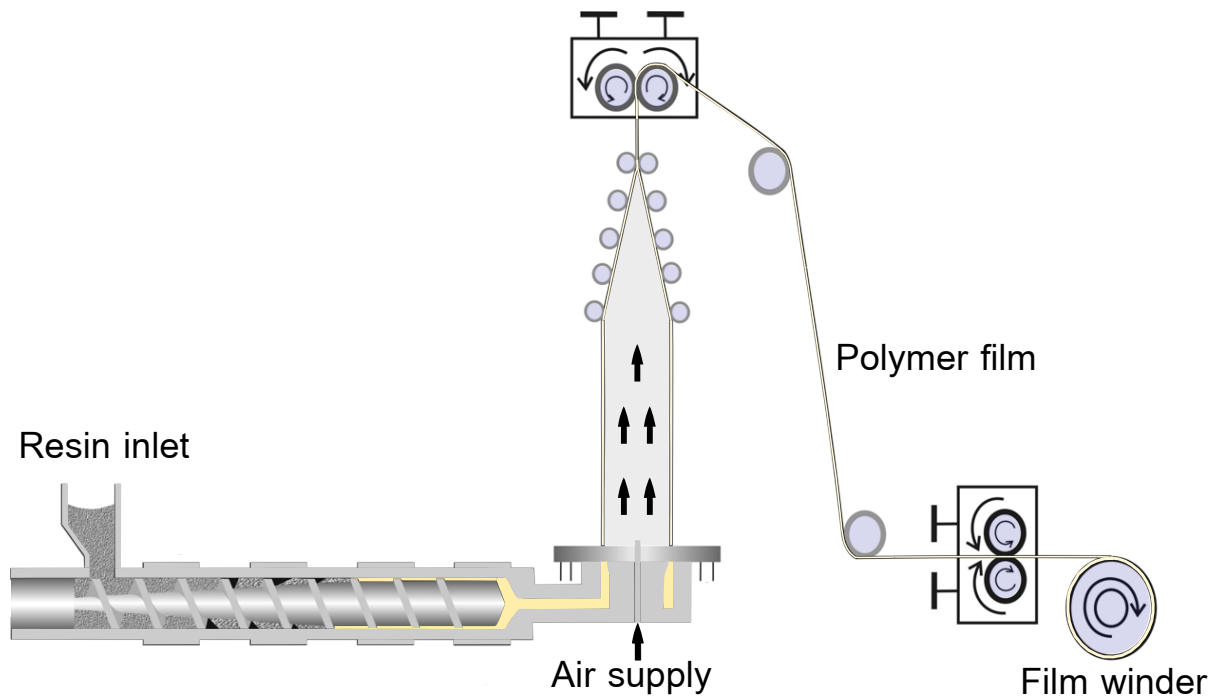
Figure 1.2: Blown film, after [34]

the ability of tropical lizards called geckos that are able to climb walls and almost any surface at amazing velocities, meaning, they can adhere to the surface and detach from it at will in a millisecond time slot. By the investigation on such an interesting ability it has been realized that, gecko toes have about 20 leaf-like layers of tissue, called scansors. Each scansor contains thousands of angled arrays of branched and hair-like fibers called setae which are consisted of stiff, hydrophobic keratin. For instance, in a type of gecko called toyko, each single setae is been measured about $110~\mu m$ long and $4.2~\mu m$ wide, which are distributed uniformly with a similar orientation and in grid-like pattern on the scansor. Furthermore, on every setae there are hundreds of nano-arrays called spatulas that make intimate contact with the surface. Every spatula is a thin stalk in an almost triangular cross-section shape. At the beginning of the 20th century, Haase noted in [35] for the first time that geckos stick by inter-molecular forces. Later on, several experiments were prepared to distinguish the exact type of the intended adhesion force and since the van der Waals force is considered as the only type that can attract to hydrophobic surfaces to adhere, it must be the sufficient mechanism in gecko setae. The important point from this study is that van der Waals force is highly independent of surface chemistry and depends on the distance between surfaces. Therefore, it can be said that gecko adhesion depends on its feet geometry. This type of construction that provides the possibility of simultaneously tilting and being peeled away with a little effort, brings out the idea of increasing effective surface area for attraction in many materials and it leads to the idea of manufacturing self-adhesive films by multi-patterning the structure of film surfaces trying to simulate the gecko effect. Furthermore, an extra unique feature discovered by gecko feet adhesion which makes it even more interesting is that, gecko setae are both extremely adhesive and extremely anti-adhesive. This claim is based on the studies showing that the gecko setae unlike any other adhesive tape, do not adhere unexpectedly and spontaneously, instead they perform the adhesion on a mechanical program of orientation, preload and drag. Therefore, if the setae are being pushed they won't necessarily perform a strong adhesion. Besides, setae do not stay dirty or get stained by surface debris unlike for example the conventional adhesives. Hence, for the first time in

history the performance of gecko setae are considered as self-cleaning adhesive [36, 37]. As mentioned earlier preparing the gecko like adhesion in the polymer films surface is still the sate of the art and must be studied for many further details, but there are some other methods available in this regard that manufacturers use it already as in mass production. From these methods it can be implied to adhesive layer Coextrusion.

Coextrusion is the procedures of forming a film composed of more than one thermoplastic layer. The main goal here is normally to produce a specific multilayer film structure in which each layer contributes a key property to the overall product performance. This process can also provide the polymer films with a thin adhesive polymer materiel coextruded on one or both side of the film surface, weather being applied on a monolayer film or multilayer of different materials. Such an action while using another method like lamination is also possible but it requires some intermediate steps of first producing each film layer individually, then being adhered to each other and it can not be done all at once as in coextrusion.
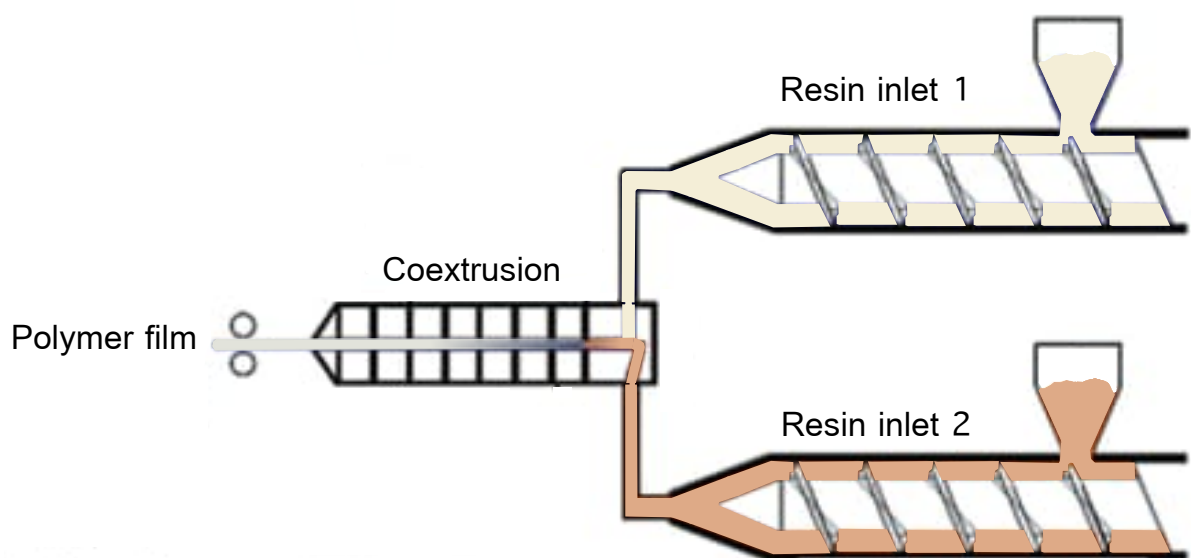

Figure 1.3: Schematics of coextrusion procedures, after [38]

The other advantage of coextrusion over lamination is that it is pretty flexible regarding the film thickness and provides the ability to produce extremely thin films which is the opposite in lamination that thickness is limited. By doing so, coextrusion often permits considerable cost savings when multilayer flexible materials are desired. Since in Coextruder container, the plastic of each layer is melted in a separate extruder or even the films are produced beforehand and then go through the coextrusion procedure. If they are prepared all at once, the materials are delivered from the extruder to a manifold or directly to the die, and combined in such a way that the resins do not blend together, That allows each layer to keep its individual identity and characteristic properties. And as it is mentioned this method can be used for both blown or cast films [30, 39].

One other significant step that shouldn't be missed in any plastic film production process is the careful surface preparation as in solvent cleaning, mechanical abrasion, or chemical treatments which provides a good interfacial strength and a durable adhered joints [40].

1.2 Advanced Measurements

The importance of a suitable test method whether for a safe and reliable design or quality control purposes is vividly explored in the history of engineering world. Although, providing a perfectly matching test method in order to generate the desired engineering data is a great challenge in this regard. The procedures of this step starts from overweening the possible test methods, then going through the availability of them, or checking if the standard methods can serve the purpose or they need an innovation, and finally validation of the innovated method to ensure the reliability of the results. The highlight outcome of such tests is to predict the life expectancy and the performance of the product under mechanical tensions as close as possible to the reality. To do so, one should possess a good understanding of environmental factors and failure mechanisms.

In the case of this study, we are looking into the challenges that self-adhesive polymeric films possibly face, and even more importantly, their performance upon those challenges. In this regard, most of the available tests of adhesives, perform only qualitative measurements which is not practical if engineering data is required. It means that, beside the developments of new usages for adhesives, which brings out the requirement for new test methods and accuracy expectancy, a limited number of tests are available to do the job [41].

Once the aim of the study and an overview of the input and output data is known, one can decide between the suitable measurement options. Based on this strategy, the intention of this study is to utilize optical displacement measurements of a mechanical test as an input to the calculations of the mechanical model. To do so, there are some standard measurement techniques of non-contact optical extensometers such as electronic speckle pattern interferometry (ESPI) and, digital image correlation (DIC) already existing. Since there is no contact with the damaged area in these techniques, they can be used until the failure occurs without getting affected. However, optical extensometers are not suitable for small displacement or small strain measurements, as there are plenty of other methods available for such purpose. For instance, Strain gauges, Linear variable displacement transducers (LVDTs), and etc.. Anyhow, unlike (DIC) and (ESPI), such contact extensometers are not in the possible choices for this study, since the whole test procedure is needed as an optical data.

Electronic speckle pattern interferometry (ESPI) is a technique to measure static or dynamic strains field in a component. It does the measurements by using laser interference fringes combined with video detection. The performance concept is based on speckle effect provided by reflected rays from the surface roughness which is illuminated with a laser beam. In fact, the microscopic roughness of the specimen surface creates a reference pattern which enables the system to determine any displacements based on correlating the reference with any further patterns. This techniques capabilities are measuring and monitoring full-field non-uniform strain fields at high resolution, vibration mode analysis and nondestructive testing. 3D strain distributions measurements for complex geometries are possible with this technique as well [42, 43].

The digital image correlation also known as DIC is a strain measurement technique. The usage of this technique have accelerated during the recent decade in the fields of material science, mechanical engineering, civil engineering, geology, and etc. The idea behind this technique is to compare two images of a component part before and after the test that causes deformation. It means, the position of the pixel subsets in the original and deformed images are correlated to one another in order to determine their displacements or strains. This determination is mostly done based upon gray intensity level, by the means of using speckle patterns namely black, white and gray sprayed on the specimen to build the required contrast.

This way the strain mapping function regarding the images can be extracted. This technique is applicable on different scales from micro to macro and the advancements over the past years have truly improved the system resolution even reaching to nano-scale by combining scanning electron microscope (SEM) with DIC. Although, as the resolution goes higher the field of vision gets smaller and providing such high resolutions increases the processing time, therefore they are more time consuming. Hence, an optimal point of setups among time, resolution, and field of view should be chosen for the desired out come. However, there is one additional factor that must be considered which is the camera and other devices pricing, as a camera possessing super high resolution and going up to millions of frames per second can be extremely expensive. Moreover, the 3D version of the system are capable of dynamic 3D displacement measurements which is called digital volume correlations (DVC) [42].

Accordingly, there are some factors out of the usual standards which are capable of affecting the measurement. Considering all the suitable techniques for this study, among the mentioned and not mentioned ones, and analyzing them based on different aspects of equipment availability, requirements limits, and costs, non of the techniques mentioned above were utilized. Although they were suitable and capable of fitting in the requirements limits pretty well, they were neither available nor essential to this study. Because the required optical input data were not being used to calculate any sort of strains and therefore a medium quality digital microscopic camera with a typical frame rate could serve the purpose very well. However, in order to improve the input data quality, the mentioned techniques above are recommended.

1.3 Outline

The aim of this thesis is to develop a novel non-local modeling method that can perform an analysis on the process of delamination for thin polymeric films and provide the information such as traction-separation curve which is beyond a common test method outcome. To this end, experiments in the form of T-peel test were designed and performed on self-adhesive, thin, flexible polyethylene films. Then the evaluation model is applied on the test outcomes in a reverse path leading us to the results ready to be inserted in the non-local model. Furthermore, modeling procedures compromises of recording film configurations during the peel test, digitizing the configuration and mathematically define them, identifying models to insert the configuration and achieve the corresponding traction-separation curves and verify each method by comparing the test and modeling results. Then finally match the results with a non-local model to identify the unknown material parameters.

The thesis at hand is divided into six chapters starting from the current Introduction chapter and followed by Chapter 2 that provides some background information about the experimental an theoretical steps of this study. Chapter 2 starts by the topics related to the practical part of the research and goes into details about the existing testing methods, material failure types and possibilities. Then the investigation continues by connecting the experimental observations and creating assumptions based on them in order to get familiarized with material physical behavior. From this stage forward, digging into the theoretical backgrounds and common methods in similar studies begins until the novelty of the proposed methods are clarified. This chapter ends each section by the reason behind the chosen path, among all the explained ones.

Chapter 3 contains graphical and theoretical details about test specimen preparation, peel test setup and procedures step by step, test outcomes and the optical data transform methods. Moreover, in this chapter all aspects of the experimental procedures are mentioned as

well as the utilized tools such as peel test machine, camera, standard test method, etc, plus graphical, mathematical and analytical softwares like Rhino, CorelDRAW, Matlab, Origin Pro and some more that were used point by point to prepare the input data for the identification step of the next chapter.

In Chapter 4, as it can be realized from its title, is composed of different methods of identification procedures to provide traction-separation curves based on the configuration of the self-adhesive PE films under T-peel test. At first there will be explanations about the idea behind the proposed novel method of the approaches as well as the mechanical theories such as the governing equations base on the non-linear beam theory, constitutive equations then follows up by the energy integral and the effective work of adhesion. The first two models called the direct approach (DA) and the complementary energy approach (CEA), are applicable on Cartesian-coordinates although, they go separate paths from the point of considering necessary boundary condition assumptions, since DA runs directly by applying the assumptions and the film configuration coordinates, in contrast for CEA, variation principles of strain energy density is taken into account and the concept of complementary energy is introduced to run the model. By realizing that the whole idea is working correctly, another method of traction-separation identification, called the exponential approach (EA), based on exponential calculations is provided to increase the accuracy of the final results. The differences of this model starts from the operation system of the calculations, that runs on configuration angles to approximate the film shape with an exponential equation, not the coordinates and polynomials.

As the identification approaches are covered, Chapter 5 continues with illustrating the results achieved from each method, plus providing the discussion on all results one by one, highlighting the pros and cones of the used methods and materials, and finally for the purpose of validation, a different method for each approach is provided that matches the results calculated from the approach to it's equivalent one from the experimental measurements. From this step forward, a non-local model is introduced to model the delamination procedure. This model operates based on modeling the notified long-range forces existing in the cohesive area and by an analogy to the pridynamic theory. The calculated traction-separation curves from the former approaches were used in this model to identify the unknown material parameters. Then again the final results were compared to the equivalent one form previous approach to check the accuracy.

Chapter 6, goes over the whole thesis, and briefly summaries the ideas and whole processes and procedures leading to the successful results. Additionally, this chapter contains the ideas to continue this study for the future by providing the direction and base requirements of the further research and finally the conclusions explaining the main outcome of such study.

2 Experimental and Theoretical Background

This chapter will briefly go through the fundamental principles of the chosen experimental an theoretical procedures of this study. Since comprehensively covering all the related topics is beyond the scope of this chapter, only the most important aspects, starting from experimental testings, through evaluations and modeling to result achievements are provided.

2.1 Types of Peel Tests and Systems

In this section some issues such as the the importance of testing adhesive strength, different type of existing adhesion tests and their functionality is going to be pointed out and explained briefly.

As a general rule to design every product, a pretest method should be prepared as the material properties of the object needs to be greater than the real forces that are anticipated to be applied during its use (i.e. geometry vs. loads, etc.). The engineering work should provide a good model consisting of experimental and analytical procedures to evaluate the intended material with useful and satisfying results. That means the material of interest of this study is not an exception to this rule either. Hence a testing method suitable to self-adhesive PE films is required. Additionally, the intended parameter of this study is mainly adhesion modeling of the mentioned films. All these initial information and the literature investigations in the following leads us to adhesion tests, either fracture tests or peel tests, as the required testing method.
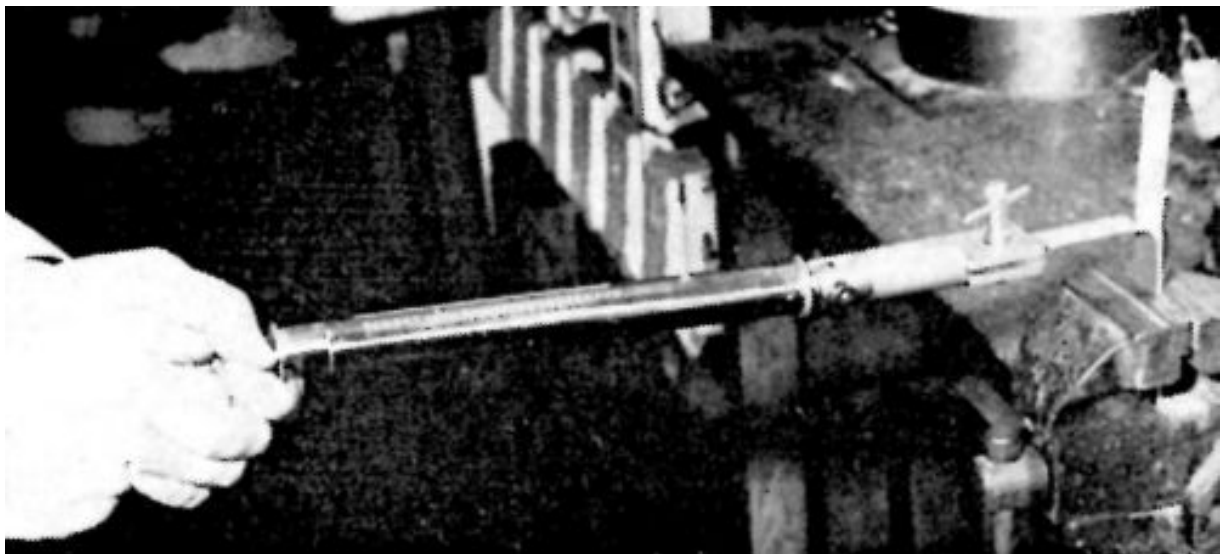

Figure 2.1: The apparatus and the adhesion testing method developed by Wittrock and Swanson [44] in 1962

Adhesion test is a simple mechanical technique used to measure the degree of adhesion between a flexible-rigid, a flexible-flexible or a relatively rigid-rigid substrates [45, 46]. To this end, to analyze the behavior of the adhesive systems various experimental techniques have been developed and some of the earlier works can be found in [20, 40, 47–53]. Adhesive joints testing possesses a long history [54], one of the earliest available pictures regarding this issue is illustrated in Fig. 2.1.

Figure 2.1 shows one of the oldest taken photos of adhesion testing methods as a peel test, which took place in 1962. The apparatus and the testing method was developed by Wittrock and Swanson [44]. In this test a vise grip on a flexible coupling is attached to the spring of a spring balance with 45 kg (100 lb) capacity. The test piece consisted of an aluminum strip or a rod rigid enough to withstand a bending force of the order of 100 lb [55].

Adhesive joint testing is crucial for ensuring the reliability of any bonded system or component. Tests are carried out for many different purposes, including materials selection, acquisition of data for design, validation, environmental durability assessment and quality control. To do so, many different test methods are available and it is important that the method used is a suitable fit for the intended purpose and can be applied in a repeatable manner [41].

Before jumping in to the different types of tests and the further topics, it might be better to have a brief review on the different modes of loading in fracture mechanics to clarify the related mode to this study with the following images.
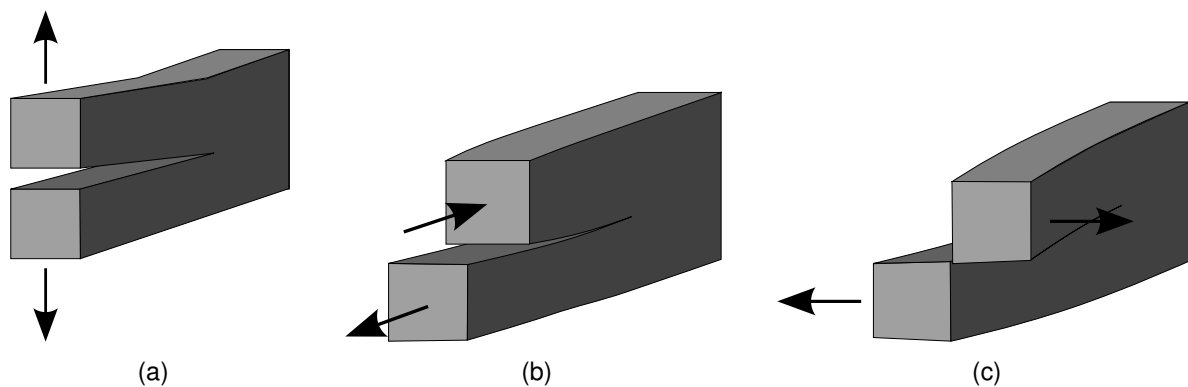

Figure 2.2: Schematics of three failure modes in fracture mechanics: (a) Mode I: opening, (b) Mode II: in-plane shear, (c) Mode III: out-plane shear

The load on an adhesive joints or a crack can be arbitrary, in 1957 G. Irwin found, any state could be reduced to a combination of three independent stress intensity factors:

- Mode I, also known as the opening mode, which refers to the applied tensile loading, Fig. 2.2(a).

- Mode II, also known as the shear mode, which refers to the applied shear stress in the in-plane direction, Fig. 2.2(b).

- Mode III, also known as the tearing mode, which refers to the applied shear stress out of plane, Fig. 2.2(c).

The adhesive strength tests can be categorized to two groups of fracture and peel tests, according to the substrate material properties which is being tested. Fracture tests are performed on bulk adhesive specimens and on adhesive joints. As explained from the beginning of this section, adhesive-joint tests are in the interest of this study. Therefore, bulk adhesive tests are not going to be discussed. The major focus will be on fracture and

peel tests of the adhesive-joint. The adhesive-joint fracture tests concern with joints formed between substrates that deform in a linear-elastic manner during the loading of the joint such that the concepts of linear-elastic fracture mechanics apply. Commonly, the substrate tested in adhesive fracture type of tests is considerably stiffer in comparison to a thin polymeric film but still flexible and not brittle. However, there is also a requirement to be able to measure the performance of adhesive joints formed between substrates that are much more flexible and may deform extensively during an adhesion test. Peel tests are typically performed at a constant rate of peeling and the standards specify such details as the width, thickness, and width–thickness ratio of the specimens.

Some of the most useful and popular Adhesive-joint tests are pointed out in the following by the bullet points.

- The mode I fracture resistance of adhesive joints is most commonly determined using the **double cantilever beam (DCB)** test and has been proven to be one of the most reliable methods in determining the quality of an adhesive joint. The details about this test was initially described in the ASTM standard (ASTM 1990) and has been developed more recently in the British standard (BSI 2001) and the international standard (ISO 2009). The DCB adhesive-joint test specimen, as shown in Fig. 2.3, includes two substrates (the double cantilevers) bonded together with a thin layer of adhesive to form the joint. During joint fabrication, an initial crack is formed at one end of the joint. The DCB test requires that the initial crack in the joint introduced by the presence of the dis-bond or releasing film be extended by applying a vertical load to the substrates. The load can be introduced via circular holes drilled through the end of the substrates, or via circular holes through the center of metallic load blocks bonded to the ends of each arm which is illustrated in Fig. 2.3 by dash lines. In the ASTM method, load is applied until crack growth occurs, at which point the loading is stopped until the crack length stabilizes. The load is then increased until the crack grows again and this process is repeated a number of times. This test method is widely used in the aircraft industry as the peel test characterizing the quality of the adhesive joint between two composite adherents [40, 46].
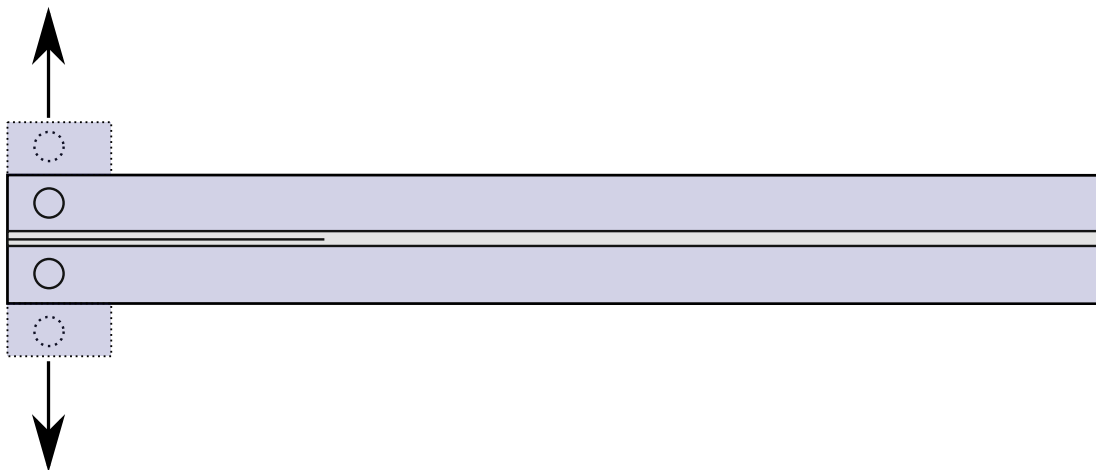

Figure 2.3: Mode I loading (opening) on a double cantilever beam (DCB) adhesive-joint test specimen; This figure is inspired by [40]

- The mode II fracture testing of adhesive joints is of course significantly more complicated than mode I testing and is still being standardized. The most popular adhesive joint test methods used In line with the mode II fracture have been the **end-notch**

flexure (ENF) tests. In the ENF tests, the specimen is loaded in either simple **3-point** or **4-point bending**. The schematics of the specimens and their loading is illustrated in Fig. 2.4. As it is also clear from the naming of the test methods, 3-point ENF has the loading in 3 points on the length of the specimen (two ends and one middle), to keep the balance and symmetry of the loading it is important that the load points are chosen in equal distances, and the load is applied in the opposite direction in the mid-point. Similarly, 4-point ENF test operates with loading applied on 4 equally distanced points along the specimen (two ends and two in the middle), the loading at the end points are again in the opposite direction of the ones applied in the middle. In both specimens, pretty similar to fabrication procedure of DCB specimens, a non-adhesive insert film is placed in the center of the adhesive layer at one end of the specimen during the manufacture of the joint and this, then acts as the crack starter in the subsequent mode II test. The 3-point ENF test was used by Chai in his detailed study of mode II fracture in adhesive joints (Chai 1986, 1988). The version of the ENF test using 4-point loading was described by Martin and Davidson (1999) for composite delamination and this has also been applied to adhesive joints. The schematics of both 3-point and 4-point ENF test are shown in Figs 2.4(a) and 2.4(b) respectively. The 4-ENF test has the advantage that stable fracture is achieved, circumventing the limitation in the conventional 3-ENF test [40].
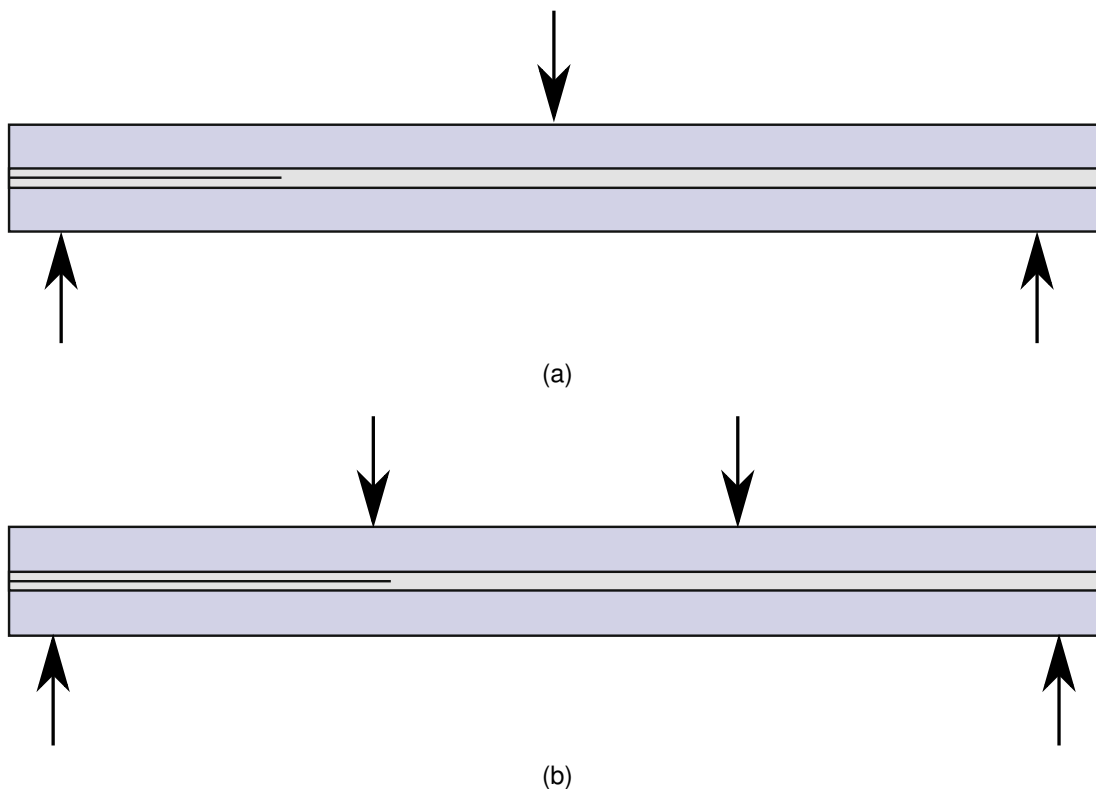

(a)

(b)

Figure 2.4: Mode II loading providing in-plane shear effect on end-notch flexure (ENF) adhesive-joint test specimens: (a) 3-point bending, (b) 4-point bending; These figures are inspired by [40]

- In addition to pure modes I and II adhesive joint fracture testing, there is a considerable interest in determining the fracture resistance of joints subject to mixed-mode (I/II) loading. Since, the adhesive joints in engineering structures will frequently experience such mixed-mode conditions in service. One of the most common test methods that

includes the mixed-mode loading of I and II is **mixed-mode flexure (MMF)** test which is also known as the **single leg bend** test. This test is now standardized by ASTM for mixed-mode delamination testing (ASTM 2004b). The specimen fabricated for MMF test consists of two substrates which are bonded to each other with a thin layer of adhesive to provide the adhesive joint. The substrates have the same dimension except one of them is some what longer than the other, which is design this way regarding to loading method of this type of test. The schematics of the MMF test specimen and the loading configuration of this method is illustrated in Fig. 2.5. The loading applied to this specimen throughout the test, is same as it is in 3-point ENF. But what makes it different and provides the mixed-mode (I/II) loading is that the loading at one of the specimen ends, is applied only on the upper substrate. The load at this point creates the mode I and the other two loads are responsible for mode II. Once more, similar to the previous test specimens non-adhesive film is inserted in the center of the adhesive layer at one end of the specimen during the manufacturing of the joint and this, then acts as the crack starter. Assuming that the failure path remains essentially the same (e.g., cohesive in the adhesive layer) it is usually observed that the fracture resistance increases as the percentage of mode II increases [40].
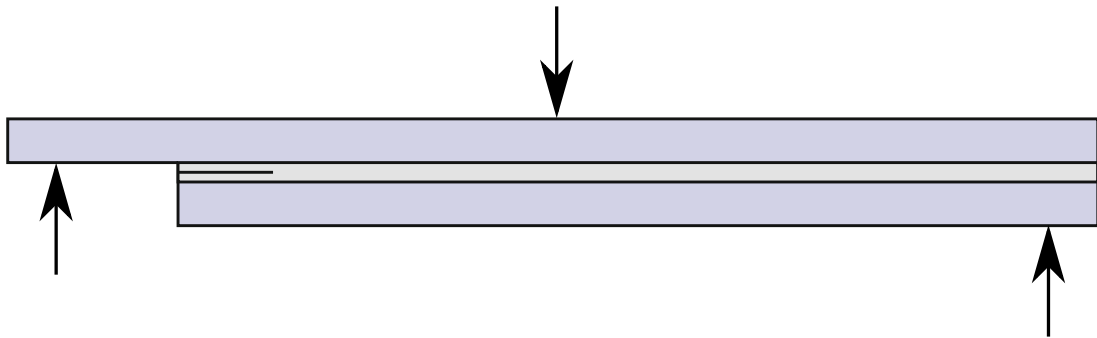

Figure 2.5: Mode I and II loading on a mixed-mode flexure (MMF) or single leg bend adhesive-joint test specimen; This figure is inspired by [40]

- In the so-called **fixed-arm peel tests**, the rigid substrate is fixed to a rigid base and the flexible substrate is peeled by a tensile test machine at a defined applied peel angle, which can vary according to the test protocols. The sketch of fixed-arm peel test samples configurations under different angles are illustrated in Fig. 2.6. Figure 2.6(a) shows a schematic of a fixed-arm peel test usual look and also more details of the rigid substrate positioning and attachment to the base under a general angle. The rigid base in such tests is attached to some wheels or a moving surface that enables the rigid substrate move horizontally in an adjustable speed in order to set the intended peel angel. Perhaps the most difficult experimental issue of the fixed-arm peel test is "ensuring that the fixed arm is (and remains) rigidly attached to the base". Additionally, the peel force is usually applied via the clamps of a tensile testing machine and the base as mentioned is fixed to a linear bearing trolley, such that the specimen can slide horizontally with minimum friction during the peeling of the flexible substrate. If the fixed arm is attached to the base using an adhesives, it requires to be ensured that it does not fail during the peel test. The usual technique of rigid substrate (fixed-arm) and rigid base attachment is to screw them together. When screws are used, it is necessary to position the screw holes in the fixed arm only at the peeling end of the joint, and put it through both the flexible and rigid substrate at the other end. The second screw is outside of the length of adhesive joint to be peeled in the test, in

other words on one end the flexible substrate is not positioned in the screw, exactly as illustrated in Fig.2.6(a). According to some standards it is also possible to use a wider rigid substrate than the flexible substrate, such that the extra width of the rigid substrate can be used to make more room for screwing down this arm to the sliding base and provide more stable attachment. Standardized peel tests describe both 90° and 180° fixed-arm peel tests (BSI 1993) as shown in Fig. 2.6(b) (first two pictures) which are the most common ones in this direction. However, the peel angle can be varied even from 45° to 180°. In the case of 180° peel test (ISO 8510-2, ASTM D 903) requires a flexible adherend to be sufficiently flexible to bend back through 180° before being peeled from a the rigid adherend at a constant peel rate.

(a)

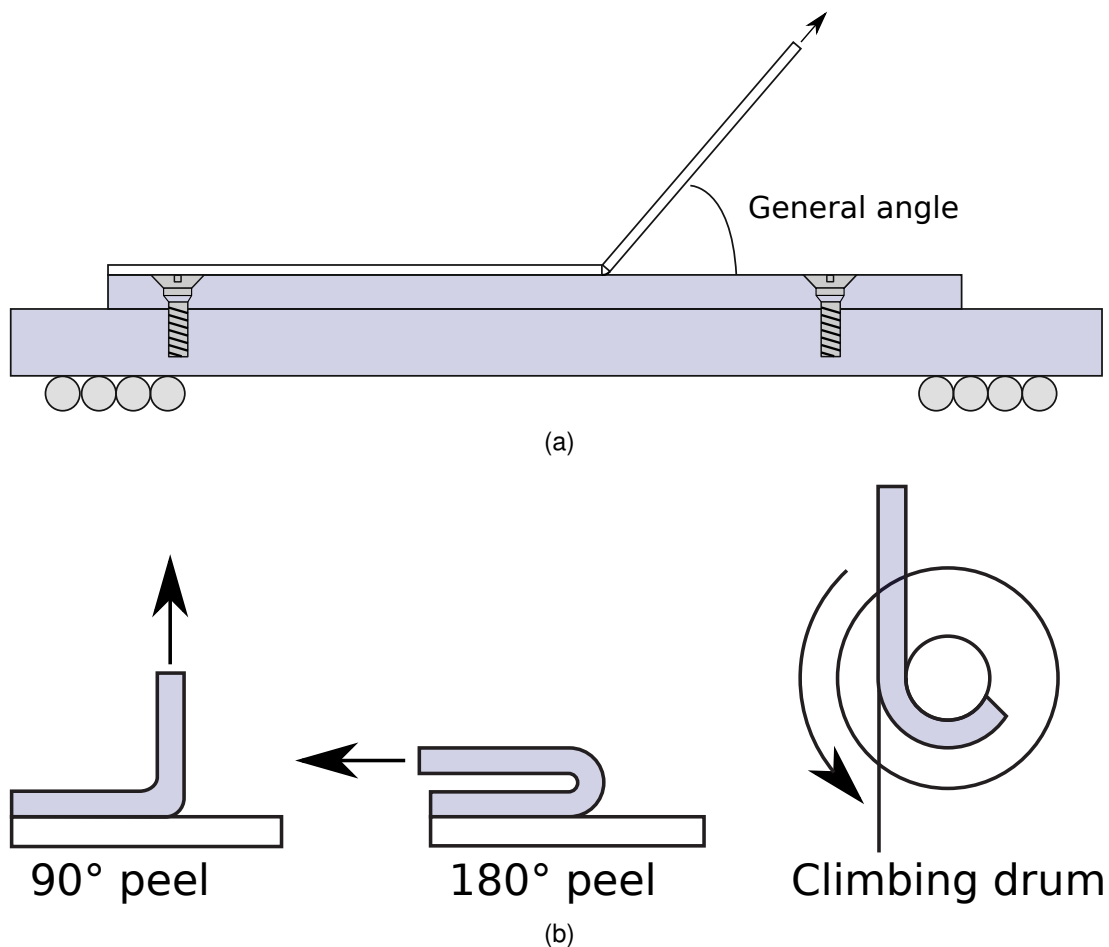90° peel   180° peel   Climbing drum

(b)

Figure 2.6: Different positioning of fixed-arm peel test specimens: (a) Detailed configuration of the specimen under a General angle with the lower arm fixed on a rolling base enabling the horizontal movement to synchronize with the peeling speed, (b) Schematics of three most common fixed-arm peel test positioning that provided the different angels; These figures are inspired by [40, 41]

Another configuration regarding the fixed-arm peel test is the floating roller test method as in the climbing drum peel test. This method enables constant angle of peel to be provided during the peel test and can be adjusted to vary the peel angle as intended. The apparatus used to control the peel angle is described in many standards such as (ISO 14676, ISO 4578, ASTM D 3167, ASTM D 1781). For instance, by attaching the

flexible substrate to a cylinder mounted on bearings which is then rotated to run the peel test. A floating roller or a climbing drum apparatus are also specified in two tests that have been standardized by ASTM (2004, 2006). The schematics of such test is illustrated in Fig. 2.6(b) (specified by the name climbing drum).

The fixed-arm peel test method is favored for non-structural adhesives, for example pressure sensitive adhesives and tapes. The climbing drum peel test, is used in the aerospace industry to determine the bonding of flexible skins to rigid sandwich structures, [40, 41].

- Probably, the most widely used peel test for the peeling of two flexible substrates is the **T-peel** test. In a T-peel test, the two flexible substrates are bonded over a part of their length. The not bonded ends are attached to the grips of a tensile or peel test machine, these two ends are positioned in a way that they provide the angel of 180° to one another. A typical T-peel test specimen and its configuration is illustrated schematically in Fig. 2.7. In this case, the substrates are peeled by the vertical movement of the testing machine upper grip, in a constant speed (providing quasi static situation) to form a separation. Preparing T-peel test specimens is simpler than that of the fixed-arm peel specimens since there is no need to attach one substrate to a fixed base and no need for a linear bearing trolley to accommodate the specimen sliding both substrates are attached to the peeling grips quite equally [40].
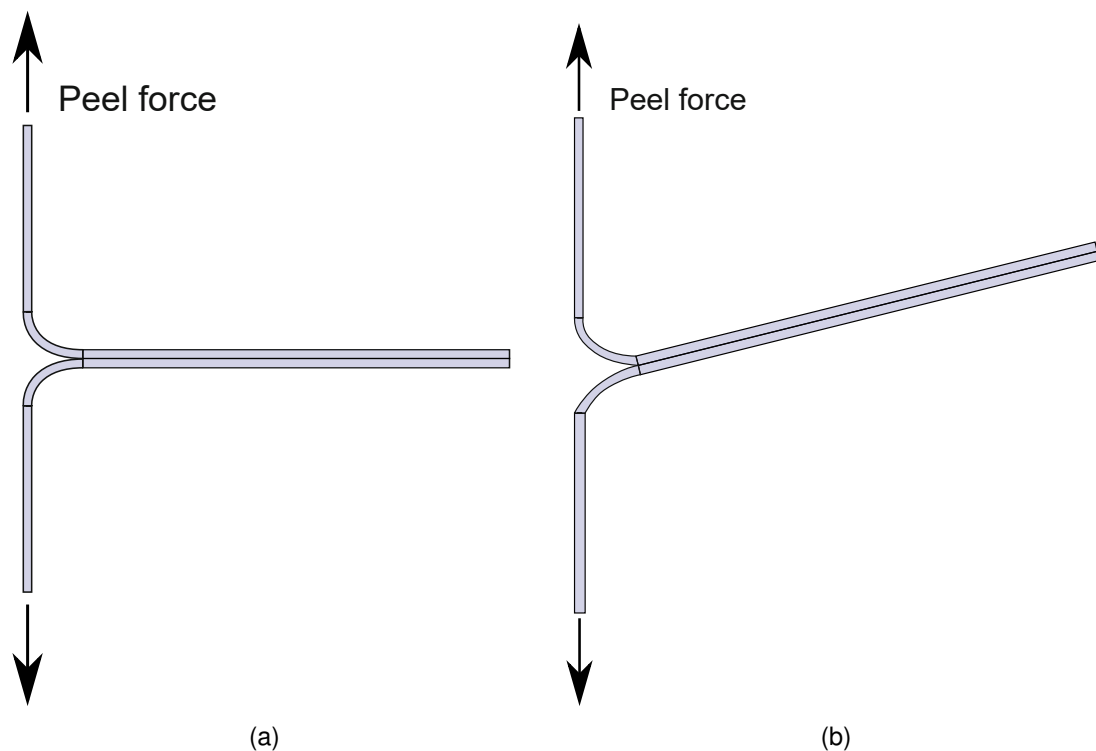

Figure 2.7: T-peel test specimens configurations during a peel test (from the transverse view): (a) Both layers of the specimen provided from one material resulting a symmetric configuration, (b) Specimen provided from different materials (different bending stiffness) resulting in asymmetric configuration; These figures are inspired by [40]

The substrates subjected to a T-peel test may or may not be of the same material. If the substrates of the peel test specimens are prepared from the same material, because of having the same bending stiffness in both layers, the loading during the peel test remains symmetric therefore the test configurations will be symmetric and

forming a "T" shape, exactly as shown in Fig.2.7(a). Otherwise, by having two different materials of different stiffness as the substrates of the specimen subjected to a peel test, the configuration of the specimen during the peel test will happen in asymmetric form and has a tendency to bend more toward the less stiffer layer, as illustrated in Fig. 2.7(b). Symmetric peeling test is a useful test configuration to evaluate the environmental durability of adhesively bonded systems. Like any other test methods, T-peel test and it's specimen preparation procedures are described in detail by (ASTM D1876) standard. Furthermore, according to the protocol (Moore and Williams 2007), loading should be performed at a constant and in a specific range of speed. The peel strength of adhesive joints is measured by a load-cell attached to the peeling grip of the testing machine. When the peel test is finalized, the measurement system provides a set of data consisting of measured peel forces at the specific values of separation (movement distance of the grip). This data can be displayed in a graph form of peel force vs. displacement. Although, the recorded peel force from the load-cell typically shows some fluctuations in a specific range. Therefore, the average value of all these fluctuated data will be considered as the average peel force.

The failure of a product, very much depends on the opening mode of its adhesive joint. This opening mode, as described earlier, can take place based on single loading mode or the mixture of the modes [45, 46]. In order to chose a compatible test method, many aspects according to many parameters specially the type of the material, opening modes and further specific parameters of interest for the study are taken in to account. Therefore, in the case of this study it is known that, the adhesion properties of some self-adhesive PE films are going to be modeled. If at least one of the substrates is flexible the separation of layers in the form of a peel test is considerably easier, as only a restricted region of the adhesive is under tension at any given time [36]. The term 'flexible' refers to the ability of the adherend to bend through 90° without breaking or cracking [41]. Now based on the mentioned previous studies it can be said that, the most suitable test for an adhesive joint that includes two flexible substrates form the same kind of material such as laminated plastic films or two layers of self-adhesive films is a T-peel test [45].

The analysis of peeling of adhesive joints has a long history because peeling is important in many industrial processes and products. The evaluation of adhesive performance via the use of peel tests is a complementary extension of these tests and the analysis of such tests is highly developed. One of the major attractions of peel tests is their practical simplicity. This is generally borne out in practice but, in both testing and data interpretation, attention to detail is important if reliable and useful results are to be obtained [54]. Regarding the experimental data evaluations and theoretical backgrounds of this study there are brief explanations in the following sections.

2.2 Adhesion vs. Cohesion

Adhesives have been used for nearly 70 years to serve many purposes. Applications related to adhesive bonding are today very diverse and can be found in all types of industries as an alternative to mechanical joints. For instance, in engineering applications, since they provide many advantages over conventional mechanical fasteners. One of the most desired advantage is that they provide a more uniform stress distribution along the bonded area, which enables the joint to have a higher stiffness and load transmission, reducing the weight and thus the cost [40].

For better understanding the provided information about the testing material in this study, it is essential to briefly imply the fundamental differences between adhesion and cohesion. It is clear that scientifically these two terms refer to quite different issues and they cannot be used instead of one another. However, it is now common to use the word "adhesive" or "adhesion" in a more general sense to refer to any clinging property (for example, glues and tapes can be called adhesives). Therefore, these matters are going to be simply clarified in the following.

Adhesion is the attraction between two separate substances, different or alike, resulting from intermolecular forces which is established between them. This concept is different from that of cohesion, which only involves intermolecular forces inside one substance such as the adherend or adhesive bulk layer. The intermolecular forces that exist in adhesion and cohesion are mainly van der Waals type forces , which will be addressed in the following subsection [56]. Kinloch imply to the concept of adhesion more simply as: "An adhesive may be defined as a material which, when applied to surfaces of materials can join them together and resist separation" [57]. Figure 2.8 shows the schematics of a basic adhesive joint, which is consisted of at least tree layers. That means, two layers of so called adherends (substances that are desired to be adhered to one another, either from two different materials or the same) and one layer of adhesive in between the adherends to perform the adhesion.

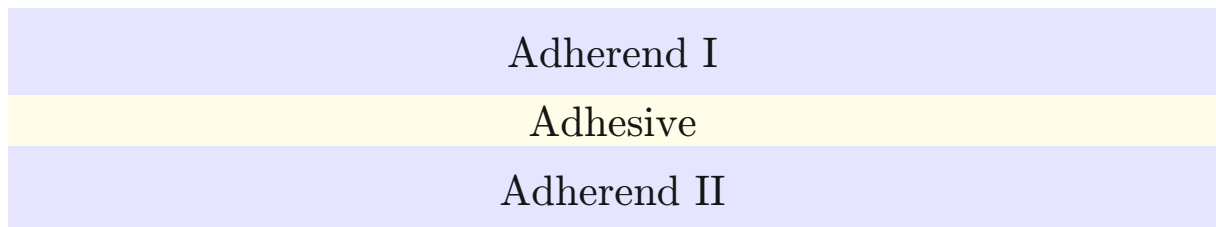| Adherend I |
|:---:|
| Adhesive |
| Adherend II |

Figure 2.8: Schematics of a basic adhesive joint system, consisting of three layers of adherends and and adhesive in between

As explained before an adhesive joint is a joint of different materials that can resist mechanical loading. However, failure can happen in any product or joint under different circumstances with different outcomes. Adhesive testing has a long history and traditionally joint testing has emphasized two issues, first, the failure load (e.g. ultimate load or continuous peeling load) which was discussed in the previous section and second, the mode of failure that results in various degrees of adhesive or cohesive failure as the key parameters [41].

Regarding the adhesive joint failures there are few possible scenarios that can happen during fracture or a peel test. The important issue here is whether some adhesive material remain on the substrate after the separation is complete (which is referred as the cohesive failure) or the adhesive film separates entirely from the adherend and recovers its integrity being ready for further use with almost unchanged performance (which is referred as adhesive failure). In other words, if the separation occurs within one of the layers or through combination of the layers of adhesive joint, it means that, the bond between the adherends and adhesive layer happened to be stronger than the molecular bond with in the adhesive film (so-called the layers cohesion is affected), otherwise if the separation takes place at the interface with one of the substrates it is understood that, the adhesion was weaker than that of the cohesion. The joint system may choose between different separation mechanisms (interfacial or cohesive, with further choice in a layered system). At first, it usually chooses the weakest mechanism in terms of force since it triggers separation first and thereby relieves the stress on the other possible mechanisms. Nevertheless, there is no guarantee that the fracture path will be along the interface. Stress distributions depend significantly on local geometrical

features such as crack sharpness and peel angle [36, 41].

Figure 2.9 illustrates the different possibilities of adhesive and cohesive failures in schematic forms. As it is clarified by a pink line in the pictures adherends bonded with adhesives or sealants break by adhesion, cohesion, or a combination of the two. Figure 2.9(a) shows the adhesive or interfacial failure that can happen in both interfaces. Cohesive failure, unlike that of the adhesive, can happen in different forms(according to mechanical properties of each involving substrate), such as:

- An entire cohesive failure within only the adhesive layer or one of the adherends (The adhesive strengths of some adhesives are great enough that the cohesive strength of the layers fails before the adhesive bond), as illustrated in Figs 2.9(b) and 2.9(c).
- Cohesive failure happening through all layers and moving forward with no specific pattern during separation, in this scenario the existence of adhesive failure in some parts of the joint is also possible as illustrated in Fig. 2.9(d).
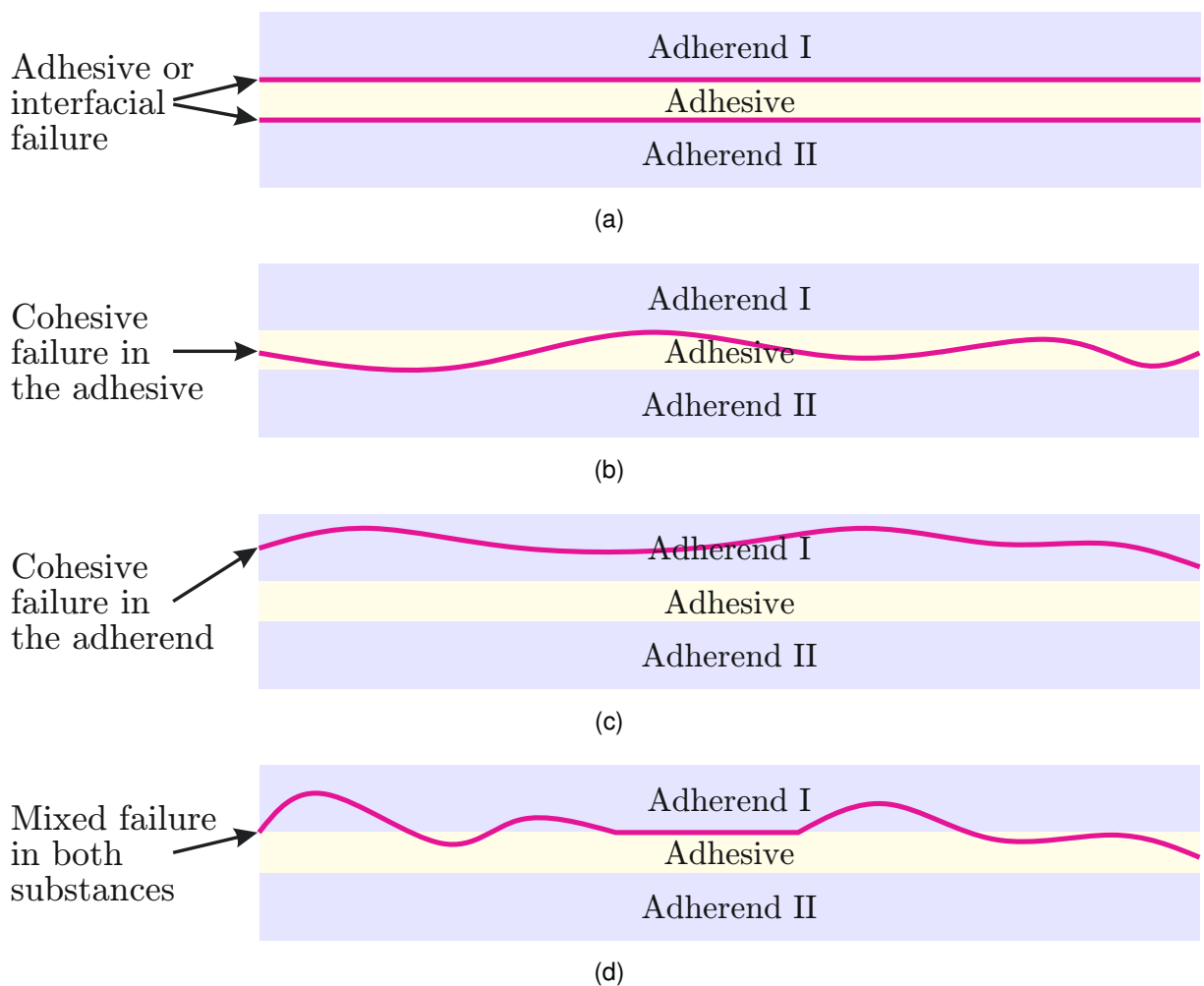

Figure 2.9: Schematics of four common ways that adhesive system failure takes place (pink line shows the separation path): (a) Adhesive failure happening in the adhesive-adherend interface, (b) Cohesive failure happening within the adhesive, (c) Cohesive failure happening within the adherend, (d) Cohesive-adhesive mixed failure happening through the whole specimen

In the case of this study, as explained in the introduction chapter, the tested material were fabricated from polyethylene substance with the self-adhesive properties which resulted in an

adhesive failure during the peel tests. For further and deeper information on adhesives and adhesion, many books such as those of [40, 57–62] and several articles from international journals (International Journal of Adhesion and Adhesives, The Journal of Adhesion and Journal of Adhesion Science and Technology) dealing with this subject can be mentioned.

2.2.1 Local vs. Non-local Interactions

In general terms, it is believed that the interactions within a material are always non-local, if we consider them in an atomic and molecular level. This argument is basically true due to the fact that atoms have a finite distance from one another. However, the interatomic distances are much smaller than the geometrical features of a larger scale problem, therefore, locality becomes an excellent approximation. Even though, local approximation faces some limits [63].

In order to comprehend the local and non-local interactions concept, an overview of attractive bonds within the materials in detail is required. In this regard, it is beneficial to know that the bond existing between the particles to bring them to each other, are divided into five main types of the Van der Waals bond, the ionic bond, the covalent bond, the metallic bond and the hydrogen bond. They certainly act in different strength because of some explainable material characteristics [64].

Moreover, adhesion or cohesion can be also categorized by the type of the bonding namely physical or chemical which can mean existence of local or non-local interactions over the interfacial area. The mentioned five main bond types can also fit in to these two categories. The chemical bonding includes the covalent and metallic bond, while the physical bonding consists of the ionic and Van der Waals bonding with or without permanent electrostatic moments [65]. These bonding types are present within the adherend or adhesive and also can occur between the two, at their interfaces. In the concept of adhesion, the focus is mostly on the bonding at the interface. The comparison in the following parts might provide adequate information to have a better understanding about the differences of these types [66].

To be more specific with the definition of interface it can be said that in this scientific direction, this term is used when one of the materials, in a liquid state (the adhesive), is brought into contact with the other solid one (the adherend) and then solidifies. In other words, interface is where two solid materials (with or without adhesive in between them) stick together [56].

Although the chemical bonds is quite strong especially in comparison to the others, it is pretty difficult to be produced in a dense manner across an interface. In the daily life there are plenty of chemical bonding created between the substrates. For instance, in the cohesion of gold to gold an interface is created at first but it disappears essentially by the bond of all atoms in the interface. However, for some other systems of unlike substrates such as metal-ceramic or polymer-polymer interfaces, the chemical bonding is much more tricky and may end up with very limited bonding and much lower strength [66, 67].

In some cases pure chemical bonding occurs and in some others physical, but this doesn't mean that the mixture of bondings cannot exist in an adhesion. For example, the existence of electrostatic or Van der Waals forces that develop between molecules hold the substances together in most of the adhesive systems. However, the additionally existence of surface chemical bonds may enhance the strength of the bond between the substrate-adhesive significantly [36, 37, 56].

To consider the majority, the intermolecular interactions existing in an adhesion or cohesion are mostly from Van der Waals type bonds [40]. This bond is generally very weak but it is always present. Therefore, there is often a significant contribution of stronger bond present

at the interface in addition to Van der Waals such as those from permanent dipoles [66]. Van der Waals forces are also basically from dipole type, but not permanent. It is formed when the electron cloud surround the nucleus which is never rigidly attached in place and is displaced slightly off-center from the nucleus. In this situation a non-zero electric dipole moment is created whose external electric field is no longer zero. Therefore, this temporary produced field by the first atom can couple with the nearby atoms in a way to produce a weak, mutually attractive force. The pairwise potential energy of this force can vary inversely with the separation [64]. Plenty of detailed discussions regarding this subject can be found by Gutowski and Good et al. [68, 69].

Based on the former brief clarifications about the bonding force kinds, it is time to focus on local and non-local topic. The direct interaction of physical objects that are in proximity implies the simplest definition for local interaction, and exactly in opposite, if a material point interacts with a point further (in a finite radius) than its immediate points it is from non-local type. The validity of locality can become questionable in many situations, especially if small features and micro-structures influence the entire macro-structure, then local assumptions should be avoided.

Non-local theories were of interest from the past. Formerly Eringen et al. in 1977 tired to provide non-local constitutive relations while keeping the equilibrium and kinematic equations in the local form in order to stay in a simplified form. In other words, they applied their non-local continuum theory on the modeling of a Griffith crack (local theory). This way they were able to predict a physically meaningful finite stress field at the crack tip, while the local theory predicts infinite stresses at the crack tip. Hence, it has become more common in non-local theories to provide the non-locality by constitutive relations. Either through integral-type models in continuum mechanicsor gradient-type models including high order derivatives [70].This type of non-local continuum theory has the advantages of capturing macroscale effects as well as the effects of molecular and atomic scales by the means of taking the long-range effects into account [71].

In principle non-locality arises from the existence of a concept called long-range forces within a material or between the interface of adhered ones. It can be claimed that the forces involved in chemical bonding are assumed short-range and mainly attractive which are considered as local interactions. In contrast, long-range attractive forces can be created through physical bonds of both electrostatic forces (coming from permanent dipoles) or van der Waals forces which can interact with the particle not only near by [72]. Additionally, by having the suitable circumstances in the problem, even the short-range forces can combine and turn into long-range ones if many particles are taken together and modeled as a unified structure. By doing so they are capable of creating the effect of long-range forces. Bobaru et al. supports this idea by mentioning a simple example in his book [63], which is brought briefly in the following.

They believe that the quantum mechanical forces as in Van der Waals, between two atoms in space can be calculated by $F_{vw} = cr_{vw}^{-7}$, where r_{vw}^{-7} is the separation distance and c is a constant. If non-locality arise as explained earlier by combining many atoms and taking long-range forces instead of short-range forces, it results the force value to become a function of distance from one surface to the other. This leads to $F_s = c_s D_s^{-2}$ suggested by Israelachvili [37] to calculate the net force between the surfaces with the distance value of D. The increase in the exponent of the distance factor, is also because of the idea of combination to create long-range forces. Theoretically, it is possible to model each atom individually based on the first idea, but considering the number of atoms in each materials, it would be an inefficient method. Therefore, the idea of considering long-range forces in continuum-like model seems to be the better choice [63]. In fact this type of non-locality

arises from the modeling decision for the system, illustrating that in some cases it is possible to choose non-local modeling regardless of underlying physical interactions in the system. However, many non-local models tend to fail when there is a discontinuity in the system. This problem occurs in the models which include spatial derivative in their equations. In order to avoid such problems, in the year 2000 a scientist called Silling represented a specific non-local theory that did not include spatial derivatives, which was called the peridynamic theory[73].

To do so, the peridynamic formulations take displacements instead of their derivatives into account. Since the aim of this theory was to be applicable on discontinuities such as a crack, it utilizes spatial integral equations based on reformulated equation of motion in solid mechanics. In this regards, the governing equations of this theory can be defined at the fracture surfaces and the damage is considered as a part of its constitutive laws. Such feature of peridynamic theory allows the modeling of crack initiation as well as its propagation choose an arbitrary path. As an other highlight feature of peridynamic theory we can point to its ability of linking different length scales providing the possibility of multi-scale failure prediction. As a general statement on this method it can be said that, internal forces are considered as non-local interactions between material points in a continuous body and the constructive model contains damage as well [74].

Like many other theories, peridynamic theory has also been going trough evolution in different directions based on the requirements of the study cases. As mentioned earlier, the original peridynamic theory was formulated by Silling in 2000 [73]. The main assumption of this theory was taking the pairwise forces in an equal magnitude which resulted in a disadvantage of limiting the property range of the material that are supposed to be modeled. For instance, the the Poisson's ratio of the material had to be quarter of the isotropic materials. Moreover, this model does not perform properly on capturing incompressibility condition, since, it is not able to differentiate volumetric deformations from distortional. However, the "bond based peridynamic theory" was later provided based on this method. In 2007 [75], Gerstle et al. introduced a "micropolar peridynamic model" to overcome the material properties limitation of the former approach. The idea behind this method was to add the pairwise moments to the interactions mentioned in "bond-based peridynamics". This way the limitation for material properties regarding isotropic materials was successfully solved, yet, the performance of this model on capture the incompressibility condition is not clear. Hence, Silling et al. [76], on the same year (2007), came up with a more general formulation that resulted in producing "state-based" peridynamic theory. This time they were able to develop the theory in a way that could solve the limits facing the "bond-based" theory. As it is also mentioned in its name, it contains peridynamic states of infinite dimensional arrays caring peridynamic interactions data. Three years later (2010), in order to explain the influence of indirect forces between the material points, Silling extended the former theory (state-based) and succeeded to present the "double state" peridynamic theory [77]. On 2011, the momentum and energy conservation laws of peridynamic theory were derived by Lehoucq and Sears [78]. By doing so, they were able to show that non-local interaction concept is inherent to the continuum conservation laws. Meanwhile, Silling extended his former peridynamic theory as well [79]. This extension was performed in the direction of bridging different length scales based on a method called "coarse-graining". This method functions by reflecting the structural properties at a lower scale to its upper scale utilizing a mathematically consistent technique.

Based on former studies on peridynamic theory, it is shown that it can predict the behavior of vast material types such as linear elastic, nonlinear elastic, plastic, viscoelastic, and viscoplastic [76, 80–83]. It's been also used for damage modeling from so many aspect of different length scales, including macro to nano. The highlight performance of peridynamic

theory, regarding this study, is the additional term to the peridynamic response function that represents van der Waals forces included by Silling and Bobaru [80]. There are numerous references as journals articles and books available in peridynamic theory field and the origins of the this theory was explained briefly in this section, however going through the details of the whole development procedures and reviewing all methods is not in the concern of this study.

In the case of this study there is no sign of chemical bond or adhesion between the layers of the self-adhesive polymer films. According to the peel force measurement results, which will be presented in the following chapters, it can be seen that the adhesive force between the films is from physical and therefore the van der Waals type. It is also noticeable that, by bringing the layers closer to each other during sample preparation from one point forward they started to attract one another, which brings us again to the long-range forces and non-local interactions.

2.3 Effective Work of Adhesion Approaches

In the present section the previous works and backgrounds on the subject of "effective work of adhesion" will be briefly implied.

Initially it is better to provide a simple and clear definition of the phrase "The effective work of adhesion". "The work of adhesion is the amount of work that is done when two adherent surfaces are parted and removed to a large distance from each other. This quantity, $W\mathrm{adh}$ may be either positive or negative; if positive the two surfaces will bond and the higher the value of $W\mathrm{adh}$ the stronger the bond. Conversely, if it is negative, no bonding will occur" so is defined in [84].

Commonly the standard approach in processing of a peel test results is to determine the effective work of adhesion regarding the specimens. Such analysis of peel test was performed for the first time by Rivlin in 1944 (reprinted in Rivlin, 1997). In this article he referred to the adhesion properties of a surface by "the tacky characteristics". Since, separation of an object from such surfaces is associated with the relatively high amount of work that has to be done, and he believed that the tackiness may be associated with a high effective work of adhesion [50, 85].

In this regard, he performed some experiments with adhesive tapes (used as surgery plaster), in which the variation of the effective work of adhesion is measured as a function of detachment speed of the adhesive from the adherend. The experiments carried out by rolling the mentioned adhesive tape onto a polished stainless steel plate which was placed approximately vertical, meanwhile, a weight was attached to the upper end of the tape so that the tape peeled off slowly from the stainless steel plate as the weight fell down in a quasi-static situation. He proposed the following equations to calculate the effective work of adhesion. If the attached mass to the end of the tape is m and the stainless steel plate is positioned vertically forming the angle θ, then the potential energy lost by the weight, in stripping off a length l of the tape, could be found by:

$$U_\mathrm{m} = \mathrm{m}gl(1 + \cos\theta)$$

He claimed that, the potential energy of U_m is equal to the work necessary to strip off a length l of the tape at the speed from gravity acceleration. Therefore, the effective work of

adhesion per unit area is obtained by $\frac{mg}{b}(1 + \cos\theta)$, where b is the width of the tape [85]. By simpler means, in this study Rivlin ignored the deformations of a peeled film and that provides us with the relationship between the effective work of adhesion and the peel force derived for inextensible films with the peel angle of 90° to the horizon as follows:

$$F_{\text{peel}} = bY$$

Kendall extended the mentioned approach of Rivlin in [86–88] by taking into account the elastic strain energy, but restricted the analysis to small deformations. In this regard, he also admitted that adhesion and surface energy are related, implying the definitions of adhesion and surface energy, which are the *force* required to separate two surfaces and the *work* required to separate them respectively. However, considering only these two parameters, wasn't realistic. Therefore, based on the previous works of Griffith [89] regarding the fracture of rigid bodies, Kendall believed that fracture of solids depends not only on surface energy but also on the geometry and elastic properties of the materials. Hence, a theory of adhesion must also take the elastic and geometric effects into account. He derived the theory of peel strength from an energy balance approach. The total energy U_T in the system is the sum of several energy terms, consisting the following principal components of the surface energy U_S, the strain energy U_E, the potential of the load U_P and the thermal energy U_L. From the principle of energy conservation, this sum does not change when a small linear strain is applied, meaning:

$$U_T = U_S + U_E + U_P + U_L, \qquad \frac{\mathrm{d}U_T}{\mathrm{d}s} = 0$$

He added that, by Imagining an elastic film with the thickness of d and Young's modulus of E, involving a length of Δc_l in the peeling film between the arbitrary points of A and B, being peeled at an angle of θ from a rigid substrate under a constant force F_{peel}, the mentioned components of the total energy contributed to the energy changes as in the following:
A surface energy term $-bY\Delta c_l$ due to the creation of new surfaces (Y being the adhesive energy, that is the experimental energy required to fracture unit area of interface or in other words the work of adhesion), a potential of the load term $F_{\text{peel}}(1 - \cos\theta)\Delta c_l$ due to the movement of the rigid glass plate applied force, and an elastic term due to extension of the film in the direction of the applied force.
The elastic term, which is the result of the region AB being stressed, has two components: a component $-F_{\text{peel}}^2\Delta c_l/bdE$ which is the work done at constant force in stretching the region between A and B, and a component $-F_{\text{peel}}^2\Delta c_l/2bdE$ which is the amount of recoverable strain energy stored in the stretched element. The material is assumed to undergo small, linear elastic strains in this instance. In the cases with no thermal energy changes the value of U_L can be avoided from the consideration. Adding up all these energy changes and assuming energy conservation gives

$$-bY\Delta c_l + F_{\text{peel}}(1 - \cos\theta)\Delta c_l + \frac{F_{\text{peel}}^2\Delta c_l}{2bdE} = 0$$

Dividing all terms by b and Δc_l yields

$$\left(\frac{F_{\text{peel}}}{b}\right)^2 \frac{1}{2dE} + \left(\frac{F_{\text{peel}}}{b}\right)(1 - \cos\theta) - Y = 0$$

This equation, quadratic in F/b, shows how the three terms, elastic, potential and surface, interact. In order to simplify and achieve more clear equation, the terms can get organized and the final equation of Kendall [88, 90] takes the following form

$$F_{\text{peel}} + \frac{1}{2}\frac{F_{\text{peel}}^2}{C_T} = Yb$$

where $C_T = Ebd$.

These assumptions of Kendall are quite similar to the case of this study, and therefore this method was the suitable choice to calculate the surface energy and to be used as a verification method for the results which is going to be illustrated in the Chapter 4.

In the cases of stronger adhesion (if the bending stresses imposed by the peel force are sufficiently large) that can cause plastic yield of the adherend during the peel test, and we can refer to the work of Gent and Hamed in 1977 [91]. Clearly, an ideal elastic-plastic solid follows a linear stress-strain relation until the yield stress, and yield strain are attained. Hence, they implied that the energy dissipation mechanism provided by plastic yielding requires higher total peel force than that of without yielding. For this purpose, the magnitude of this additional energy dissipation was determined experimentally by them for a simple elastic-plastic strip adhered to a rigid substrate. Moreover, they calculated the peel force required to propagate a bend in an elastic-plastic strip, using elementary bending theory. At last, they concluded from their study that the value of which these forces contribute to the total peel force in a peeling experiment is governed by the strength of adhesion, relative to the thickness, deformability of the adhesive and yield stress of the adherend. In addition to this study, the dissipation of energy was taken into account by Kinloch et al. in 1994 [49] and Hadavinia et al. in 2006 [92] in processing results of peel tests for elasto-plastic materials. Further works in this regard is devoted to transverse shear strains of the peeled film that are additionally taken into account by Thouless and Yang in 2008 [93].

2.4 Cohesive Zone Model

The cohesive zone model, usually abbreviated as CZM, is a concept in fracture mechanics where defines the fracture as a gradual phenomenon. One of the noticeable advantages of this model is that, it is not limited to modeling a single crack tip and is able to provide the description of crack nucleation and growth through different times and length scales.

In CZM the crack surfaces separate across an extended crack tip or cohesive zone, although cohesive tractions resist against this separation. One of the fundamental matters in the simulation of system with CZM is the definition of cohesive interactions along fracture surfaces. Generally speaking, these cohesive interactions are a function of displacement, or in better words, separation during a fracture or peeling. If the fracture surfaces separate

greater than a specific characteristic length, complete failure will happen. This aspect in CZM is called the traction-separation relationship of the fracture surfaces [94].

The concept of the cohesive zone model has been widely used to investigate and analyze the process of delamination or the various material failure phenomena, such as fatigue crack growth [95–99], crack growth along adhesive bond joints [100–103], discrete fracture processes of homogeneous and inhomogeneous material systems [104], etc.

Cohesive zone models are usually presented as a function of both normal and tangential tractions in terms of separation. Mostly the general behavior of the traction-separation relationship is in a way that with increasing the opening displacement (separation), the traction over the interface rises until a maximum amount called $\sigma_{\max}$, afterwards it decreases until it vanishes (or it has so low value that considered as vanished).In the point that traction is vanished a complete separation is occurred and is called the opening displacement point δ_n or δ_t for normal and tangential separation respectively [105].

The traction-separation relationships behave globally similar. Therefore, it is believed by many scientists that two independent parameters of the cohesive energy and one of the traction or separation are sufficient to model a cohesive zone, which means the form of the traction-separation relation is not important. Although, it is proved by a lot of researchers that the form of the traction–separation relations for CZMs plays a very critical role in determining the macroscopic mechanical response of systems [104]. Hence, there is a great variety in traction-separation laws which are caused by some number of factors which affect the resulting failure behavior and the form of the curves. The description of the traction-separation forms are presented by Chandra et al. in 2002 [104] which is summarized in the following table to have an overview on this topic.

Table 2.1: Various traction-separation relationships in the order of exploration year, this table is extracted from Chandra et al. in 2002 [104]
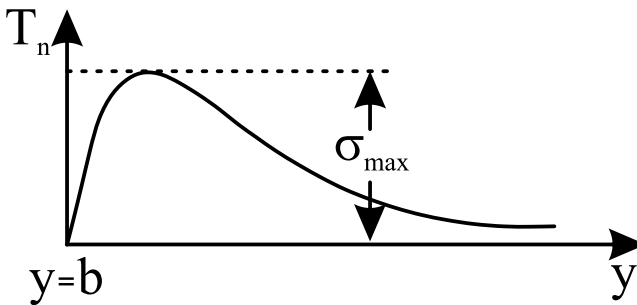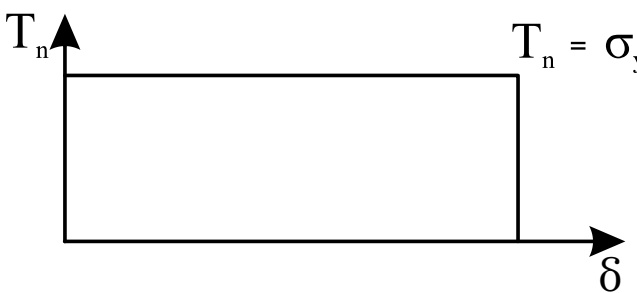
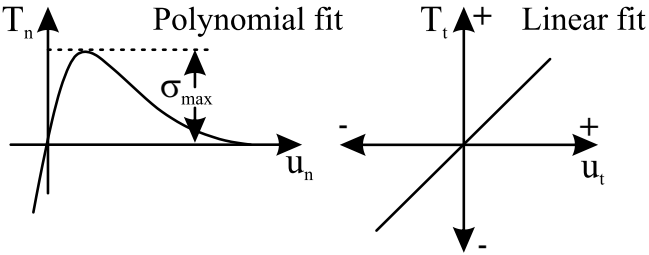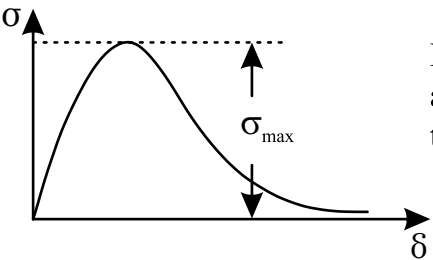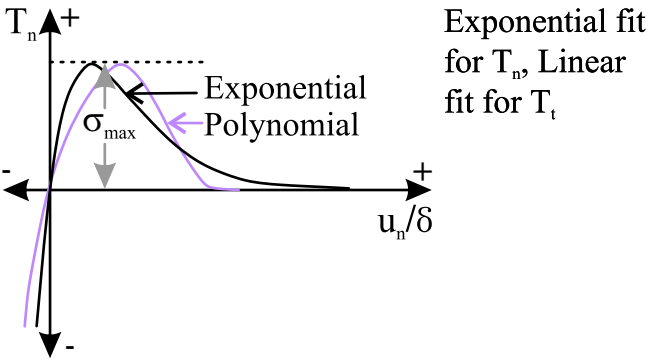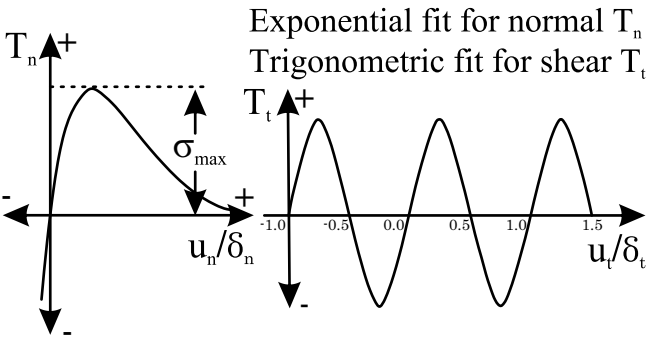| Author (year)	Proposed model	Comment
Barenblatt (1959, 1962)		The first to propose the cohesive zone concept
Dugdale (1960)		Cohesive stress equated to yield stress of material

Table 2.1: Continued on next page
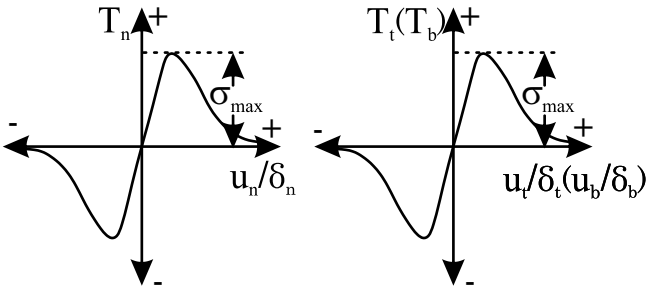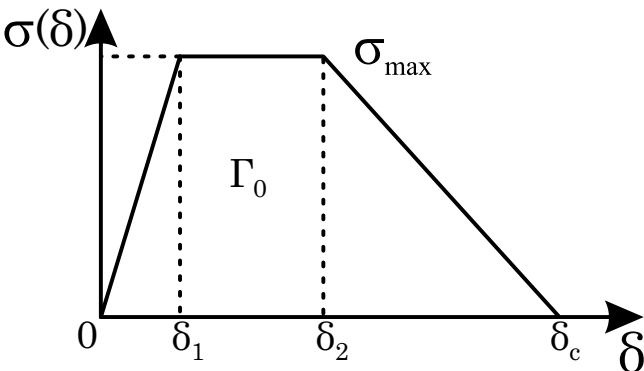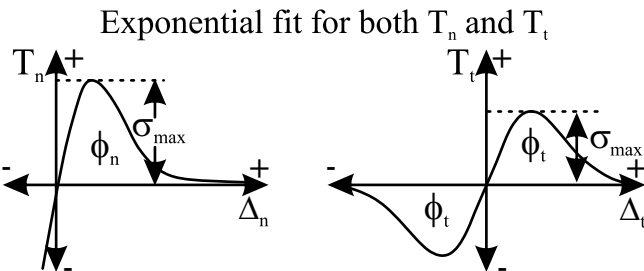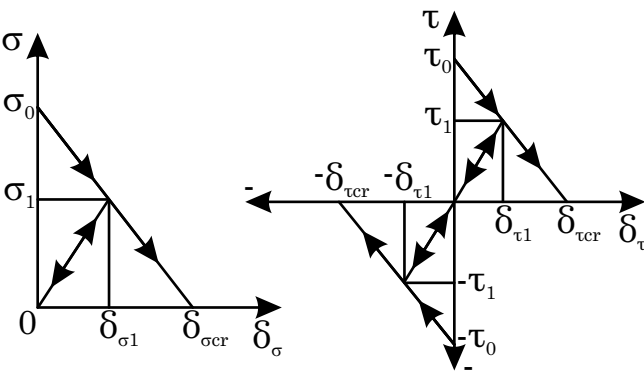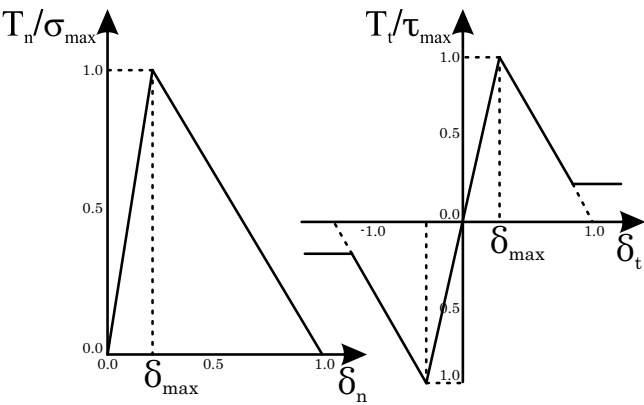
Author (year)	Proposed model		Comment
Needleman (1987)			Phenomenological model; predicts normal separation
Rice and Wang (1989)		Model based on atomic fit of the type $(1+x)e^{-x}$	Phenomenological model; predicts normal separation
Needleman (1990a)		Exponential fit for T_n, Linear fit for T_t	Predicts normal separation
Needleman (1990b)		Exponential fit for normal T_n Trigonometric fit for shear T_t	Periodic shear traction to model Pieriels shear stress due to slip
Tvergaard (1990)			Quadratic model

Author (year)	Proposed model	Comment
Tvergaard and Hutchinson (1992)		Claims shape of separation law are relatively unimportant
Xu and Needleman (1993)		Claims shape of separation law are relatively unimportant
Camacho and Ortiz (1996)		Uses additional fracture criterion; predicts failure by both shear and normal separation in tension and by shear separation in compression
Geubelle and Baylor (1998)		Bilinear model; ascending curve can be matched to initial stiffness of the material

By doing a brief research on CZMs, it can be realized that there are already several constitutive relationships developed in this regard. As mentioned earlier, the effective traction vs. separation define various cohesive relations respect to the shape of the curves, such as polynomial [106, 107], trapezoidal [108], exponential [109], bilinear [110], etc. as shown in

the figures of Table 2.1 [94]. The most popular proposed CZMs are illustrated in Table 2.1 in the order of their exploration year, including the name of the scientist who invented them.

- **Barenblatt**, Basically CZMs were presented as a possible alternative to the concept of fracture mechanics in perfectly brittle materials [104, 111]. The concept of the the cohesive surface formulation or CZM was originally proposed by the pioneering contributions of Barenblatt [112, 113] in 1959 and 1962 which was focused on finite strength of perfectly brittle materials. Barenblatt proposed the first CZM as a distribution of cohesive forces in the region ahead of a tensile crack which increases to a finite limit to the opening traction as opposed to the infinite opening traction of the linear elastic solution for a mathematically sharp crack. In [112, 113] Barenblatt focused on his work on brittle or quasi-brittle failure, where deviations from linear elasticity are bounded to a region close to the crack tip. [111].

- **Dugdale**, Later, if one traces CZMs back to the work of Dugdale [114] in 1960, he or she will face the extended version of this concept to perfectly plastic materials [94]. Dugdalee [114] introduced a similar cohesive zone model as well, to investigate yielding at a crack tip and size of the plastic zone. In his model the traction in the cohesive zone was assumed to be constant and equated to the yield stress of the material when the separation was smaller than a critical value. The aim of this study was to directly calculate the gauge of yielding of thin ideal elastic–plastic steel sheets containing slits as a function of the applied load [94, 111].

- **Needleman**, Ulike Dugdale, one of the first people who used polynomial or exponential traction-separation relations to study the debonding which happened in metal matrices was Needleman since 1987 [66, 107, 109] see Table 2.1 for parts Needleman, 1987, 1990a, 1990b. Later on since 1993, **Needleman and Xu** used the previous models to provide newer method studding the void nucleation and dynamic fast growing cracks at the interface. In this regards, Needleman himself implies that "his contributions were the introduction of cohesive surfaces into initial/boundary value formulations without any initial crack so that crack nucleation can be modeled and the introduction of a formulation (with X.-P. Xu) of multiple cohesive surfaces allowing for shear as well as tensile decohesion [111, 115]".

- **Rice and Wang**, This model was introduced in 1989 and it assumes that the interfacial region is a two joined elastic continua that interact with each other as in adhesion type. For this sort of interaction, they implied that stress vs. separation are related like $\sigma = \sigma(\delta)$, which provides the corresponding curve in Table 2.1. It is also assumed that these two solids separate without dislocation or any other in elastic processes and there is no shear happening parallel to the interface [116].

- **Tvergaard**, In 1990 a quadratic traction-separation relation was introduced by Tvergaard which was used to describe the interfaces of whisker reinforced metal matrix composites. Two years later, in 1992 **Tvergaard and Hutchinson** [117] used a traction-separation model in the shape of trapezoidal to calculate the resistance of a crack growth in a elasto-plastic material, as well as in the peeling of adhesive joints [104].

- **Camacho and Oritz**, As it is illustrated in Table 2.1, in 1996, these two scientists used a linear traction-separation formulation. By adding a fracture criterion, this model was utilized to simulate the propagation of multiple cracks along arbitrary paths in brittle materials [118].

- **Geubelle and Baylor**, A bilinear traction-separation model was introduced by them in

1998 to simulate a spontaneous crack or delamination initiation and propagation in thin composite plates under low-velocity impact [110].

In most of the CZMs except Dugdale's and Camacho et al.'s model; see Table 2.1, the traction–separation graphs are as described earlier, increasing interfacial separation the traction across the interface reaches a maximum, then decreases and eventually vanishes leading to a complete failure or delamination. It is believed by many scientists that the main difference between the various CZMs lies in the shape or the constants that describe the shape of the model. Moreover, generally speaking, the exponential model by Xu and Needleman (1994), as it is also observable in Table 2.1, provides smooth traction-separation curves and therefore is believed to be more stable than discontinuous models, such as the bilinear model of Guebelle and Baylor [104].

The usual or standard method in processing/simulating the result of mechanical tests such as peel test, fracture, etc. is to use a local traction-separation law. The procedure which is used the most in this regard, is to assume a specific idealized shape of the traction–separation curve, like the ones introduced already in Table 2.1, to simulate the test and to identify parameters in the traction-separation law. For instance, parameters such as energy of adhesion (area below the traction–separation curve), critical opening displacement, etc. Such a method is applicable if the type of the traction-separation law is provided by using theoretical, experimental and computational methods. For example, for a double cantilever beam specimen a traction-separation relation was calculated based on the J-integral or if the physical properties of the adhesive joint are well-defined, its interaction potentials are applicable using Lennard-Jones potential to compute the local traction–separation curve numerically [50, 94, 119–121].

In the case of this study, the critical point is the identification of the traction-separation curves, specifically calculated for the materials chosen for our tests, from the results of their peeling experiments. Therefore, unlike the usual procedures of CZMs, in this study the shape of the interfaces during the separation is taken into account and by extracting the required parameters from the peel tests, the corresponding traction-separation curve were obtained by going in a reverse procedure.

2.5 NURBS

As it is already mentioned in previous section, the procedure of this study goes in a reverse path therefore in order to complete the identification step the configuration and shape of the film during the separation is required in a digital form. One of the most precise ways to do, so is to use NURBS and extract the required data. The details of this step will be explained in Chapter 3. In the following we briefly review the background of the NURBS and how it can be created.

If we go some years back in a time before the computers existed, people such as engineers, architects, artists, etc., basically who required to design something like device parts, roads, bridges and so on, had to do their job on paper and use various rulers and tools based on the design. For instance, in order to draw straight lines and circles or circular arcs, tools like rulers, T-square, and compasses were used respectively. Obviously without computers, design world faced a lot of challenges such as not being able to draw major amount of interesting shapes which are not just circles or ellipses. Such problems took place specifically in ship building. Therefore in this case, the designers could use a long, thin and flexible stripe of wood, plastic or even metal as a drawing tool which was called "spline". Figure 2.10

illustrates a spline, this tool was held in place with nails or lead weights. The outcome of such a design was a smooth curve with possibly various curvatures because of the nails positions. The elasticity of the spline material provided it to take the shape that minimized the energy of bending.. Therefore, it could create the smoothest possible shape between the nails. Afterwards, when computers were invented and were also used as designing tools, the mathematical behaviour of such curves were investigated so that they can be applicable by computer aided design tools [122].
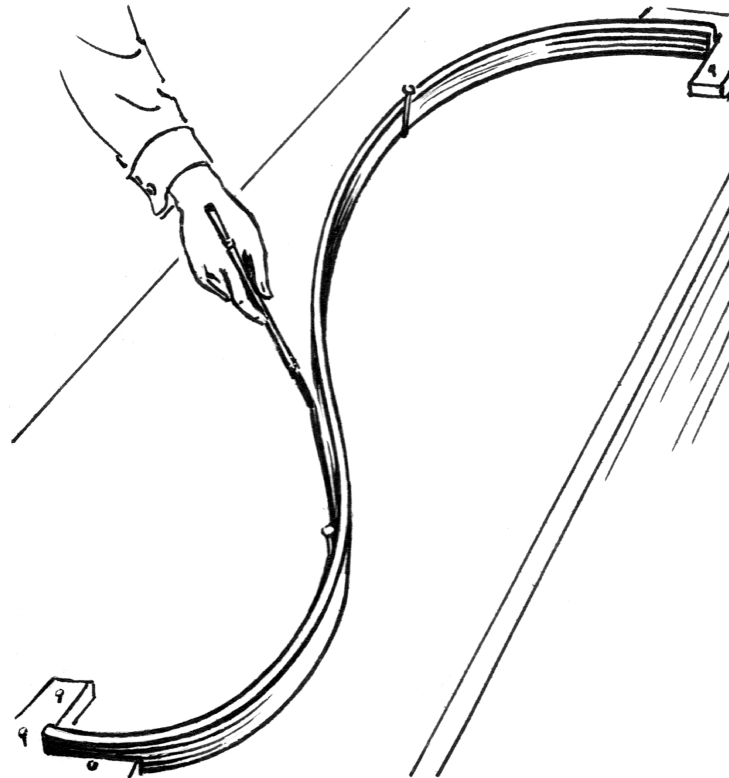
Figure 2.10: The sckematics of a spline which is held in place by some nails at a number of predetermined points [122]

Since 1946, spline shape attracted the attention of mathematicians to study and define them mathematically. By investigating so, piecewise polynomial equations were derived and a scientist named I. J. Schoenberg called them spline curve or spline function after the mechanical spline tool. The pioneer work in this regard, was started by the parallel work of Renault engineer Pierre Bézier, and Citroën's physicist and mathematician Paul de Casteljau but since Bézier published his results earlier the curves were named after him [123].

Non Uniform Rational B-Splines, or in a short form called NURBS, grew out of the mentioned pioneer work of Pierre Bézier. As it is also clear from the name, NURBS is a mathematical model that uses basis splines, or B-splines. Nowadays B-splines are widely used in computer graphics in order to draw curves and surfaces which provides a great flexibility and precision. By using the rational and nonuniform rational type of the B-spline, this precision and flexibility grows even much higher. Therefore, a modeling system can use NURBS for wide range of curves and surfaces from straight lines and flat planes to precise circles and spheres as well as intricate piecewise sculptured and conic surfaces. This makes NURBS unique and the best choice to be used in computer-aided design (CAD), manufacturing (CAM), and engineering (CAE), in order to design or model automobiles, aircraft, ships, shoes, shower shampoo bottles, etc., or for an animated character or computer game, or even as the motion

path for that character [123, 124].

To get familiar with the terminology and definition of NURBS we need to know what does each word of Non Uniform Rational B-Splines stands for. Starting from spline, which is mentioned earlier and is representing a piecewise polynomial function with a desired order. The term B-splines refers to the basis spline functions, that can be defined through a number of ways such as divided differences of truncated power functions by Curry 1947 [125] and Schoenberg 1946 [126], blossoming by Ramshaw 1987 [127], or a recurrence formula by Cox 1972 [128] and de Boor 1972, 1978 [129, 130]. In this study the recurrence formula is used, since it is the most useful method also for computer algorithms. This method defines the basis functions by two parameters called **Knot vector** and **control points**. A knot vector is a non-decreasing sequence of real numbers showing coordinates in the parameter space and is written as $Z = \{\zeta_1, \zeta_2, ..., \zeta_{n+p+1}\}$, where $\zeta_i \in \mathbb{R}$ is called the ith knot, ζ is the knot vector, i is the knot index, $i = 1, 2, ..., n + p + 1$, and p is the polynomial order, n is the number of basis functions which is used to build the B-spline curve. If the knot vector is known, the B-spline basis function of p-degree (order $p + 1$) which is denoted by $N_{i,p}(\zeta)$ can be defined by the following relations [131, 132].

$$N_{i,0}(\zeta) = \begin{cases} 1, & \text{if } \zeta_i \leq \zeta < \zeta_{i+1}, \\ 0, & \text{otherwise.} \end{cases}$$

For $p = 1, 2, 3, ...$, the basis functions will be defined differently based on the next equation

$$N_{i,p}(\zeta) = \frac{\zeta - \zeta_i}{\zeta_{i+p} - \zeta_i} N_{i,p-1}(\zeta) + \frac{\zeta_{i+p+1} - \zeta}{\zeta_{i+p+1} - \zeta_{i+1}} N_{i+1,p-1}(\zeta)$$

Knot vectors may or may not be **uniform**. They are categorized in this way that, if the knots are equally spaced in the parameter space they are considered as uniform, and reciprocally when the knots are unequally spaced, the knot vector is **non-uniform**. The values of knots can be repeated although for limited amount of times. These multiplicities are limited, because they imply important information about the properties of the basis function. A knot vector is considered to be open if the first and last knot in the group is repeated $p + 1$ times, and this is the maximum amount of times that a knot can be repeated (can't go higher than the polynomial order). This brings us to the continuity concept in NURBS which has multiple different levels. The continuity level in each joint of NURBS can be calculated from the multiplicity of the corresponding knot by $C^{p-\mathbf{m}}$, where $\mathbf{m}$ is the single knot multiplicity value. As implied earlier, starting from the open ends of a NURBS curve, it will give us $C^{p-(p+1)} = C^{-1}$ that means there is no continuity in those points of staring or ending of a curve. Now if we go one step further to positional continuity $C^{p-p} = C^0$ it means that the ending posits of two piece of curves or surfaces are attached, however, they may still meet at an angle or make a sharp corner. The third would be the tangential continuity achieved by $C^{p-(p-1)} = C^1$ meaning, the first derivative of the left and right limit at the joint are coincide. The highest level of continuity with considering the curve-degree is achieved at the points where their corresponding knot is not repeated and there is only one number for that knot available in the knot-vector, providing us with C^{p-1} [131, 132].

By providing the basis functions based on the knot vectors and polynomial order, B-spline curves can be constructed with a linear combination of the basis functions.To this end, as

mentioned earlier, another parameter called the control point is also needed, which is the vector-valued coefficient of the basis functions or in other words they are the coordinates denoted to the location of the points shaping the curve [131, 132]. The B-spline curve of degree-p is defined as the following:

$$C(\zeta) = \sum_{i=1}^{n} N_{i,p}(\zeta)B_i$$

where $B_i \in \mathbb{R}$ are the control points corresponding to the basis function of $N_{i,p}(\zeta)$, $i = 1, 2, ..., n$.

Clearly, in this subject, if one likes to dig into the details there is a vast area of research available with also a lot of challenges which is required to be solved. However, going deeply into this subject is out of the intentions of this study. Since NURBS were utilized to precisely digitize the deformed shape of the polymer films during the peel test, providing more and complicated details about NURBS is considered unnecessary.

3 Materials and Experiments

3.1 Materials

The polymeric films tested in this study were fabricated of linear low density polyethylene (LLDPE) with the thicknesses of less than $23\,\mu\mathrm{m}$. Figure 3.1(a) illustrates the schematic view of the constituent layers of the films, which includes a bulk layer of transparent flexible polyethylene films and one layer of very thin polymeric cling material co-extruded to the bulk layer. They were produced by POLIFILM company in different thicknesses for different using purposes. Figure 3.1(b) shows the actual picture of a two-layer specimen of the mentioned films with the thickness of $23\,\mu\mathrm{m}$ subjected to T-peel test, positioned in between the clamps of a tensile testing machine, from an angled view.

The films exhibit self-adhesive behavior because of the mono-layer co-extruded polymeric cling material. Therefore, this study deals with pure adhesive interactions, which leads to smooth cling surface on the films after the peel test performance. The cling surfaces didn't show any loss of adherence quality or sign of any extra particle like micro-crazes or fibrils remaining from the other cling layer after being peeled from one another. Hence, it is safe to say that, no cohesive failure mechanisms was observed during peeling. The differences between the Cohesive and Adhesive interactions and failures are discussed in detail in chapter 2.
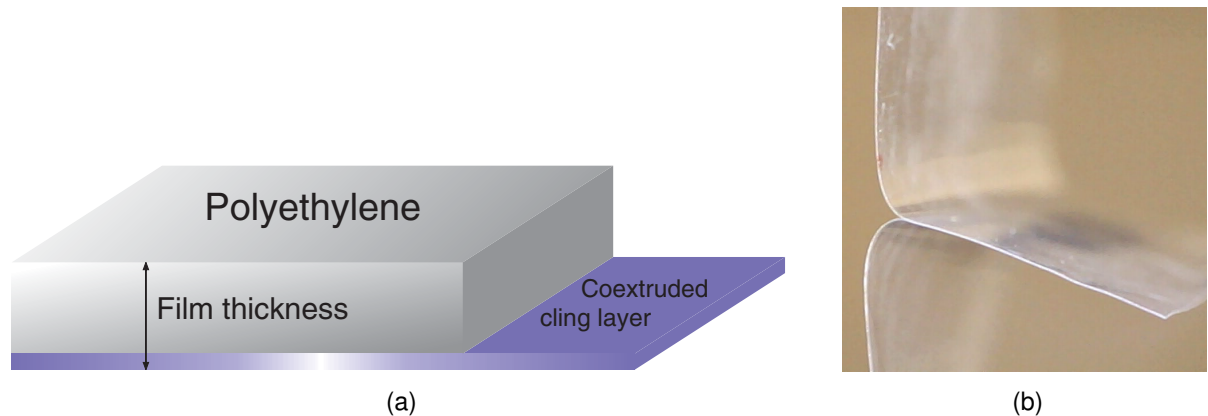

Figure 3.1: (a) Schematic structure of the mono-layer co-extruded polyethylene film used for the experiments of this study; (b) Two layers of the identical polyethylene films under T-peel test after being adhered to each other

The basic information about the films such as the sample name, thickness, etc. is illustrated in table 3.1. As mentioned earlier, polyethylene films were tested in four different thicknesses of $12, 17, 20$ and $23\mu\mathrm{m}$. According to the total thickness of the films, the cling layers were co-extruded in two different percentage of 14% and 17%. As it is observable in table 3.1 the samples were named based on their total film thickness and cling layer percentage. Although the cling layers were co-extruded in only two different percentages, it is obvious that as the

Table 3.1: Basic information of the polyethylene films used for the experiments of this study

Sample name	Film thickness	Cling layer thickness	Cling layer percentage	Cling material
12/14	12 μm	1.68 μm	14%	CL1
17/14	17 μm	2.38 μm	14%	CL1
23/14	23 μm	3.22 μm	14%	CL1
12/17	12 μm	2.04 μm	17%	CL1
20/17-CL2	20 μm	3.4 μm	17%	CL2

film thickness changes, the absolute value of the cling layer thickness would change too. All the samples were made of identical materials for the film. But the polymeric cling material co-extruded to sample $20/17 - CL2$ was different than the others. The exact information about the co-extruded cling material and what are they made of, were confidential to POLIFILM company and was not allowed be revealed. Therefore, $CL1$ and $CL2$ were assigned to the cling materials so that the differences can be distinguishable. Because, the final results of traction-separation behavior of the films is considered as a property of the cling material. It means, the traction-separation behavior changes if the cling material is changed, like in the case of sample $20/17 - CL2$. But as long as the cling material are the same, it is expected that variations in the thicknesses of the films **do not** affect this behavior in the other four samples.

3.2 T-Peel Extension

As the details about the existing peel test methods were explained fully in Chapter 2, it can be realized that among all of them, T-peel test is the most suitable peel test method for performing experiments on two layers of identical flexible, thin films with self adhesive properties. Therefore, the T-peel tests were performed according to the ASTM 1876 standard as well as the sample preparation.
The schematics for the experimental procedure is presented in Fig. 3.2. According to the mentioned standard, the dimension of the samples were $25\,\mathrm{mm}$ to $65\,\mathrm{mm}$ for the width and the length respectively. For sample preparation, two layers of similar polymer films were cut with the mentioned dimensions, then they were laid on top of another while the cling surface of both films came together and were pressed to each other by a roll with the mass of $1\,\mathrm{kg}$. This rolling and compression process of the layers were not necessary for the whole area of the films, it had to be done only on the area which was supposed to be peeled by the testing machine. Since the cling surfaces of the films had the tendency to absorb dust or humidity, to reduce adherence possibility of extra particle on them, the samples were prepared in a closed and clean environment with a relatively steady air flow. In order to provide statistically reliable results in the further steps, five samples were prepared for each polymer film.
To perform the T-Peel test, the ends of each layer of the samples, which were not adhered to each other, were put in between the top and bottom clamps of a tensile testing machine. As it is illustrated in "T-peel test" part of Fig. 3.2, the yellow pieces embedded in the right grips of both top and bottom clamps represent a rubber material which provided perfect grip on thin layers such as our tested polymer films in between the clamps. These clamps were installed
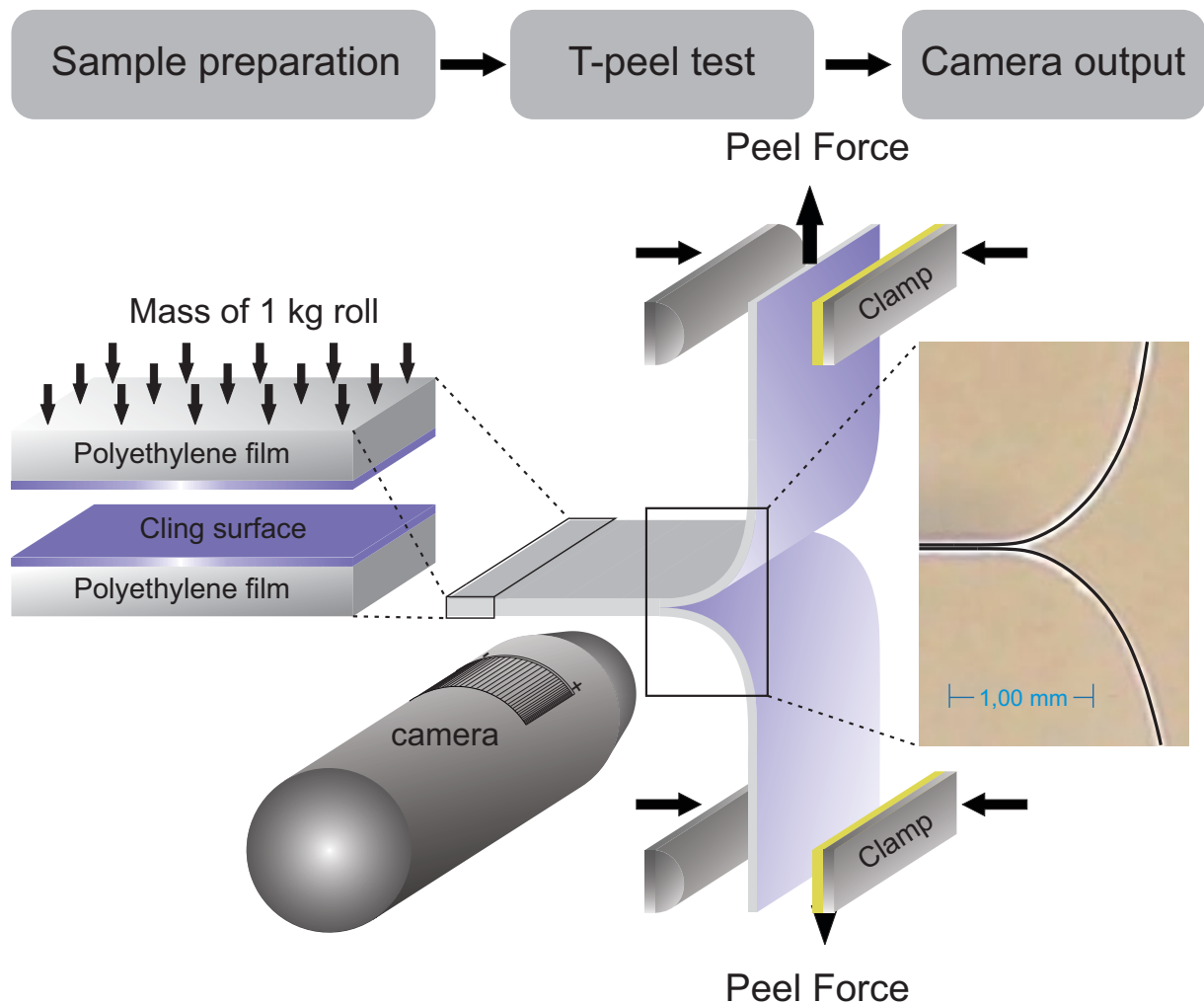
Figure 3.2: Schematic sketch of the experimental procedure starting with preparing the samples form identical layers of polyethylene film (left); Then the T-peel test which is recorded from the transverse view by a microscopic camera (middle); Picture of the deformed shape of the film from transverse view as the camera output (right)

exactly in front of each other, in the same vertical line, to provide a symmetric and equal peel force on both ends of the sample. Again, based on the mentioned standard of ASTM 1876, the initial distance between the clamps of the tensile-testing machine was $60\,\mathrm{mm}$ with the steady peel rate of $100\,\mathrm{mm/min}$ to provide the quasi static situation during the peel test. The length of peeled part of each layer of films by the machine was $10\,\mathrm{mm}$. Each sample had two layers and only the upper grip of the machine did the movement to peel the layers. Therefore, the displacement of the upper grip was minimum $20\,\mathrm{mm}$ so that it could complete the peeling procedure and totally separate the layers until the end.

The force which is required to peel the layers from one another can be measured by the load-cell attached to the end of the top clamp on tensile testing machine. But the measured peel force values do not provide the adequate data for further evaluation steps. Therefore, the other required additional data here is the deformation shape of the films during the peel test which can be provided from the T-Peel test experiments. Regarding the extraction of this information from the experiments, a USB digital microscopic camera was located perpendicular to the transverse view of the samples and grips, during the peel test, as illustrated in middle step of Fig. 3.2. So that it could record the the whole Peel test performed

on each sample from the transverse view. From which, the bending shape of the films during the peel test could be extracted later as an image. In the final step of Fig. 3.2 an image is shown as an actual example of camera output. As it was mentioned in the sample preparation explanations, in order to have statistically reliable experimental results five samples were prepared to be tested from each polyethylene film variety. Hence, there were five recorded peel test videos available for each film type which is 25 videos overall by the end of the experiments. These videos provided the configuration of the films in the whole peel test duration.
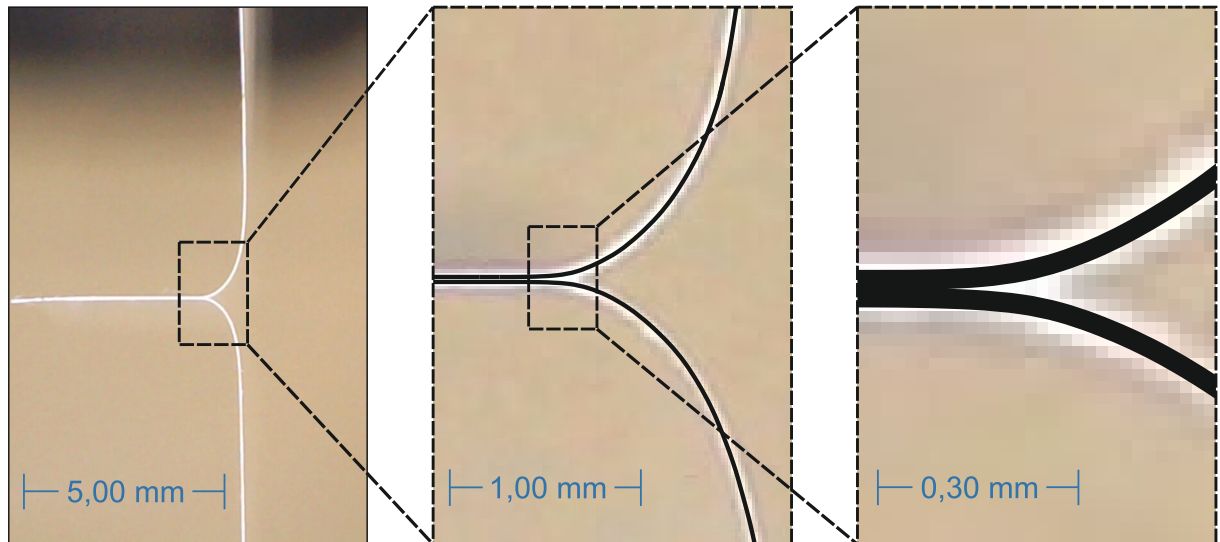

Figure 3.3: Extracted picture from the T-peel test recorded video (left); Magnified 5 to 8 times with respect to the original photo to feature the deformed shape of the films in the delamination zone vector, black lines are drawn by B-spline technique in Coreldraw (middle and right)

In order to have better imagination of the extracted deformed shape of the films from the recorded peel test videos, Fig. 3.3 is provided in three different magnitudes. As mentioned earlier the polymer films were originally transparent, but because of light reflection they appeared in white color in pictures. Such picture as Fig. 3.3 (left) is the camera view during the peel test. Then if we zoom in to the first picture with the magnitude of five, we see Fig. 3.3 (middle), which shows the delamination area more clear. The black lines in Fig. 3.3 (middle and right) are vector lines drawn on the shape of the films to make us able to process the deformed shape of the film in evaluations, which will be explained in detail in the following parts. Finally, by taking an even closer look at the delamination area (separation area of the films), the zone of adhesive interactions, which is indeed in the interest of this study, is visible in Fig. 3.3 (right). According to the symmetric essence of T-peel tests, only the deformed line of one layer was taken into account for further evaluations. Because the other layer possesses the same interacting forces and behavior but in the opposite direction.

3.2.1 T-peel Test Equipment

Such a digital microscopic camera as illustrated in Fig. 3.4(a) was used to record the whole T-peel test. Although it was not a high worthy or super professional camera, it had high microscopic magnification ability. There were eight LEDs around the camera lens with adjustable light power, which could provide an optimal and clear lighting for the recording

<div align="center">(a)</div>

<div align="center">(b)</div>

<div align="center">(c)</div>
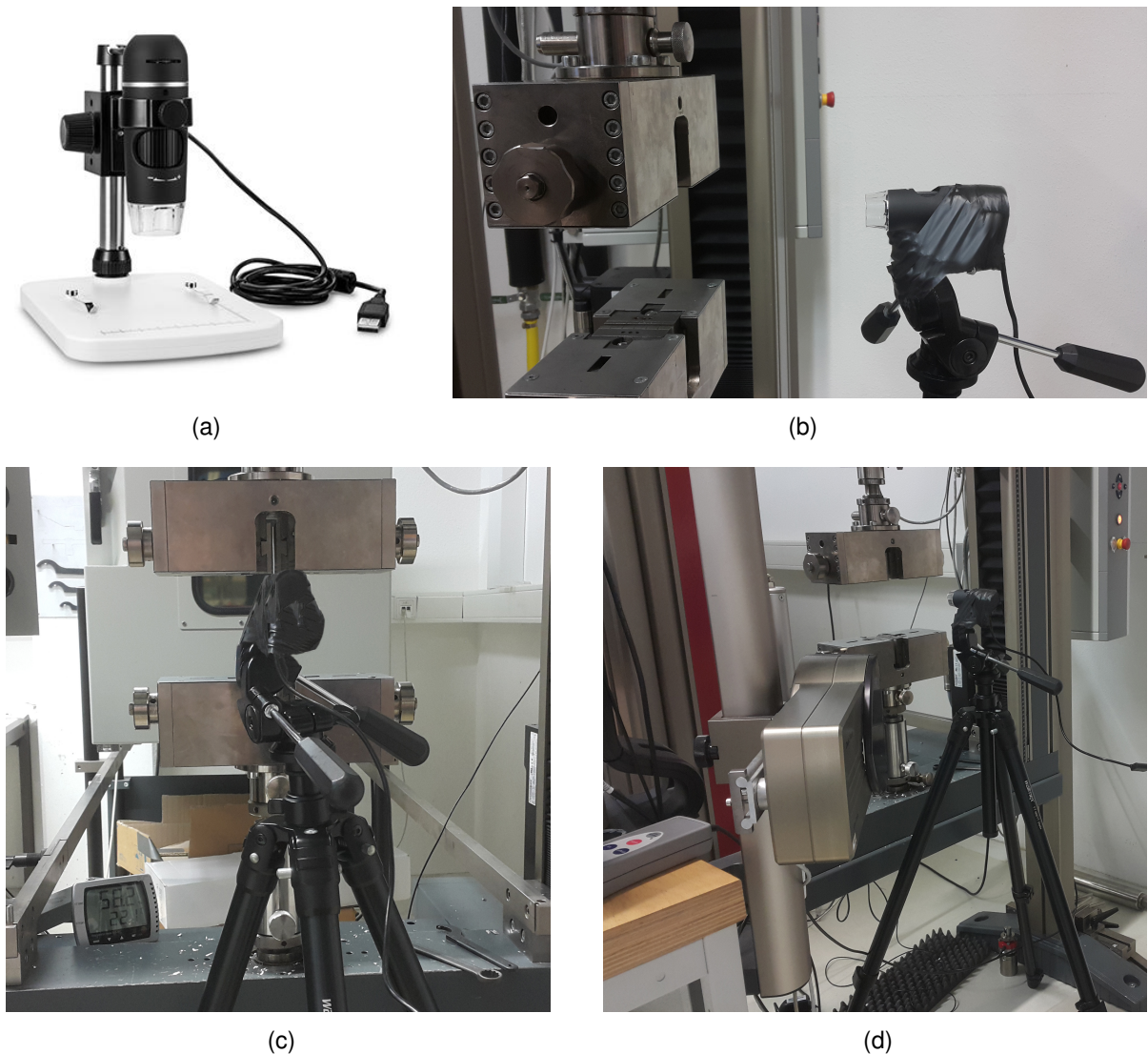

<div align="center">(d)</div>

Figure 3.4: (a) Digital USB microscopic camera, used to record the film configuration during T-peel tests [133]; (b)-(d) T-peel test-setup, camera position with respect to the transverse view of the clamps from three different angles of view

object. T-peel tests were recorded in $\times 30$ zoom in magnification with the frame rate of $10\,\mathrm{frames/s}$. Overall it can be said that, for such transparent thin film the camera showed a pretty satisfying performance.

The actual test-setup is shown from three different angles of view in Figures. 3.4(b)–(d). The position of camera with respect to the tensile testing machine is visible in the pictures. The camera had the ability to get as close as $3mm$ to the objects and zoom in even more than $\times 50$ but in this study the best distance between this camera and the recorded object was about $20-30cm$. Because during the peel test the top clamp moves vertically and upward, it moves the delamination area of the films in the same direction. So if the camera was placed too close it wouldn't be able to fit the delamination area during the peel test in the same frame from the beginning until the end. In addition, the camera had to be placed exactly perpendicular to the clamps in order to record the best transverse view of the films.

Figures 3.5 represents the actual picture of tensile-testing machine and the load-cell attached to it. This was the devise used for the T-peel test experiments. Both the tensile-testing machine and the load-cell were produced by Zwick/Roell company that is the world's leading
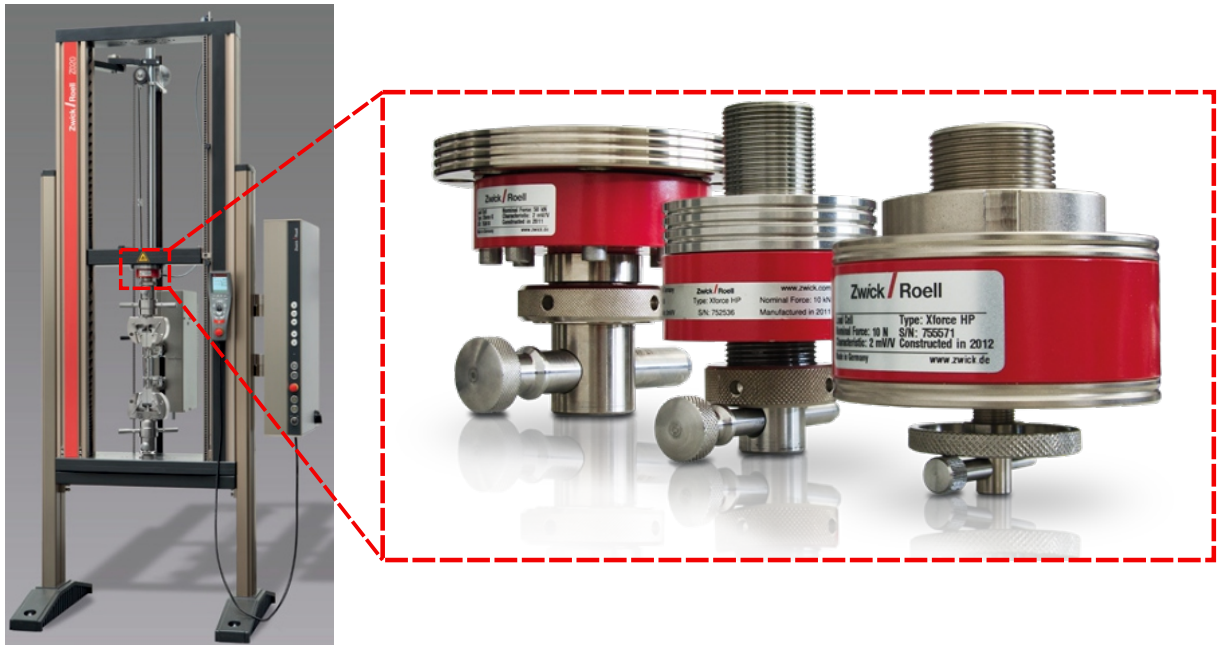
Figure 3.5: Tensile testing machine used to perform the T-peel tests and the load-cell attached to the machine to measure the peel force both from Zwick/Roell company [134]

supplier of testing machines for materials. Since the required force measurement range was in "mN" scale, a very sensitive load-cell had to be used. Therefore, from the Xforce HP models of the load-cells the one with the $5\,\mathrm{N}$ nominal force could Measure the intended range of peel force. The outcome of such load-cells are the the measured peel force in specific time steps vs. the displacement of the top clamp. Since the sensitivity of the load-cells are high, there is always some small range of fluctuations in the measured peel force values. These data can be represented as a graph which is showed in Fig. 3.6 with more details.

In fact, the measured peel force is the common output of such test. Figure. 3.6 shows the Idealized force vs opening diagram beside schematics of the films subjected to the vertical forces of the clamps. Since the fluctuations of peel force in measurements were caused because of load-cell sensitivity, they could be neglected and F_{peel} was determined as follows:

$$F_{\mathrm{peel}} = \frac{F_{0.2} + F_{0.8}}{2} \tag{3.1}$$

where $F_{0.2}$ and $F_{0.8}$ are force values corresponding to displacement values of $0.2 \times u$ and and $0.8 \times u$, respectively, u is the displacement of top clamp of the testing machine, and b is the width of the sample. Any median or average line corresponding the measured values are also valid. The important point to keep in mind is that peel force values corresponding to the beginning and ending parts of the peel test which behaves like a linear line with high slope, shouldn't be considered in the calculations. This measured F_{peel} is normally used to calculate the work of adhesion which can be computed for in-extensible or linear-elastic films based on the presented methods by Rivlin and Kendal respectively, which are explained in 2. However, the peel force measurement alone doesn't provide enough input data to evaluate the delamination procedure and analyze the behavior of adhesive systems. Therefore, the actual configuration of the films during peeling was needed for further evaluations and the measured peel forces were used at the final step to verify the calculation methods.
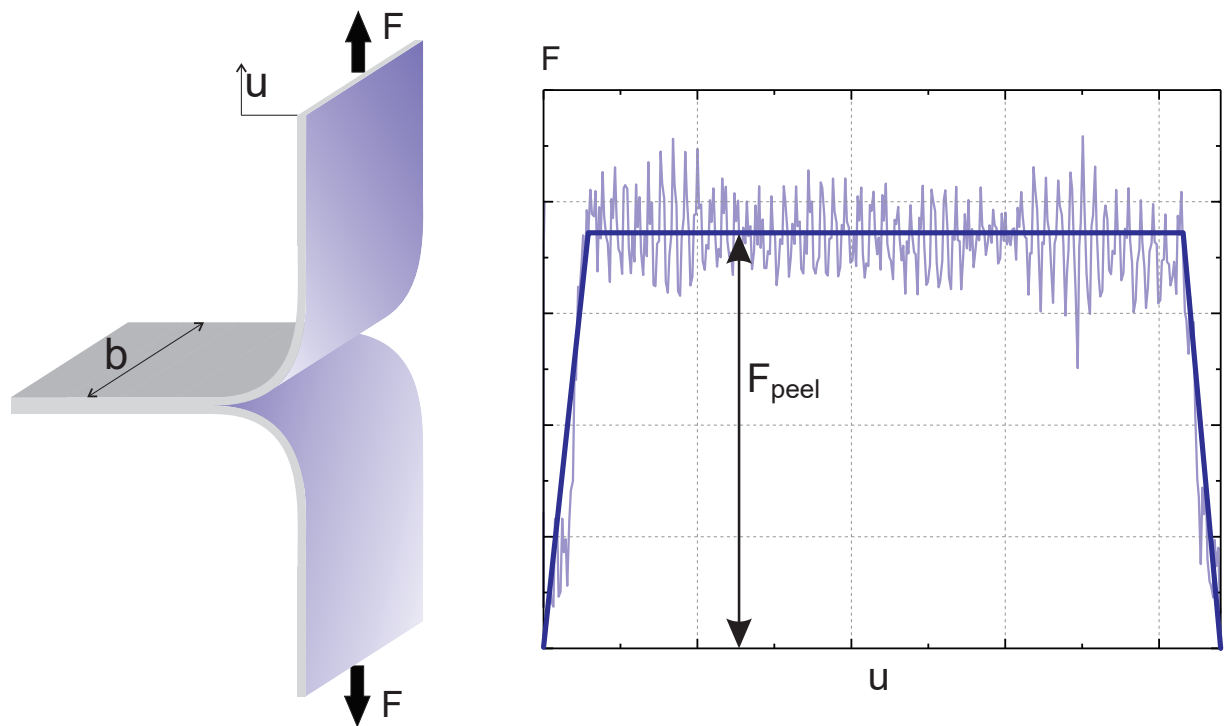
Figure 3.6: Schematic sketch of symmetric configuration of the sample during T-peel test (left); Idealized peel force as F vs. displacement of the top clamps as u diagram for peel force evaluation (right)

3.3 Procedure for Process of the Images

In the following chapters it will be fully explained that why the exact configuration of the films during the peel tests were essential to calculate their corresponding traction-separation curves. These configurations can be mathematically defined by estimating their Cartesian coordinates or the angles that define the actual orientation of the deformed films. To this end, the extracted images of the peel tests were processed based on the following procedures.

Vector line creation by B-spline technique in Coreldraw

Vector line inserted in Rhino and the corresponding identical NURBS rebuilded
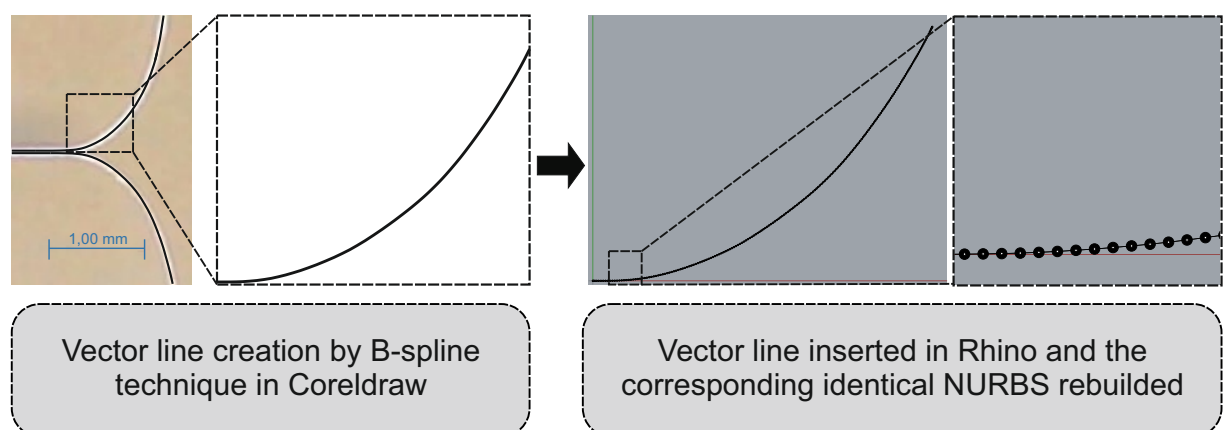
Figure 3.7: Digitization procedure of the film configuration: Vector line corresponding to the deformed film drawn in Coreldraw software (left); The line inserted in Rhino software environment to provide its identical NURBS and extract the illustrated control points (right)

In order to provide digital form of the film configuration from the pictures, a vector line was

drawn on the film deformation in CorelDraw software, using the B-spline technique as it is illustrated in the left part of the Fig. 3.7. Afterwards the vector line was inserted into Rhino software to build the NURBS (Non-uniform rational B-spline) identical to the vector line. Curve estimation method by NURBS has a complicated but accurate procedure, which is explained in detail in chapter 2. Right part of the Fig. 3.7 shows the mentioned rebuild NURBS corresponding to the vector line of deformed film, in Rhino software environment and if we take a closer look, its corresponding control points are visible. By building the NURBS in Rhino, the mathematical information about the line such as the knot vector, control points, order of the line, etc. can be extracted. The amount of these values are modifiable as wanted, but under consideration of some accuracy factors. For instance, the NURBS won't be accurately identical to the actual deformation if its order is too low, or the control points are too few. Going in the opposite direction is also not a good idea, over-increasing these factors do not always mean NURBS will match the original line better. They have to be in an optimum ratio that the consumed time for the further evaluations and calculations on the line be worthy of those factors increase amount. Because from a point forward increasing the control points, the order, or the knot vectors do not show significant effect on the NURBS matching accuracy, and it only increases the evaluation time consumption.

Now applying all the necessary mathematical operation of this study on NURBS is an unnecessarily complicated and time consuming work in our case. Furthermore, by transforming the NURBS to another data types that are insertable in the evaluation model of the following chapters, the evaluation duration is significantly decreased meanwhile the final results are still in the same accuracy level. The further calculations of the model are programmed in MATLAB software. As mentioned before, from this step forward the mathematical data corresponding to the deformed shape of the films can be used in different forms, such as by estimated polynomial equation, estimated exponential equation using Cartesian-coordinates or angles of the deformed line respectively as shown in schematic Fig. 3.10 and 3.8.
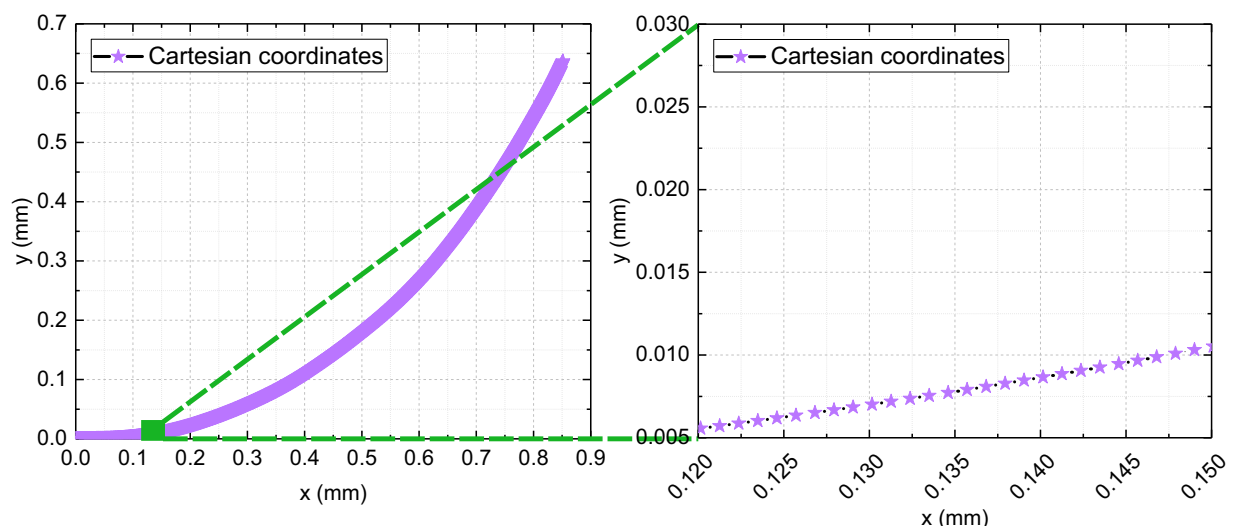
3.3.1 Numerical

Figure 3.8: Digitized data corresponding to the film configuration extracted as Cartesian-coordinates from the NURBS

As it is already mentioned to avoid all the unnecessary complications with the pure NURBS data calculations, they were evaluated in MATLAB to provide their corresponding digitized

data as Cartesian-coordinates. Extracted numerical values from BURBS as Cartesian-coordinates, were a quite accurate method in line digitization. Because infinite numbers of coordinates can be generated from NURBS. However, to use the numerical values shown in Fig. 3.8 as they were, all the further calculations of traction-separation curve identification had to be modified to numerical methods. Such as "Gaussian quadrature" for integration or "Complex Step Differentiation" needed to be involved to proceed the identification step. In the numerical methods, one can go deeply in to the details and increase the calculations accuracy as much as needed by increasing the numbers without any limits, but that doesn't always happen to be true. Since, increasing the numbers in numerical methods will generally bring out higher time consumption, or increase the errors too. These Cartesian coordinates corresponding to the film configuration were extracted from the NURBS in the numbers of 1, 10 and, 100 thousand points. Due to the presence of high order differentiation for identification of traction-separation curve in chapter 4 using the numerical methods were not the best choice.
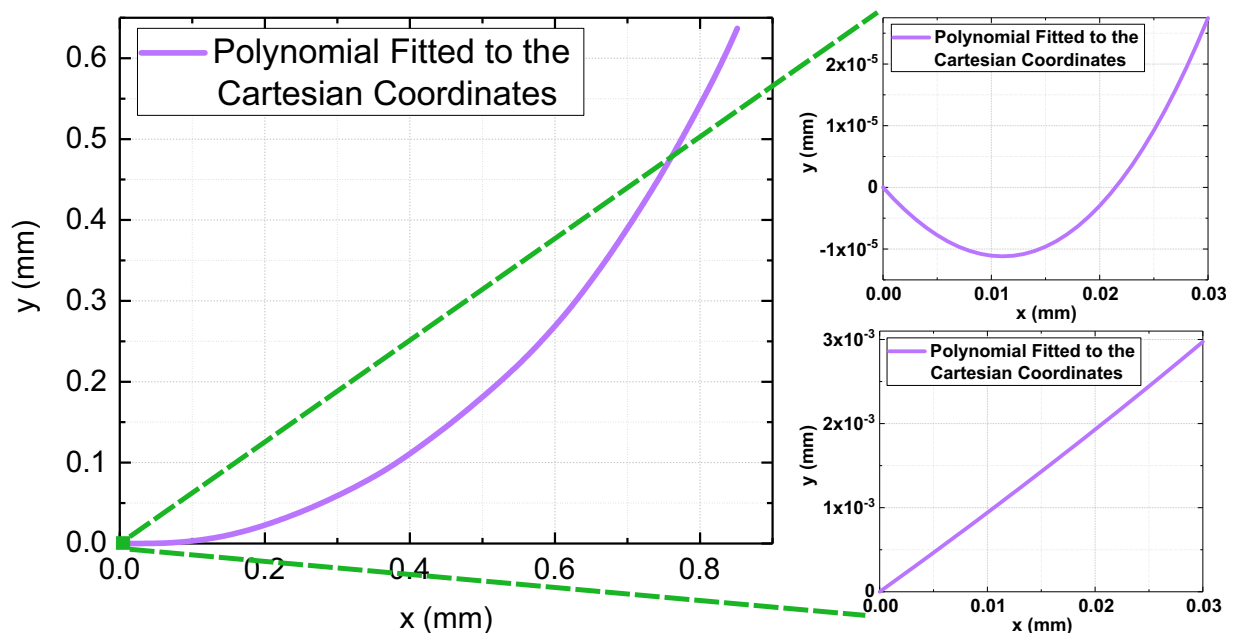
3.3.2 Polynomial

Figure 3.9: Polynomial fitted to the Cartesian-coordinates corresponding to the film configuration during T-peel test (left); Incorrect behavior of the fitted polynomial in delamination area (top right); Corrected fitted polynomial in delamination area (bottom right)

Another alternative to mathematically define the deformed shape of the film would be using the Cartesian-coordinates to estimate their corresponding polynomial equation. It is certain that all of these methods to define the line have small but in some cases neglect-able drawbacks in accuracy factor. The polynomial estimation of the film configuration method was not an exception either. For instance, it is not always possible to get a perfectly fitted polynomial equation. If we take a very close look at the beginning of the delamination area estimated by polynomials in Fig. 3.9 (left), it is mathematically possible that the approximated polynomial line shows such a behavior as Fig. 3.9 (top right). But from the physics point of view this behavior is practically wrong. Since the action of the experiment is to separate the

layers and the peel force is upward, so the "y" values shouldn't be decreasing in any stage of the experiment. However, this problem can be fairly solved by not using the automatic fitting commands of the softwares, instead finding the polynomial coefficients by the least-square method, where some conditions can be applied on the coefficients approximating procedure to prevent such problem as in Fig. 3.9 (top right) from happening. One simple condition in this direction is to add $dy/dx > 0$ to the fitting polynomial, this way the approximation will show such behavior as shown in Fig. 3.9 (bottom right). In addition, different orders of the polynomials were tested in [50] and it was proven that increasing the order doesn't necessarily lead to better accuracy and there is an optimum value for the order if using polynomials is chosen.

Hence, by taking the optimum value of the polynomial order into account, the best fitting polynomial equation to the lines were estimated. Eventually, based on the identification steps, the corresponding traction-separation curves with acceptable behavior could be calculated. They are both explained in detail in chapter 4.

3.3.3 Angles

The last but not the least, was another alternative procedure to describe the deformed centerline of the film which was the approximation of the deformed shape of the films based on the angles representing orientation of line as shown in Fig. 3.10. If we zoom in to the film configuration vector line it can be seen that φ represents the angle between the tangent of deformed line and the hypothetical x-axis. In this method of line description, the further calculations to identify the traction-separation curve needed to be modified. Therefore, an approximate analytical solution to the equations of the non-linear beam theory was derived and utilized to fit the deformation curves from experiments. However the main theory remains the same, unlike using a polynomial the calculations can't be followed based on x and y variables or Cartesian-coordinates. Although, in the first step, to provide the intended angles the Cartesian-coordinates corresponding to the line were needed.
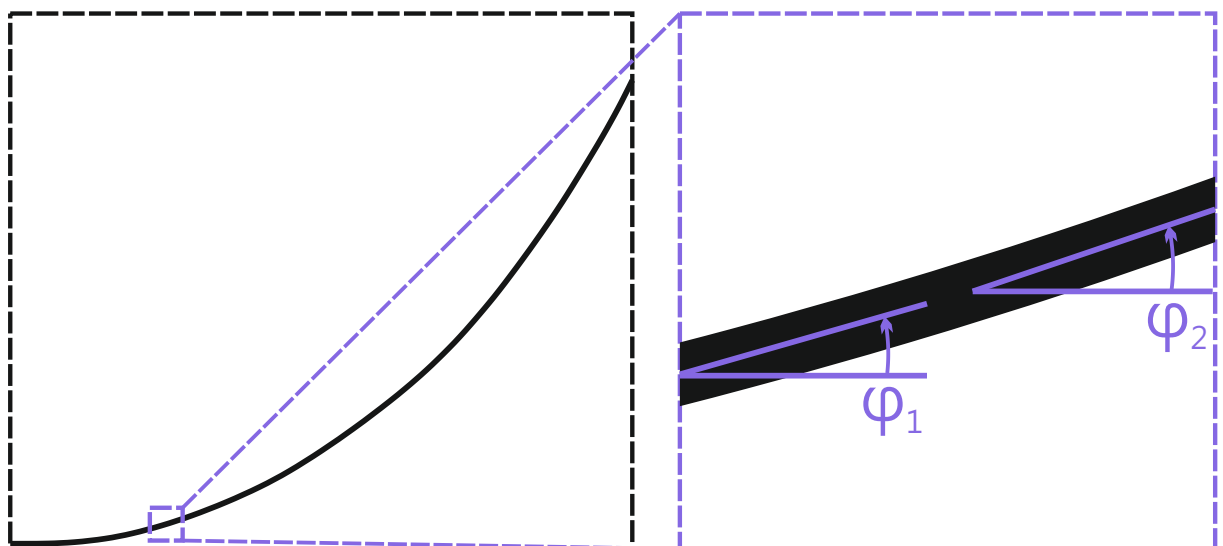
Figure 3.10: Angles of tangent to the line orientation defining the configuration the digitized vector line

The angles extracted from this step were used to estimate an exponential equation fitting the data in very close range of approximation and the intended delamination area. Then

the exponential equation could be inserted directly into the identification model to provide the traction-separation curves. In this model, which is explained with all the details in the following chapter, all the results are based on φ and as a function of y.

4 Identification

This identification chapter is primarily based on [50], where further information and details can be found. In the modeling methods that are related to traction-separation curves, normally they are planed as following. Regarding the subject of a study, experimental, and modeling procedure, a traction-separation law is chosen. Then based on the equations of that law the missing parameters of the study can be obtained. But in the case of this study the problem is solved in a reverse path which is the novelty about the provided model. Thus the traction-separation behavior of a self-adhesive polymeric films were identified from their deformation configuration during the T-peel test. Now, with the idea behind this method the traction-separation curves special for the wanted case can be generated by performing their related modifications on the model.

In this section the governing equations are presented to describe the equilibrium configurations of a thin flexible polyethylene film for the given forces F_{peel} and q. To this end the non-linear theory of beams [135–137] will be applied. Furthermore, the the energy integral is derived and classified as Eshelby-type conservation law [138]. Finally the traction separation curves are presented based on three different approaches of: direct approach, complementary energy approach and exponential approach.
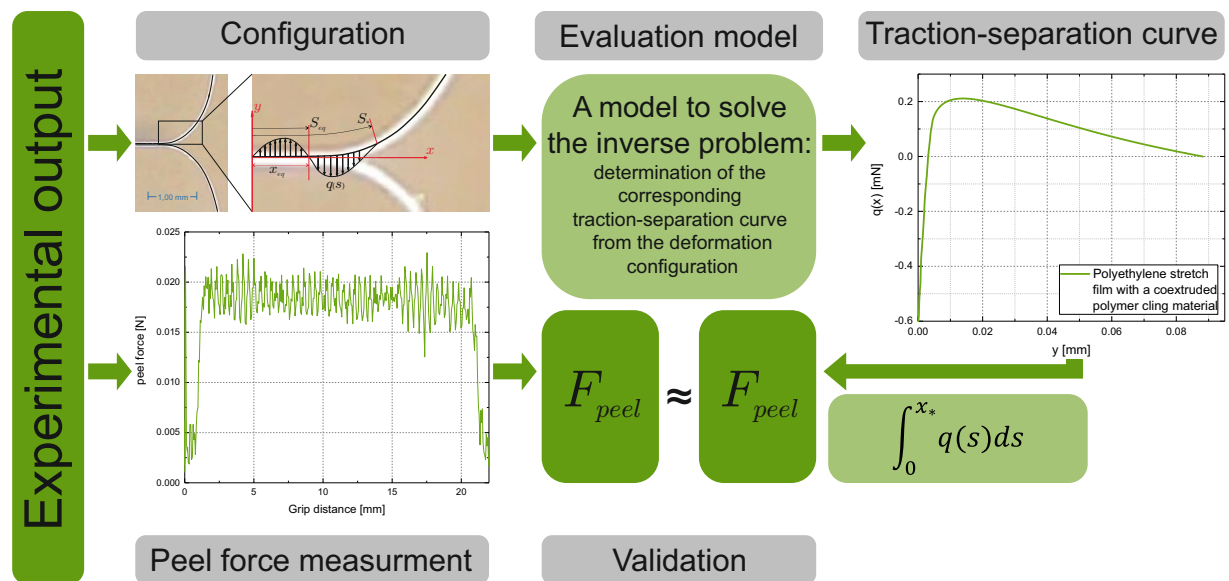
Figure 4.1: The procedure representing modeling traction-separation curves identification and model validation based on the identified and measured results comparison

Figure 4.1 represents an overview of the modeling procedure to identify the Intended traction-separation curve. This procedure takes the experimental outputs as an input in different directions until they are used, to be matched in the validation step. At first the digitized form of the film configurations during the peel test is taken into account to be inserted in to the identification model. The inverse model is run, using the film configuration data. The modeling output is the traction-separation curve corresponding to the inserted configuration. By an integration along the traction-separation curve with respect to the length of the curved

film, the peel force (F_{peel}) can be obtained. Now the second output of the experiments which is the measured peel force from the test is used to validate the calculated peel force. The validation step can be done either by peel force comparison or in the case of direct approach by the surface energy comparison, which is also related to the peel force values. The whole procedure will be explained in detail in further sections.

4.1 Non-linear Beam Theory
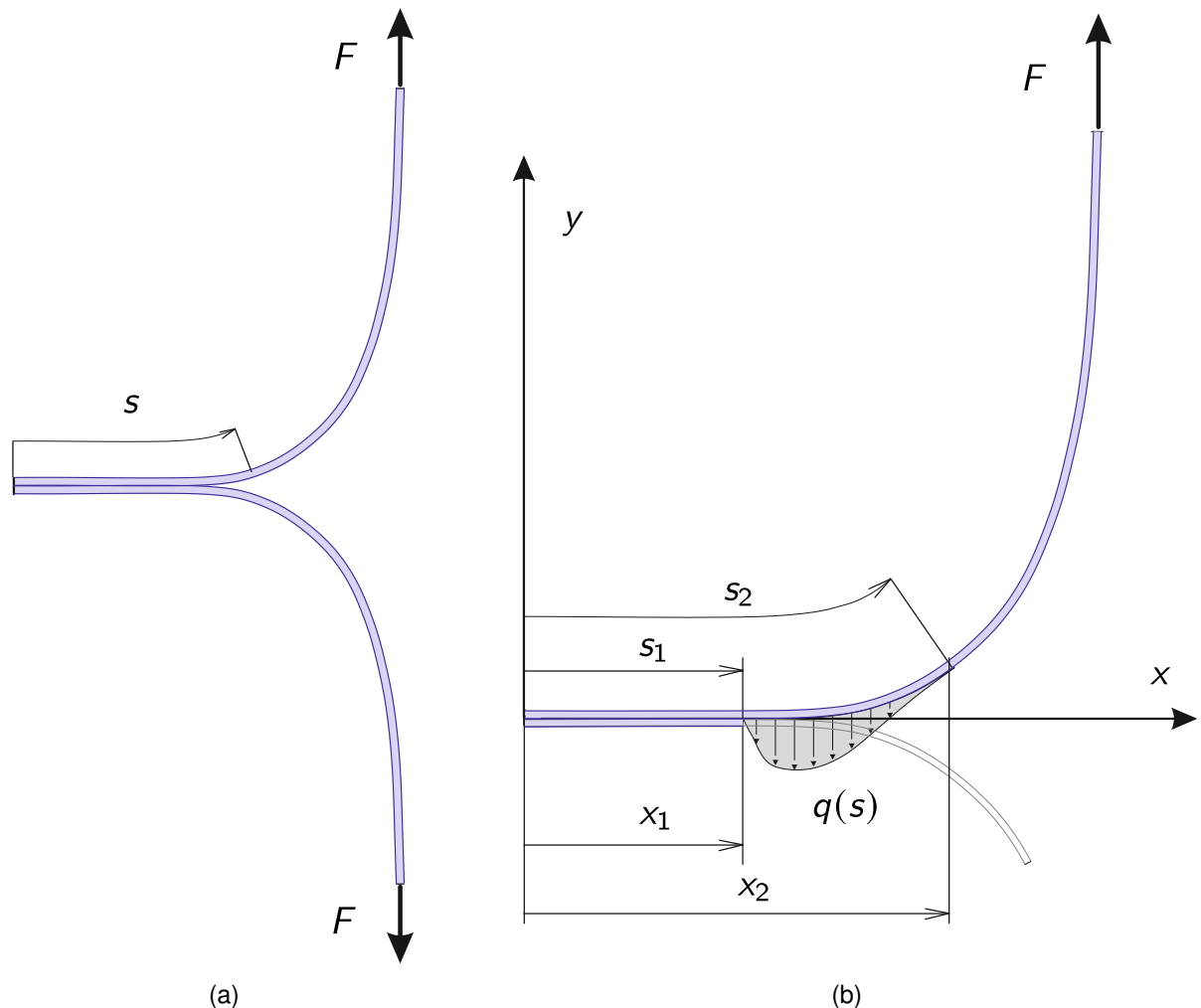
Figure 4.2: Schematics of deformed configuration of flexible films in a T-peel test [50]. (a) Loading and deformed shape of film, (b) force distribution within the zone of adhesive interaction $q(s)$, Arc-length parameter s and corresponding Cartesian coordinates

Figures 4.2(a) and 4.2(b) illustrate the schematics of two layers of flexible films subjected to T-peel loading and a distributed force q of adhesive interaction between two films respectively. The clamps of the tensile testing machine attached to the two ends of the films have vertical displacement during the T-peel test and both layers of the peeling films are from the same material. Hence, it can be realized that, the the deformed configuration of the of the films is symmetric. From the symmetry of the deformed configuration it is obvious that, the horizontal component of the interaction force is zero and only the vertical (peel) force has

to be considered for further identification steps. It means, under the assumption of slow quasi-static peeling the resultant force of q is in equilibrium with the applied peel force F.

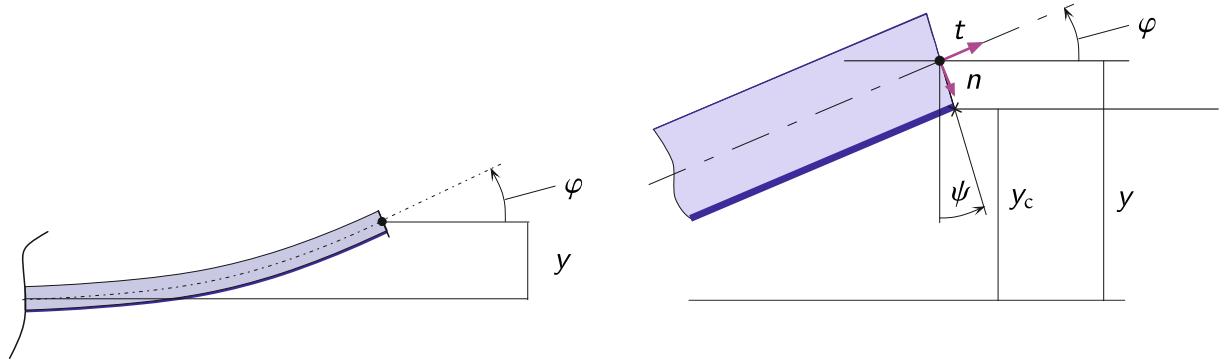### 4.1.1 Governing Equations for Thin Films in a T-peel Test

Figure 4.3: Basic kinematical characteristics in a schematic cross-section of film configuration with the coordinate

In the following equations s is the arc-length parameter in the deformed state characterizing positions of cross sections of the deformed film and $[x, y]$ represent the Cartesian coordinates corresponding to the mentioned configuration, Fig. 4.2.

$$x_c = x - \frac{h}{2}\sin\psi, \qquad y_c = y - \frac{h}{2}\cos\psi \qquad\qquad (4.1)$$

As illustrated in Fig. 4.3, the actual orientation of a cross section is described by the angle $\psi(s)$, while $\varphi(s)$ is the angle between the tangent to the deformed line and the x-axis. The tangent and the normal unit vectors to the deformed center-line are specified by **t** and **n**, respectively. For a cross section with $[x, y]$ coordinates and the rotation angle ψ, the lower point of the cling layer is defined by x_c and y_c coordinates as they are derived in the following relations of Eq. (4.1)

$$\frac{dy}{ds} = \sin\varphi, \qquad \frac{dx}{ds} = \cos\varphi, \qquad y' = \tan\varphi, \qquad (...)' = \frac{d(...)}{dx} \qquad (4.2)$$

Figure 4.4 (a and b) illustrates the schematic deformed configuration of the flexible film under T-peel test and the free body diagram for the zone of adhesive interaction respectively. In Fig. 4.4(a) the distributed interaction force q and the point B, where the interaction force takes zero value and changes the sign is also shown. The curvilinear coordinate of this point is specified by s_{eq} with the corresponding Cartesian coordinate of x_{eq} and y_{eq}. From the equilibrium conditions for the moments it follows, that the interaction force q must change the sign. Indeed, for the beam shown in Fig. 4.4(a) the equilibrium condition for the moment with A as the reference point yields

$$\int\limits_{s_{eq}}^{s_*} q_+(l-x)ds - \int\limits_{0}^{s_{eq}} q_-(l-x)ds = 0$$

where $s*$ represents the curvilinear coordinate of a point where q approaches to zero ($x*$ and $y*$ are the corresponding Cartesian coordinates). It is obvious that if q_- is zero, then the equilibrium condition is not satisfied.
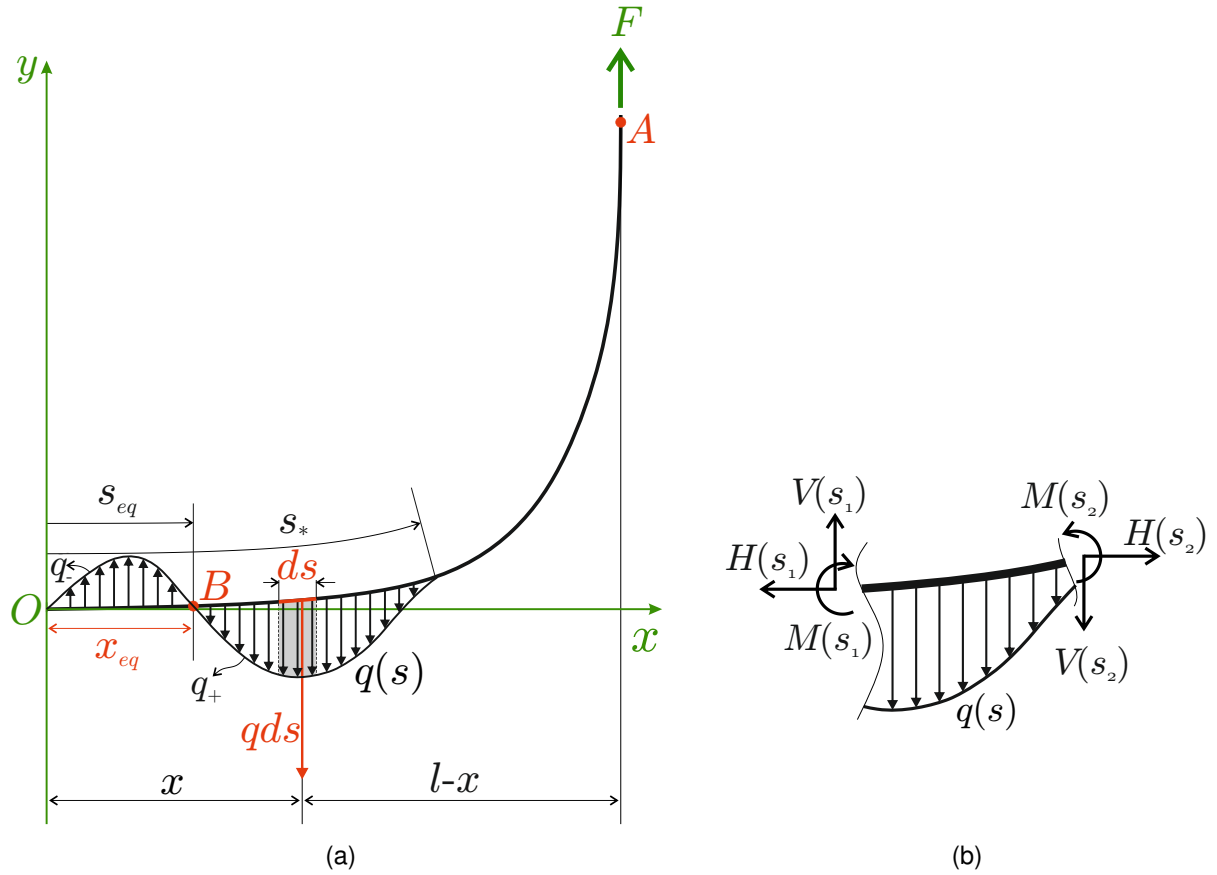
Figure 4.4: Free-body diagram inside the zone of adhesive interaction defining the parameters of governing equations for (a) the whole film (b) a part of the film with coordinates s_1 and s_2

Figure 4.4(b) illustrates a free-body diagram for a part of the thin film defined by the coordinates s_1 and s_2 within the zone of adhesive interaction. The mechanical interactions between the cross sections are characterized by the normal force N, the shear force Q and the bending moment M. With the balance of forces and moments for the line element with arbitrary coordinates s_1 and s_2 the following equilibrium conditions can be derived

$$\frac{\mathrm{d}H}{\mathrm{d}s} = 0, \qquad \frac{\mathrm{d}V}{\mathrm{d}s} = -q, \qquad \frac{\mathrm{d}M}{\mathrm{d}s} = Q + \frac{h}{2}q\sin\psi \qquad (4.3)$$

where H is the horizontal and V the vertical component of the force vector, respectively.

Integrating Eq. $(4.3)_1$ provides $H = const$, and the integration constant is zero since the force F is applied in the vertical direction. With $H = 0$ both the normal and the shear force can be related to the vertical force and the angle φ as follows:

$$N = -V \sin \varphi, \qquad Q = V \cos \varphi \tag{4.4}$$

For the forces and the bending moment the following constitutive equations can be formulated

$$N = \frac{\partial W}{\partial \lambda}, \qquad \lambda = \frac{\mathrm{d}s}{\mathrm{d}s_0},$$

$$M = \frac{\partial W}{\partial (\lambda \chi)}, \qquad \chi = \frac{\mathrm{d}\psi}{\mathrm{d}s},$$

$$Q = \frac{1}{\lambda} \frac{\partial W}{\partial \gamma}, \qquad \gamma = \psi - \varphi, \tag{4.5}$$

where W is the strain energy density per unit length of the undeformed film, $\mathrm{d}s_0$ is a line element in the reference state, λ is the local stretch, χ is the local curvature and, γ is the transverse shear strain. Specifying the strain energy density, Eqs. $(4.2) - (4.5)$ together with boundary conditions can be applied to find the deformed configuration of the rod for the given force F and the distributed force q. Vice versa, if y, λ, and ψ are given then one may find the distributed adhesive force q applying Eqs. $(4.2) - (4.5)$.

4.1.2 Energy Integral and Effective Work of Adhesion

For the interaction force q it can be assumed that a potential U_q exists such that

$$q = \frac{1}{\lambda} \frac{\mathrm{d}U_q}{\mathrm{d}y} \tag{4.6}$$

The strain energy density is a function of three arguments: λ, $\lambda\chi$, γ and, y. Taking the derivative of the strain energy density W with respect to the coordinate s and applying constitutive equations (4.5) it is obtained

$$\frac{\mathrm{d}W}{\mathrm{d}s} = N\frac{\mathrm{d}\lambda}{\mathrm{d}s} + \lambda Q\frac{\mathrm{d}\gamma}{\mathrm{d}s} + M\frac{\mathrm{d}(\lambda \chi)}{\mathrm{d}s} \tag{4.7}$$

With Eqs. $(4.3) - (4.5)$, Eq. (4.7) takes the following form

$$\frac{\mathrm{d}}{\mathrm{d}s}(W - M\chi\lambda) = -q\lambda\frac{\mathrm{d}y_c}{\mathrm{d}s} \tag{4.8}$$

Equation (4.8) is the conservation law for the non-linear beam theory. Within the tree-dimensional theory of elasticity similar Eshelby-type conservation laws are discussed in [138, 139]. By taking Eq. (4.6) into account, the following integral of Eq. (4.8) can be derived,

$$W + U_q - M\lambda\chi - N\lambda = C \tag{4.9}$$

where C is an integration constant. For inextensible films with $\lambda = 1$, Eq. (4.8) is known as the energy integral of Euler's elastica [136]. In [50] it is shown that, by analogy to the J-integral in fracture mechanics the quantity $\Gamma = M\lambda\chi + N\lambda - W$ provides the energy release rate for T-peeling of flexible films. For $s = l$ we observe that $\Gamma(l) = F\lambda(l) - W(l)$ and W depends only on the stretch $\lambda(l)$. Therefore, the following relationship between the peel force F_{peel} and the specific energy of adhesion Υ can be obtained [50].

$$F_{\text{peel}}\lambda_l - W(\lambda_l) = \Upsilon b, \qquad \lambda_l = \lambda(l), \tag{4.10}$$

Where b is the width of the film samples. The relationship (4.10) is derived in [140] based on the energy balance equation for flexible hyperelastic films. For an inextensible film the Rivlin's formula follows from Eq. (4.10)

$$F_{\text{peel}} = \Upsilon b \tag{4.11}$$

Assuming small elastic strain of the peel arm such that $\lambda_l = 1 + \varepsilon_l$, $\varepsilon_l \ll 1$ where ε_l is the engineering strain, and with the linear-elastic law $N = C_T\varepsilon_l$, where C_T is the tensile stiffness of the peel arm we obtain

$$W(l) = \frac{1}{2}F_{\text{peel}}\varepsilon_l = \frac{1}{2}\frac{F_{\text{peel}}^2}{C_T} \tag{4.12}$$

Equation (4.10) takes the form

$$F_{\text{peel}} + \frac{1}{2}\frac{F_{\text{peel}}^2}{C_T} = \Upsilon b \tag{4.13}$$

With $C_T = Ebh$, where E is the Young's modulus and h is the total thickness of the one layer film, Eq. (4.13) is the Kendall's relationship between the peel force and the effective work of adhesion [88].

4.1.3 Variational Principles

Taking the first variation of the strain energy density and applying constitutive Eqs.(4.5) it is obtained

$$\delta W = N\delta\lambda + \lambda Q\delta(\psi - \varphi) + M\delta(\lambda\chi) \tag{4.14}$$

With Eqs. (4.3)–(4.5) and (4.7), Eq. (4.14) can be transformed to

$$\delta(W + U_q) = \lambda\frac{\mathrm{d}}{\mathrm{d}s}(M\delta\psi - V\delta y) \tag{4.15}$$

Integration of Eq. (4.15) provides

$$\int_{s_1}^{s_2} \delta(W + U_q)\frac{1}{\lambda}\mathrm{d}s = \left[M\delta\psi - V\delta y\right]_{s_1}^{s_2} \tag{4.16}$$

where s_1 and $s_2 > s_1$ are arbitrary coordinates of the cross sections. The variational equation (4.16) includes the strain energy density and the potential of the distributed force q. With a direct variational method applied to Eq. (4.16) one may compute equilibrium configurations of the film for the given forces. Such a procedure would be efficient if the traction-separation law $q(y)$ is known a priori.

To analyze the inverse problem, let us introduce the complementary energy Ω by the Legendre transformation

$$\Omega = N\lambda + \lambda Q(\psi - \varphi) + M(\lambda\chi) - W \tag{4.17}$$

With Ω the following constitutive equations can be formulated:

$$\lambda = \frac{\partial\Omega}{\partial N}, \qquad \lambda(\psi - \varphi) = \frac{\partial\Omega}{(\partial\lambda Q)}, \qquad \lambda\chi = \frac{\partial\Omega}{\partial M} \tag{4.18}$$

Taking the first variation of Ω and applying Eqs. (4.3)–(4.5) it is obtained

$$\delta(\Omega + \lambda Q\varphi) = -y\delta(\lambda q) + \lambda\frac{\mathrm{d}}{\mathrm{d}s}(\psi\delta M - y\delta V) \tag{4.19}$$

The integration provides the following complementary energy type variational equation:

$$\int\limits_{s_1}^{s_2} [\delta(\Omega + \lambda Q \varphi) + y\delta(\lambda q)]\lambda^{-1}\mathrm{d}s = \left[\varphi\delta M - y\delta V\right]_{s_1}^{s_2} \tag{4.20}$$

4.2 Assumptions

In order to formulate the identification procedure let us simplify the initial constitutive Eqs. (4.2)–(4.5) applying the following assumptions:

- The deformed lines show that the thickness of the films is much less than the length of them within the zone of non-zero curvature. Furthermore, for the considered T-peeling samples we expect that the transverse shear deformation is negligible. Therefore, in this study we apply the shear-rigid model, by setting $\gamma = 0$ which results in $\psi = \varphi$.
- Based on the experimental data it is concluded that the axial strains of the peel arm are small such that $\lambda = 1 + \varepsilon$ and $\varepsilon \ll 1$.

By setting $\psi = \varphi$ and applying Eq. (4.2) the local curvature can be expressed as follows

$$\chi = \frac{\mathrm{d}\varphi}{\mathrm{d}s} = \frac{\mathrm{d}\varphi}{\mathrm{d}x}\cos\varphi = -\frac{y''}{(1 + y'^2)^{\frac{3}{2}}} \tag{4.21}$$

From Eqs. (4.3) and (4.4) the membrane force can be computed as

$$N = -M'\frac{y'}{(1 + y'^2)^{\frac{1}{2}}} \tag{4.22}$$

Assuming the linear-elastic response of the peel arm the bending moment is proportional to the curvature

$$M = \mathrm{B}\chi \tag{4.23}$$

where B is the bending stiffness Eqs. (4.21) and (4.22) yield

$$\frac{N}{\mathrm{B}} = \frac{y'}{(1 + y'^2)^3}[3y''^2 y' - y'''(1 + y'^2)] \tag{4.24}$$

4.2.1 Direct Approach

With the assumed small strain ε and the linear-elastic response of the peel arm, interacting force potential of U_q is obtained from Eq. (4.9) as the following

$$U_q = \frac{1}{2}B\chi^2 + N \qquad (4.25)$$

With Eqs. (4.21) and (4.24), Eq. (4.25) takes the following form:

$$\frac{U_q}{B} = \frac{1}{(1+y'^2)^3}\left[\frac{1}{2}y''^2 + 3y''^2y'^2 - y'''y'(1+y'^2)\right] \qquad (4.26)$$

Eq. (4.26) can be used to calculate the potential U_q of the adhesive force for the digitized configuration of the tested films $y(x)$. Since the approach based on Eq. (4.26) is achieved directly from the constitutive equations and the effective work of adhesion is related to the deformed shape of the film, it will be called direct approach (DA). The challenge with this approach is that in Eq. (4.25) three derivatives of $y(x)$ are required. Even though a relatively high quality images are used for digitizing the film configuration with vector lines, interpolation errors are unavoidable in mathematically defining the line and higher derivatives may be inaccurate leading to non-stable identification.
The force of adhesive interaction q can be evaluated as follows:

$$q(x) = \frac{U_q'}{y'} \qquad (4.27)$$

In this case, the fourth derivative of the function $y(x)$ is required, which would lead to loss of accuracy in evaluating q.
Despite the fact that, a high order of derivation of the deformed film configuration is included in evaluations, we still can expect qualitatively reasonable results if $y(x)$ is not too sensitive to derivatives. Furthermore, the accuracy level of the Direct Approach results can be checked by comparing the energy of adhesion calculated from two methods. First from the maximum value of the potential $U_{q\mathrm{max}}$ calculated in Eq. 4.25, which can be computed as follows:

$$Y = \frac{U_{q\mathrm{max}}}{b} \qquad (4.28)$$

And second from the Kendall formula mentioned in Eq. 4.13 by inserting the average value of measured peel force during the experiments, tensile stiffness and , the width of the tested samples in the following equation.

$$Y = \frac{F}{b} + \frac{1}{2}\frac{F^2}{C_T b} \qquad (4.29)$$

4.2.2 Complementary Energy Approach

As mentioned before, an alternative solution to avoid the high number of derivatives is the use of the Complementary Energy (CE) variational principle (4.20). With the assumption of shear rigidity and the small axial strain Eq. (4.24) can be simplified as follows:

$$\int_{s_1}^{s_2} \left[\delta \left(\frac{M^2}{2B} + Q\varphi + N \right) + y \delta q \right] ds = \left[\varphi \delta M - y \delta V \right]_{s_1}^{s_2} \tag{4.30}$$

Considering $y(x)$ and $y'(x)$ as the functions that describe the deformed film configurations and can be identified from experimental results, the variational Eq. (4.30) can be formulated as follows based on the mentioned assumptions:

$$\int_{x_1}^{x_2} \left[(1 + y'^2)^{\frac{1}{2}} \delta \left(\frac{M^2}{2B} \right) + (\tan^{-1} y' - y') \delta V + y(1 + y'^2)^{\frac{1}{2}} \delta q \right] dx = \left[\varphi \delta M - y \delta V \right]_{x_1}^{x_2} \tag{4.31}$$

According to Ritz Method for the bending moment M, the vertical force V and the adhesive force q the following polynomial series approximations are applied:

$$\frac{M(x)}{B} = \sum_{i=0}^{m} D_i x^{i+2},$$

$$\frac{V(x)}{B} = \sum_{i=0}^{m} D_i (i+2) x^{i+1},$$

$$\frac{q(x)}{B} (1 + y'^2)^{\frac{1}{2}} = -\sum_{i=0}^{m} D_i (i+2)(i+1) x^i \tag{4.32}$$

With Eq. (4.32) the equilibrium conditions of Eq. (4.3) are exactly satisfied. By inserting Eq. (4.32) into Eq. (4.31) and performing some transformations the following system of linear algebraic equations with respect to unknown coefficients D_k are obtained:

$$\sum_{k=0}^{m} R_{ik} D_k = f_i, \qquad i = 0, ..., m, \tag{4.33}$$

where

$$R_{ik} = \int_{x_1}^{x_2} (1 + y'^2)^{\frac{1}{2}} x^{i+2} x^{k+2} \mathrm{d}x$$

$$f_i = \int_{x_1}^{x_2} \left[(y' - \arctan y')(i+2)x^{i+1} + y(i+2)(i+1)x^i \right] \mathrm{d}x$$

$$+ \left[\arctan y' x^{i+2} - y(i+2)x^{i+1} \right]_{x_1}^{x_2} \tag{4.34}$$

To estimate the accuracy of the presented approach, the peel force can be determined from the distributed adhesive force $q(s)$ as follows

$$F = \int_0^{s_*} q(s) \mathrm{d}s \tag{4.35}$$

Where s_* is the curvilinear coordinate corresponding to the critical opening displacement. With $\mathrm{d}s = (1 + y'^2)^{\frac{1}{2}} \mathrm{d}x$ and Eq. (4.27) the peel force F_{peel} can be computed from the deformed film configuration.

$$F = \int_0^{x_*} (1 + y')^{\frac{1}{2}} q(x) \mathrm{d}x = -B \sum_{i=0}^{m} D_i (i+2) x_*^{i+1} \tag{4.36}$$

Now with Eq. 4.36 which is defined as a function of x the peel force corresponding the evaluated film configuration can be obtained to be compared with the measured one from the experiments.

The potential of the adhesive force distribution can be obtained with respect to Eq. 4.27, and therefore by applying the following formula

$$U_q(x) = \int_0^x q(\zeta) y'(\zeta) \mathrm{d}\zeta \tag{4.37}$$

4.2.3 Exponential Approach

The third option to obtain the traction-separation curves, is to change the defining method of film configurations. As mentioned earlier in this approach the deformed film configuration is defined by angle φ and exponential equations instead of approximating it polynomials.

Therefore, the further calculations should be modified to match the inserting data too.
An important feature of this approach is that it satisfies kinematic and static boundary conditions for the T-peeling. Furthermore, the obtained interaction forces satisfies equilibrium conditions. In order to formulate the robust identification procedure of exponential approach, Eqs (4.2)-(4.5) are simplified applying the assumptions mentioned in section 4.2. Therefore, by setting $\varphi = \psi$ and applying Eq. (4.2), the local curvature can be expressed as follows

$$\chi = \frac{\mathrm{d}\varphi}{\mathrm{d}s} = \frac{\mathrm{d}(\sin\varphi)}{\mathrm{d}x} = -\frac{\mathrm{d}\cos\varphi}{\mathrm{d}y} \qquad (4.38)$$

Assuming the linear-elastic response of the peel arm the bending moment is proportional to the curvature as in Eq. (4.23) and negligible transverse shear deformation, Eq. (4.9) yields

$$U_q - \frac{1}{2}M\chi - N = C \qquad (4.39)$$

Applying the boundary conditions $N = 0$, $M = 0$ and setting $U = 0$ for the left free edge of the film it is obtained $C = 0$, therefore

$$U_q = \frac{1}{2}M\chi + N \qquad (4.40)$$

Specifying $\Lambda = \cos\varphi$ the following expressions can be derived from Eqs. (4.2)-(4.6) and (4.23)

$$M = -\mathrm{B}\Lambda^\bullet, \qquad N = \mathrm{B}\frac{1-\Lambda^2}{\Lambda}\Lambda^{\bullet\bullet},$$

$$V = -\mathrm{B}\frac{\sqrt{1-\Lambda^2}}{\Lambda}\Lambda^{\bullet\bullet},$$

$$U_q = \mathrm{B}\left[\frac{1}{2}\Lambda^{\bullet 2} + \frac{1-\Lambda^2}{\Lambda}\Lambda^{\bullet\bullet}\right], \qquad (4.41)$$

where

$$(...)^\bullet = \frac{\mathrm{d}(...)}{\mathrm{d}y}$$

In order to compute the interaction force distribution $q(y)$ it is needed to approximate the function $\Lambda(y)$ from the deformed configuration of the beam centerline. High quality vector images of the deformed films and B-spline approximations provide both the deformed line $y(x)$ and its first derivative $y'(x)$ with satisfactory accuracy. However, the experimental curves generated from images usually have a scatter of the order of magnitude of the film

thickness. This leads to the loss of accuracy by computing the higher derivatives. As shown in [50], non-physical oscillations are observed for the curvature, if the deformed centerline is approximated by polynomials.

Another alternative procedure could be to approximate the deformed line based on the equations of the beam theory. However, closed-form solutions to Eqs (4.2)-(4.6) are only available for the geometrically-linear case (small strains and cross section rotations) and special types of the traction-separation laws, e.g. linear, triangular or piecewise linear laws [141, 142].

To derive a suitable approximation for the function $\Lambda(y)$ it is assumed that for a part of beam the interaction force is negligible. By setting $q = 0$, Eq. (4.3)$_2$ can be integrated providing $V = const$. With the boundary conditions for $s = l$ we obtain the vertical force $V = -F_{\text{peel}}$. The normal force is computed from Eq. (4.4)$_1$ as follows

$$N = F_{\text{peel}} \sin \varphi \tag{4.42}$$

For $q = 0$ the force potential takes the constant value $U_q = U_0$. The energy integral (4.40) takes the form

$$U_0 = \frac{1}{2} M \chi + F_{\text{peel}} \sin \varphi \tag{4.43}$$

With the boundary condition $M = 0$ for $s = l$ and $\varphi = \pi/2$ we obtain $U_0 = F_{\text{peel}}$. Taking into account Eq. (4.23) the energy integral (4.43) can be formulated as follows

$$\frac{1}{2} B \chi^2 = F_{\text{peel}}(1 - \sin \varphi) \tag{4.44}$$

Let us note that Eq. (4.44) is known as the energy integral of Euler's elastica, as mentioned in [136]. It can be used to compute the function Λ for a part of the film. Indeed from Eq. (4.44) it is obtained

$$\frac{1}{2} B \Lambda^{\bullet 2} = F_{\text{peel}}(1 - \sqrt{1 - \Lambda^2}) \tag{4.45}$$

Taking into account that Λ is a decreasing function it is obtained

$$\Lambda^\bullet = -\sqrt{2 \tilde{F}_{peel}}(1 - \sqrt{1 - \Lambda^2})^{1/2}, \qquad \tilde{F} = \frac{F_{\text{peel}}}{B} \tag{4.46}$$

By integration, the following relation between Λ and y is derived

$$\Psi(\Lambda) = \sqrt{2\tilde{F}_{\text{peel}}}(y - y_0), \qquad \Psi(\Lambda) = \int_{\Lambda_0}^{\Lambda} \frac{d\tilde{\xi}}{(1 - \sqrt{1 - \tilde{\xi}^2})^{1/2}}, \qquad \Lambda_0 = \cos\varphi_0 \qquad (4.47)$$

where y_0 and φ_0 are the opening and the corresponding angle of rotation for a point of the beam with the coordinate s_0. The integral in $\Psi(\Lambda)$ can be formulated in a closed analytical form in terms of elliptic functions. For the purpose of the identification, it is useful to approximate the solution (4.47) by the use of elementary functions. Indeed the solution (4.47) is only valid for a part of the beam where the interaction forces are negligible. For this part the angle of rotation is close to $\pi/2$ and we can assume $\Lambda^2 \ll \Lambda < 1$. In this case, the differential Eq. (4.47) takes the simplified form

$$\Lambda^\bullet = -\sqrt{\tilde{F}_{\text{peel}}}\Lambda, \qquad (4.48)$$

with the solution

$$\Lambda(y) = A\exp(-\alpha y), \qquad \alpha = \sqrt{\tilde{F}_{\text{peel}}} \qquad (4.49)$$

where A is the integration constant. The function (4.49) approximates the cross-sectional rotation only for a part of the beam and satisfies the boundary condition $N = F_{\text{peel}}$ for the top right edge. To improve the accuracy, the following two-terms of approximation are assumed

$$\Lambda(y) = A\exp(-\alpha y) + B\exp(-\beta y), \qquad \beta > \alpha \qquad (4.50)$$

Applying the boundary conditions for the left edge of the beam $\Lambda(0) = 1$ and $\Lambda^\bullet(0) = 0$ it is obtained

$$A = \frac{\beta}{\beta - \alpha}, \qquad B = \frac{\alpha}{\beta - \alpha} \qquad (4.51)$$

To find β the least-squares method can be applied.
As explained in section 3, for the identification the centerline of the film was digitized from a photograph inserting into Rhino® software. With the B-spline approximations of $y(x)$ the first derivative $y'(x)$ and the function (4.52) were evaluated numerically.

$$\cos\varphi = \frac{1}{\sqrt{1 + y'^2}} \qquad (4.52)$$

With the proposed functions $\Lambda(y)$ the distributed interaction force q can be now computed as follows

$$q = \mathrm{B}\left[-\frac{1}{\Lambda^2}\Lambda^{\bullet\bullet}\Lambda^{\bullet} + \frac{1-\Lambda^2}{\Lambda}\Lambda^{\bullet\bullet\bullet} \right] \tag{4.53}$$

Equation (4.53) provides q as a function of the separation y. In order to compute the force distribution along the arc-length parameter s, the function $s(y)$ is required. From Eq. (4.2)$_1$ the following differential equation is derived

$$s^{\bullet} = \frac{1}{\sin\varphi} = \frac{1}{\sqrt{1-\Lambda^2}} \tag{4.54}$$

After the integration it is obtained

$$s(y) = \int\limits_{0}^{y} \frac{\mathrm{d}\xi}{\sqrt{1-\Lambda^2(\xi)}}$$

The interaction forces identified with the exponential sum (4.49) satisfy the equilibrium conditions. Indeed the equilibrium condition for the forces can be formulated as follows

$$\int\limits_{0}^{l} q(s)\mathrm{d}s = F_{\mathrm{peel}} \tag{4.55}$$

With Eqs (4.3) and (4.41) we obtain

$$\int\limits_{0}^{l} q(s)\mathrm{d}s = -\int\limits_{0}^{l} \frac{\mathrm{d}V}{\mathrm{d}s}\mathrm{d}s = V(0) - V(l) = \mathrm{B}\frac{\sqrt{1-\Lambda^2}}{\Lambda}\Lambda^{\bullet\bullet}\Big|_{y=0}^{y=y_{\max}}$$

For $y = 0$ we have $\Lambda = 1$, while for $\beta y \gg 1$

$$\Lambda(y) = \frac{\beta}{\beta-\alpha}\exp(-\alpha y), \quad \Rightarrow \quad \frac{\Lambda^{\bullet\bullet}}{\Lambda} = \alpha^2 = \tilde{F}_{\mathrm{peel}}$$

Consequently for $y = y_{\max}$

$$\frac{\sqrt{1-\Lambda^2}}{\Lambda}\Lambda^{\bullet\bullet} = \tilde{F}_{\mathrm{peel}},$$

and Eq. (4.55) is satisfied. On the other hand taking the top right point of the beam as the reference point, the equilibrium condition for the moments takes the form

$$\int_0^l q(s)(x_l - x)\mathrm{d}s = F_{\mathrm{peel}}\frac{h}{2}, \tag{4.56}$$

where x_l is the x-coordinate of the right top point of the beam. With Eqs (4.3) and (4.41) and by integration by parts we obtain

$$\int_0^l q(s)(x_l - x)\mathrm{d}s = V(0)x_l - \int_0^{x_l} V\mathrm{d}x = V(0)x_l - M(x_l) + M(0) + \frac{h}{2}\int_0^{y_{\mathrm{max}}} q\mathrm{d}y$$

With $\mathrm{d}y_{\mathrm{c}} = (1 + \chi h/2)\mathrm{d}y \approx \mathrm{d}y$ and

$$\int_0^{y_{\mathrm{max}}} q\mathrm{d}y = \int_0^{y_{\mathrm{max}}} \frac{\mathrm{d}U_q}{\mathrm{d}y_{\mathrm{c}}}\mathrm{d}y \approx U_q(y_{\mathrm{max}}) - U_q(0) = F_{\mathrm{peel}}$$

we finally obtain

$$\int_0^l q(s)(x_l - x)\mathrm{d}s - F_{\mathrm{peel}}\frac{h}{2} = V(0)x_l - M(x_l) + M(0) \tag{4.57}$$

For the two-terms exponential sum (4.50) the boundary conditions $V(0) = 0$, $M(0) = 0$ and $M(y_{\mathrm{max}}) = 0$ are satisfied. Therefore the derived interaction force q satisfies the equilibrium condition (4.56).
Equations (4.49) and (4.50) are special cases of the exponential sum which can be applied to approximate a function $f(x)$ as follows

$$f(x) = \sum_{k=1}^n A_k \exp(\mu_k x) \tag{4.58}$$

Applications of exponential sums in various physics and engineering problems as well as algorithms to compute coefficients A_k and exponents μ_k are discussed in [143–145], among others. For the problem considered in this section, the two-terms sum (4.50) is applied and the adding of an additional exponential term does not lead to an improvement of approximation. Indeed, to identify constants in higher-order exponential terms photographs within the process zone of peeling with higher resolution are required. Furthermore, the applied shear-rigid beam theory may lead to inaccurate results as the length of the analyzed process zone becomes comparable with the film thickness.

5 Identification results and Non-Local Modeling

5.1 Results and Discussion

To have an overview of the procedures done so far: By performing the experiments and evaluating the film configuration pictures from transverse view, their corresponding digitized data of the deformed films was found in the form of polynomial or exponential equations. The polynomials were inserted into identification models of direct and complementary energy approaches explained in sections 4.2.1 and 4.2.2, and the angles into exponential approach form section 4.2.3. Eventually, the following results were provided from each Approach. In order to verify the main idea of the modeling and provide higher reliability, 125 pictures were evaluate with direct and complementary energy approaches. Although the results from these approaches were correct and satisfying, the accuracy is always better to be increased. Therefore, the exponential approach was taken into account. Now that the functionality of the main idea behind the modellings is proven with high statistical results and since it was a pretty time consuming procedure to evaluate all these pictures, for the exponential approach and the non-local model, explained in Chapter 6 only one picture was taken into account and its result was compared to the same one from CEA and EA receptively. The details are explained in the following sections.

5.1.1 Film Configuration

According to the digitized data corresponding the shape of the films during the peel tests such a graph as in Fig. 5.1 is provided. It should be mentioned that, from each polyethylene films 5 samples were tested and from each test 5 pictures were randomly chosen to be evaluated. It means 25 pictures of configuration per material were evaluated. Therefore, the final results are statistically reliable. Figure 5.1 illustrates the variations in the configuration of the films during the peel test for each material as the shaded areas and the lines represent their corresponding average deformation shape.

The variations in the graphs show that, the configurations were not constant neither during the peel test of the samples from the same material, nor during a single peel test. These configuration variations occurred the least and the most in samples $17/14$ and $12/17$ respectively. Additionally, the radius of deformed films during delamination (in the case of having the same cling material) has a direct relationship with the thickness of the films, which is reasonable regarding their bending stiffness. It means, as the thickness increases, the radius of curved shape of the film increases too. The sequence of these deformations satisfies the expectations, as their corresponding average line is changing with respect to the thickness variations from sample $12/14$ to $23/14$. However, a traction-separation curve is the property of the cling material and shouldn't be affected by the thickness variations.

In the case of films $12/17$ and $12/14$ it was expected to see approximately a similar configuration range during the delamination, since they had identical cling material and the
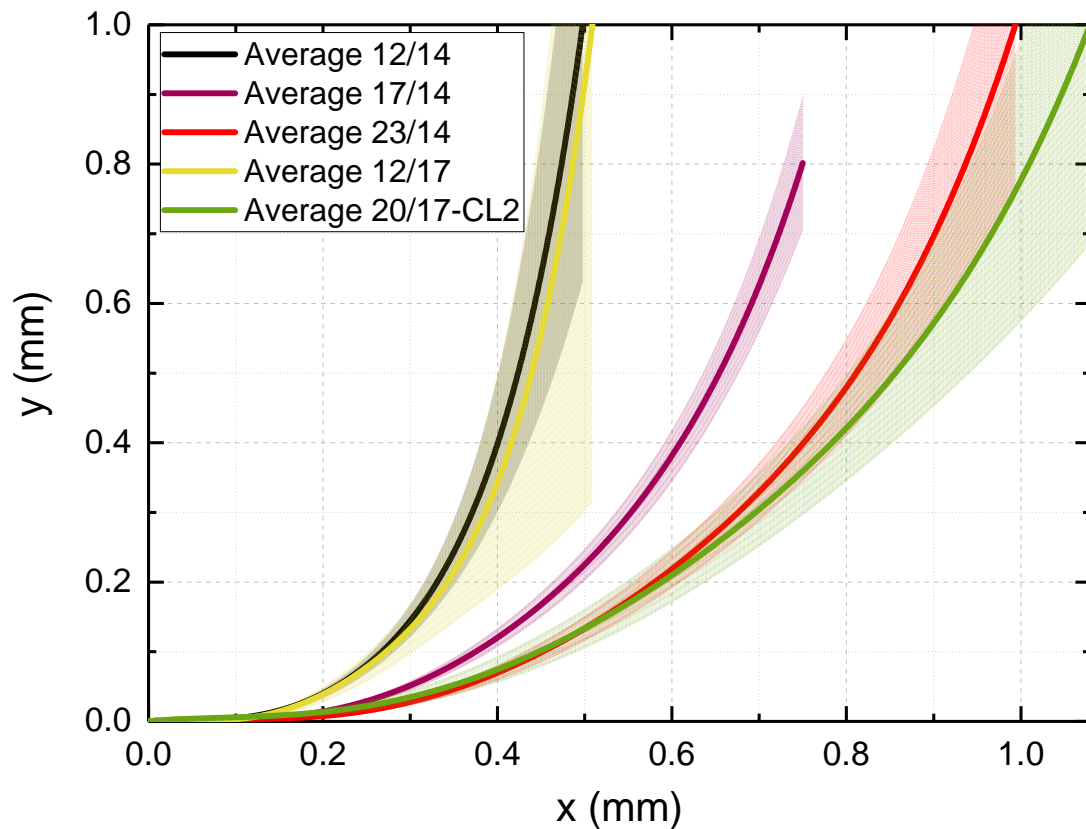
Figure 5.1: Digitized configuration of the films during the peel test, the line represents the average configuration of 25 picture frame extracted from the test videos; The light color range is the configuration variations of each sample

thickness of $12\mu m$ overall. But the experimental and evaluated data such as the average peel force values, delamination configurations, traction-separation behavior, etc. (which will be illustrated in the following pages) showed different results. Although their average configuration lines were pretty close to each other, the variation range in film $12/17$ was much higher than that of $12/14$. This wide range of configuration variation affected the final average results too. Hence, the different behavior of film $12/17$ were assumed as a result of manufacturing faults such as non-homogeneous cling layer co-extrusion. Because, even-though its configuration varied so much, the verification step of the model was still valid, the F_{peel} and surface energy values from both experiments and model were in a good accordance.

Film $20/17\,CL2$ was co-extruded with a cling material different from the other films. Therefore, the results relating this film, such as the configuration or its corresponding traction-separation behavior can not be compared with the others. But the final results of all the films were verified based on Eqs. (4.28, 4.29) and (4.33) for both Direct and Complementary Energy approaches respectively.

5.1.2 Direct Approach

To analyze the accuracy of the results, regarding the configuration approximation, different orders of polynomials defining the film configuration line, were compared by Nase et al., 2016 in [50]. To this end, different approximations with different number of terms in the polynomial series were generated applying the least-square method. The results in [50]

show that for $n > 4$, where n is the order of the approximated polynomial representing the film configuration, the increase of n has a negligible influence on the curve $y(x)$. However, the derivatives of y are sensitive with respect to the number of terms in the polynomial. Therefore, according to the results showed in [50] to avoid inaccuracy in applying the direct approach on polynomials, values of higher than 6 for n is not recommended.

According to Eq. (4.27) calculating the traction-separation curves based on direct approach, requires the fourth derivative of the film configurations during the peel tests. Beside all the possible errors in experimental and digitization procedures, when the fourth derivative of the configuration line is included in the calculations, providing error free results is clearly pretty challenging. Therefore, the accuracy expectations from the final results of this method is relatively low. So as long as the traction-separation curves of this approach can qualitatively match that of the complementary energy approach and the verification step of surface energy examining is valid based on Eqs (4.28) and (4.29), it can be claimed that the model produces satisfying results.

As it was mentioned earlier 25 pictures were evaluated for each film and therefore 25 distributed adhesive force q graphs as a function of x-coordinate were obtained for each polyethylene film by the direct approach. In Fig. 5.2 each line represents the average values of all q vs. x graphs, corresponding each film.

As it was expected, the maximum distributed adhesive force values q_{max} were similar and in a close range for the films with the same cling material, that means the first four samples showed in Fig. 5.2.

Of course because of the different configuration of the samples during the peel tests, if we consider they have similar traction-separation behavior, the corresponding x-coordinate at the same separation values y of the samples would be different as explained in the following. Figure 5.3 is extracted from Fig. 5.1. According to this figure, which is focused on the configuration lines of the films in the delamination area, it is clearly visible that for a specific amount of separation y, the corresponding value of x-coordinate increases as the films get thicker, from $12/14$ to $23/14$ (for the films with the same cling material). The vertical rectangles in Fig. 5.3 represent the variation in x-coordinate of each film corresponding to a specific amount of separation or in other words y (for instance for $y = 0.2$), which occurred during the peel tests.

As mentioned before, films $12/17$ and $17/14$ showed the highest and lowest x-coordinate variation range respectively. The last film ($20/17 - CL2$) is not considered in the comparison, because its co-extruded cling material was different. Therefore, its behavior can not be compared with the other films. Now by taking Fig. 5.3 into consideration and checking Fig. 5.2, it can be claimed that beside getting similar q_{max} values, the length of the lines on the x-axis increases in an expected sequence apart from film $12/17$. Thus, as the films get thicker the average distributed adhesive force gets longer with respect to x-axis. The results of film $12/17$ did show the similar traction-separation behavior as other samples with the same cling material in some single evaluations, but as it was also visible in Fig. 5.1 this film had a wide range of configuration variation. Therefore, many of the evaluated pictures didn't show the expected behavior, which leaded it's corresponding average Traction-Separation graph to be slightly different than the others.

If we omit the x-coordinate from the graph of Fig. 5.2 and represent the average distributed adhesive force q vs. y-coordinates, the graph called traction-separation curve is achieved. The average traction-separation curves which were identified by DA method are illustrated in Fig. 5.4. In the films with 14% of cling material co-extrusion, the average q_{max} values varied slightly from 0.2 mN to 0.3 mN. As mentioned earlier this modeling method requires the forth derivative of the film configuration line which highly affects the tr-sp curves accuracy.
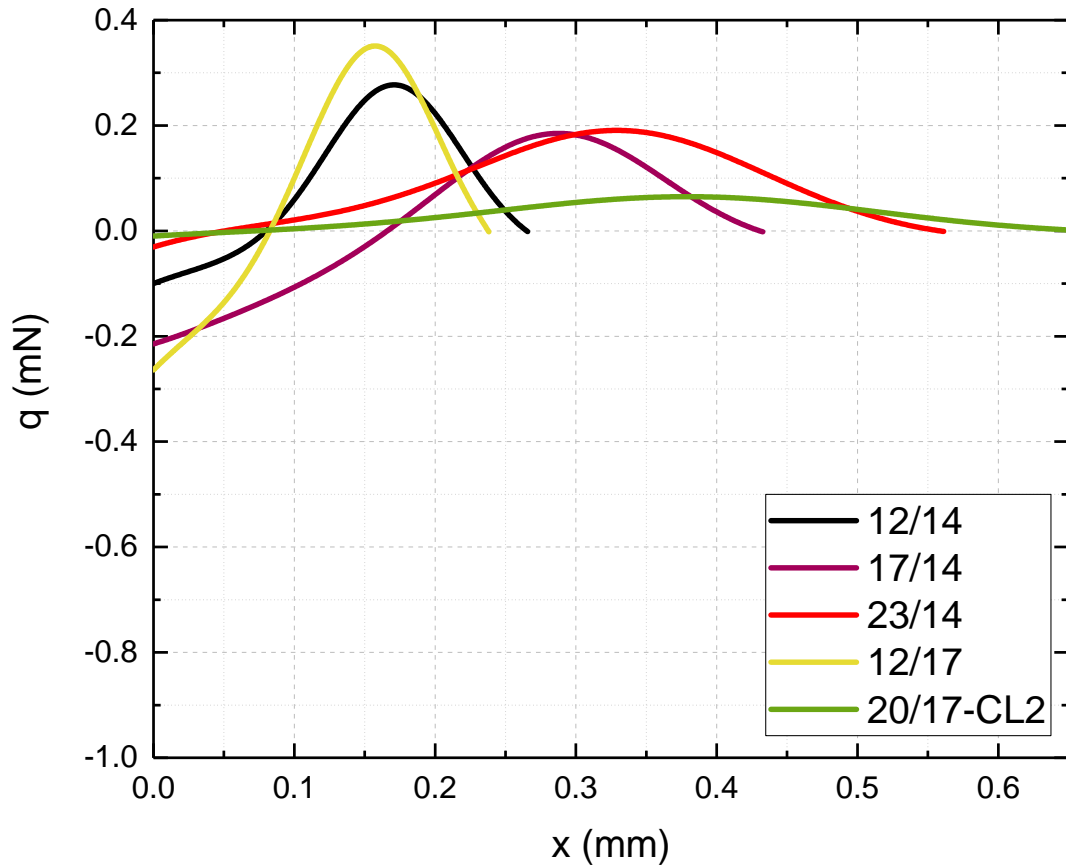
Figure 5.2: Average distributed adhesive force q of each sample as a functions of x-coordinate, identified by direct approach
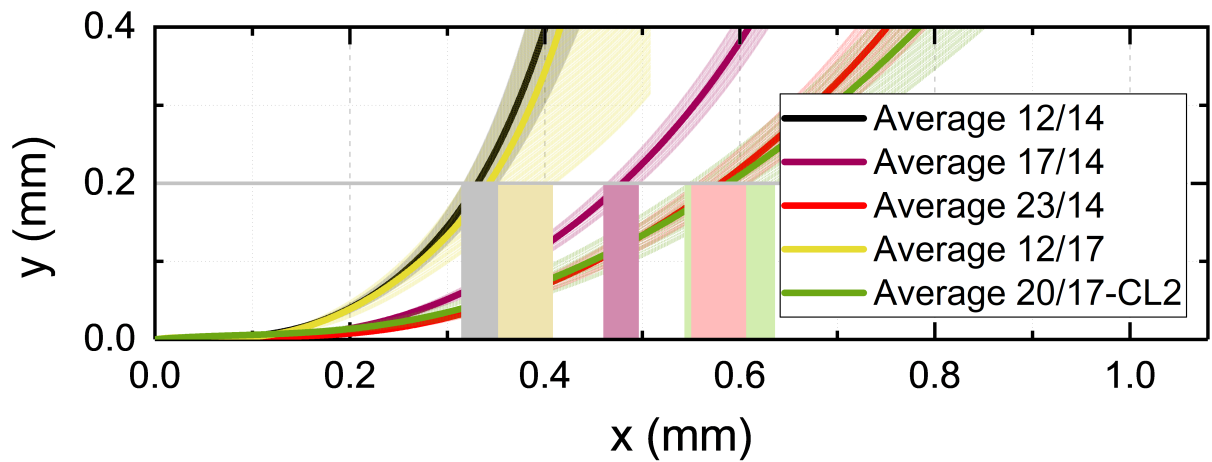

Figure 5.3: Average distributed adhesive force q of each sample vs. y coordinates identified by DA, which is known as traction–separation curves

However, the results are still in a good match with each other and showed pretty similar behavior specially the curves from film $17/14$ and $23/14$. Apart from the physical reasons which might have been affecting the configuration variations and therefore tr-sp curves on film $12/17$, digitizing both samples with 12μm thickness was a difficult procedure. Because of their sharp curvature in the configurations, providing a perfectly fitting polynomial equation to them was not the only challenge. In order to get such a sharp bending polynomial which also matches the other circumstances, the polynomial coefficients were calculated in a
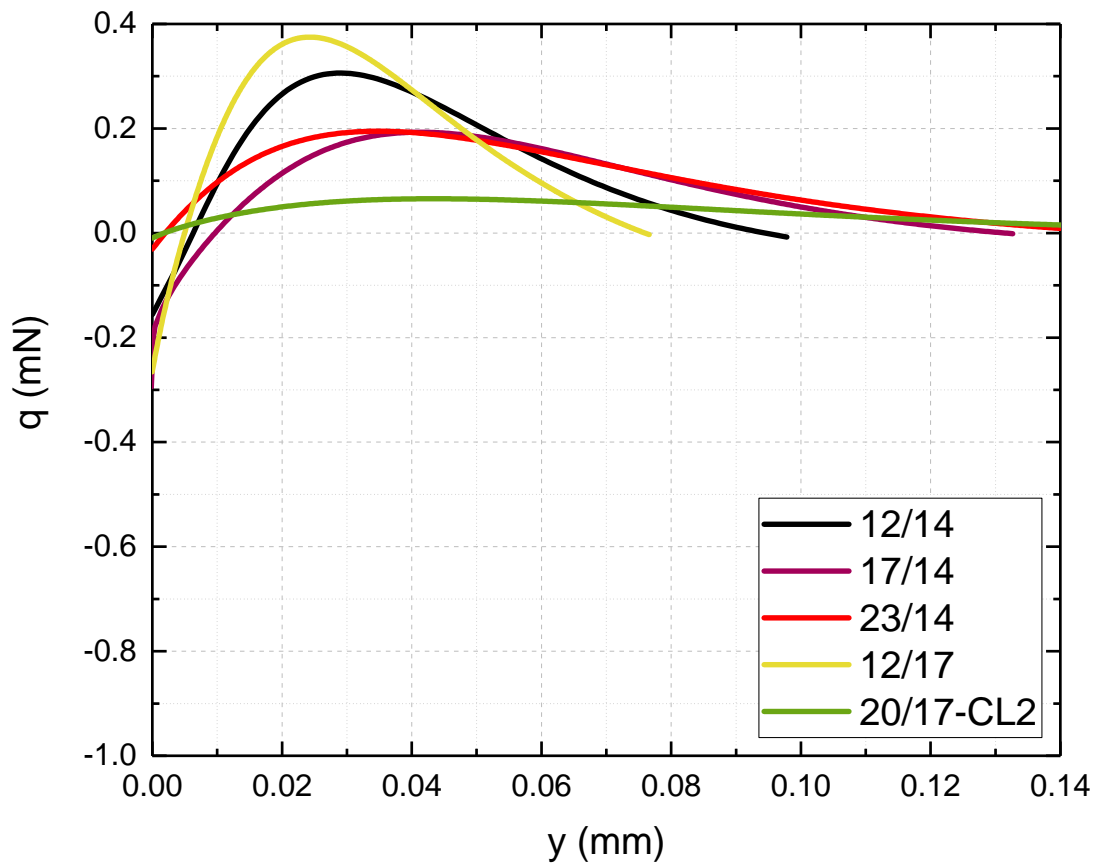
Figure 5.4: Average distributed adhesive force q of each sample vs. y coordinates identified by Direct Approach (DA), which is known as traction–separation curves

significantly higher range of value (not lower than three digits numbers) in comparison to the other samples. Although the polynomials could match the vector lines with a high accuracy but because of the high value coefficients they were more sensitive to derivations than the polynomials fitting sample $17/14$ and $23/14$. Hence, that was considered as one of the reasons why the tr-sp curves of samples $12/14$ and $12/17$ showed slightly different behavior than the others.

Once more, it is not expected that sample $20/17 - CL2$ shows the same tr-sp behavior as the others (because of its different cling material). But anyway this sample has also shown a perfectly reasonable behavior.

Figure 5.5 represents box charts containing Maximum values of the distributed adhesive force q_{max}, separation values in the equilibrium position y_{eq}, and in the critical opening displacement position y_*. As explained in section 4.1.1, the equilibrium and critical opening displacement positions are the points in which the distributed adhesive force q is zero before and after achieving to q_{max} point respectively. Clearly in the concept of exponential traction-separation curves the traction values do not become zero after reaching the maximum value as they behave like an exponential function. But here we took a point as a limit that if the distributed adhesive force value goes lower than that limit it is considered as zero and vanishes or in other word the critical opening displacement point.

Each of the diamonds illustrated in Fig. 5.5 is for representing the corresponding calculated value to a film configuration picture. As it is shown, the boxes of q_{max} values for samples with the same cling material (the firs four samples) are approximately in a similar range of distribution which is a perfectly reasonable behavior. Except in sample $12/17$ that had some
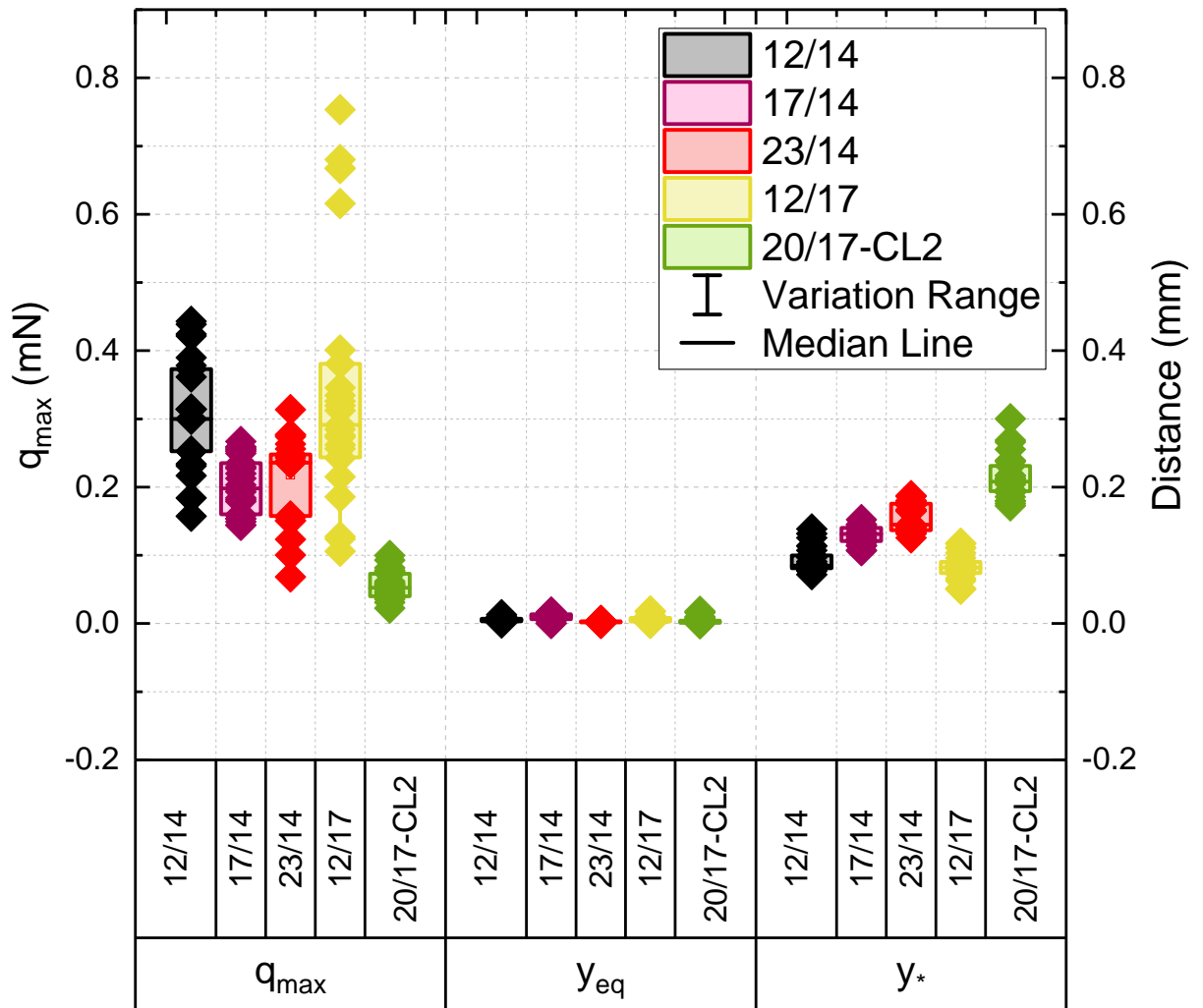
Figure 5.5: Comparison of q_{max}, y_{eq}, and y_* values, obtained from 25 evaluated pictures per sample, based on Direct Approach (DA)

q_{max} values significantly further from the median range. Such a separate results of some pictures that are the reason of different tr-sp behavior in this sample. One of the interesting information that can be taken out from this graph is by taking another look at Fig. 5.1 and comparing the distribution range of q_{max} values with the film configuration variations. They show a direct relationship, as the film configuration variations is wider, the q_{max} values are distributed in a wider range too.

As it is illustrated in Fig. 5.5, values of y_{eq} are quite similar. They even seem to behave regardless of the change of cling material in samples. But of course it is not the case, since y_{eq} parameter deals with pretty small values in comparison to the others, variations of it are also not so wide and visible as the others.

As the last parameter compared in Fig. 5.5, y_* values for each sample, which also represent the maximum separation, are not so distributed as q_{max}, but are not as dense as y_{eq} either. According to the box charts, again y_* values for the samples of $12/14$ to $12/17$ showed approximately the same range which was expected. Although, the variation range of sample $17/14$ is slightly smaller than the others. It is believed that, this is also related to the configuration distribution range from Fig. 5.1.

As mentioned earlier, according to different type of cling material co-extruded in sample $20/17 - CL2$ it can be clearly seen that, the calculated values for both q_{max} and y_* are in a

close range. But the variation range in these two parameters of this sample is not matching that of the other samples, which was also expected and reasonable behavior.

The last step in a modelling procedure, which also reveals the model value, is the result verification. That means to claim the functionality of theoretical model, the model results should be in accordance with the experimental ones. This way, it can be checked that the model works for actual experimental data or not.

Figure 5.6 illustrates two sets of box charts, showing differently calculated surface energy values of each sample side by side. In order to verify the results obtained from direct approach, these values were compared to each other. The black boxes represent the surface energy values for linear-elastic films calculated by Kendall Equation of (4.29). This equation uses the measured peel force values F_{peel} to get the surface energy of each sample. Therefore, the output values are related to the experimental data that includes five samples per PE film type that were peeled by the tensile testing machine. Five measured F_{peel} values provided five surface energy per PE film type.
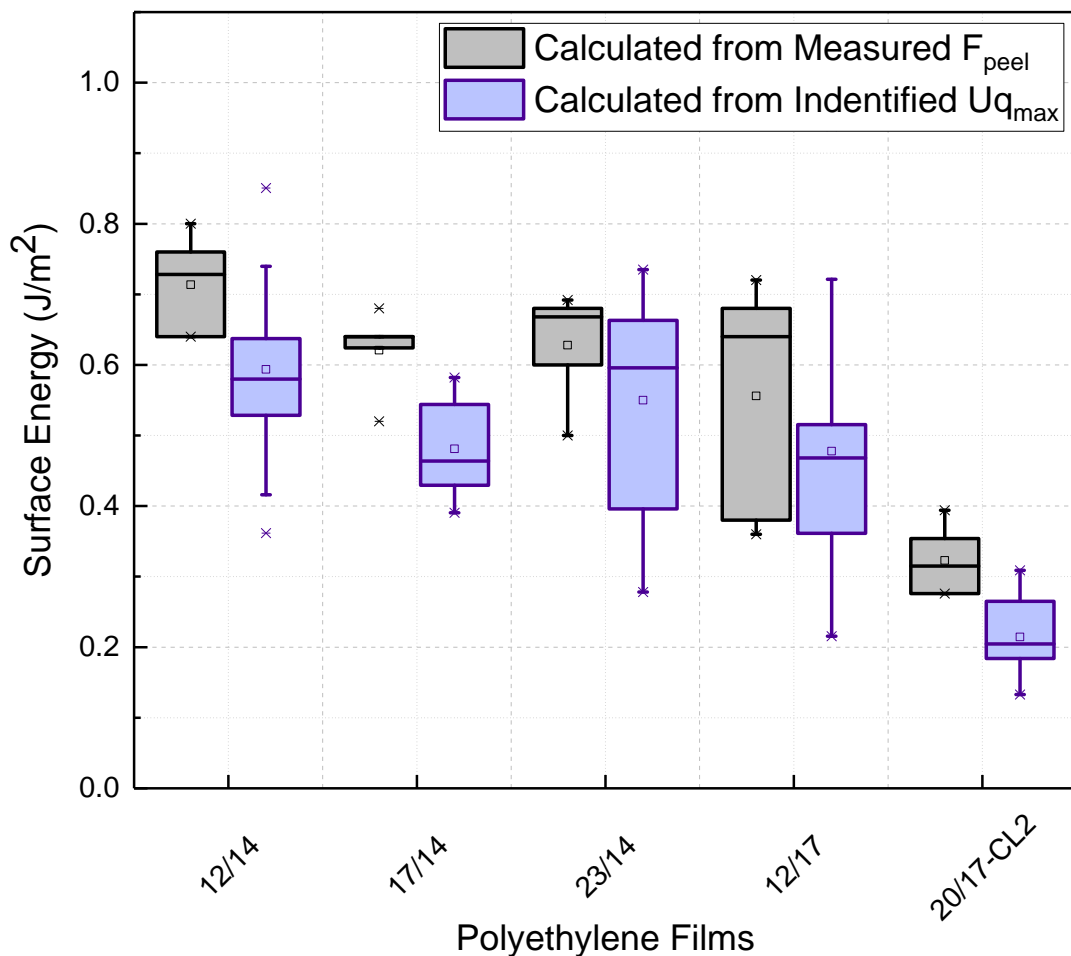

Figure 5.6: Surface energy comparison obtained directly from measured peel force values by Kendall equation of (4.29), and from the potential of maximum identified distributed adhesive force $U_{q_{\text{max}}}$ based on Eq. (4.28) to verify Direct Approach

The blue boxes in Fig. 5.6 represent surface energy values obtained from the maximum value of the potential $U_{q_{\text{max}}}$ identified by Direct Approach. The potential was calculated for each evaluated film configuration picture by Eq. (4.26). By inserting the maximum value of the potential in Eq. (4.28) the surface energy values were obtained this time from the model.

Unlike the surface energy values showed by the black boxes these blue boxes contained 25 calculated values per each PE film type. Because 25 pictures were evaluated for each PE film type.

Despite all the sensitivities and inaccuracy factors of the direct approach the final values of surface energy calculated by both methods are in a good accordance. Apart from matching values of surface energy in each PE film, these values are in a similar range for all the films with the same cling material which was expected because of having the same surface properties. Once again the distribution in the black box values is in a direct relation with the film configuration variation, as the least and most distributed values belong to films $17/14$ and $12/17$ respectively. This relation is quite reasonable, because if the configuration of a film during the peel test varies widely, it means the force which is required to separate the layers F_{peel} changes widely too. Additionally, the basic input for Kendall Equation of (4.29) was F_{peel} which transfers the changes to the surface energy values. But another fact in this case is that, generally high fluctuations in measured F_{peel} values can be the result of non-homogeneous surface co-extrusions of cling material, which is believed to be the case of film $12/17$.

The horizontal line in middle of each box represents the median of all values in that box. The median of calculated surface energies from both methods are also in a close range for each PE film type. For instance, the identified values, which means the blue box, in film $23/14$ showed higher distribution than its values of the back box, but the concentration of both values (median) are pretty close to each other. Additionally, there is something that all films have in common about the median line, that is, the median line in all blue boxes have slightly lower value than that of the black boxes, which is considered as a result of inaccuracies of DA identification method.

Film $20/17 - CL2$ is not being compared to the other ones. But since its corresponding surface energy values obtained from both methods are in close range to each other too, it can be realized that, in spite of all the mentioned drawbacks, the DA method worked properly and provided reasonable results in the case of all these PE films.

5.1.3 Complementary Energy Approach

In this section the traction-separation curves from the complementary energy approach are presented. Same as the results from DA, 25 pictures of film configurations per material were evaluated based on this approach (CEA) and again each line in the following graphs represents the average line of 25 evaluated tr-sp curves. As it was mentioned, the film configurations as an input of DA and CEA models, were all defined by polynomial series with the power of $n = 5$. According to Eqs (4.33) and (4.34) CEA method includes only the first derivative of the film configuration $y'(x)$ which makes this method less sensitive to slight fluctuations of film configuration. Therefore, more accurate and stable results are expected from this approach.

Figure 5.7 illustrates the average lines for the distributed adhesive force q of each PE film as a function of x-coordinates. If we compare this graph with the same one from DA (Fig. 5.2), we can see that the lines are qualitatively in the same sequence and range of values. For instance, average q_{max} value for films with the same cling material (all films except $20/17 - CL2$) calculated by both methods of DA and CEA varies between 0.2 to 0.3 mN approximately. However, in Fig. 5.7 the variation range of q_{max} among the same films is much lower than that of in DA and satisfies the expectations better, which means CEA results are more accurate. Moreover, this method is not as sensitive to the sharp bending configurations
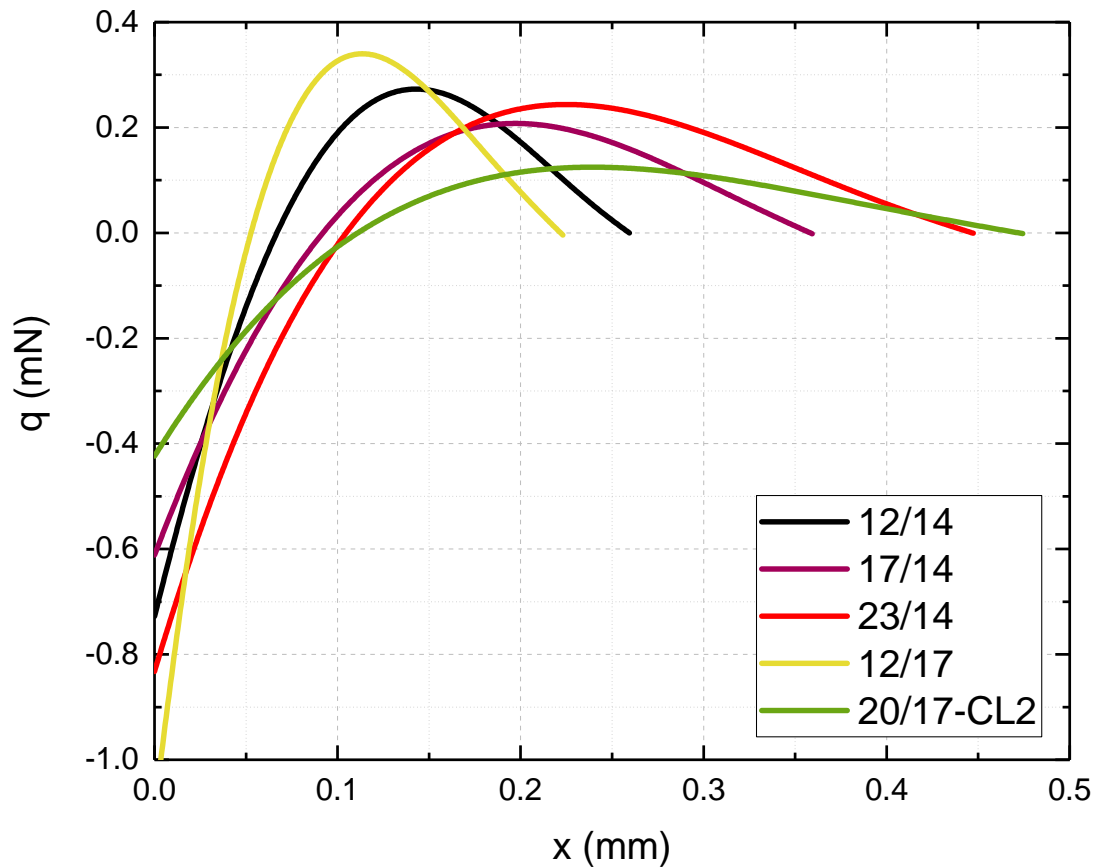
Figure 5.7: Average distributed adhesive force q of each PE film as a functions of x-coordinate, identified by Complementary Energy Approach (CE)

of films $12/14$ and $12/17$ as DA. According to CEA results film $12/17$ still shows slightly different behavior though. Which again leads us to idea of having manufacturing fault of in-homogeneity in the cling layer co-extrusion. Because both models have run multiple times on each film configuration to be statistically reliable and have provided the expected results for all films, except for film $12/17$. This only concludes the existence of a physical problem by this film.

Once more, the sequential x^* values of the films are pretty reasonable considering the similar separation values and their corresponding x-coordinate based on Fig. 5.3.

Although there was no other films with the same cling material as in film $20/17 - CL2$ to be compared to each other, the results from both approaches can be taken into account. It can be seen that, the curve corresponding to this film in Fig. 5.7 is also in a good accordance with the same one calculated by DA.

The average traction-separation curves identified by CEA is illustrated in Fig. 5.8. The first three films show a perfectly matching behavior as it is expected because of having the same cling material. They have similar values in all factors of q_{max}, y_{eq} and y^*. Since these factors have such close values on average lines, their individual values and variation ranges must be pretty close too.

The different behavior is still observable in case of film $12/17$. In the individual curves of some evaluated pictures of this film, similarity to the other curves were observed in both DA and CEA. But the problem is the wide variation range of the results by this film and it was decided from the beginning to keep all the results involved in the average line. Therefore,the not matching curves can't be omitted or otherwise the results cant be statistically reliable
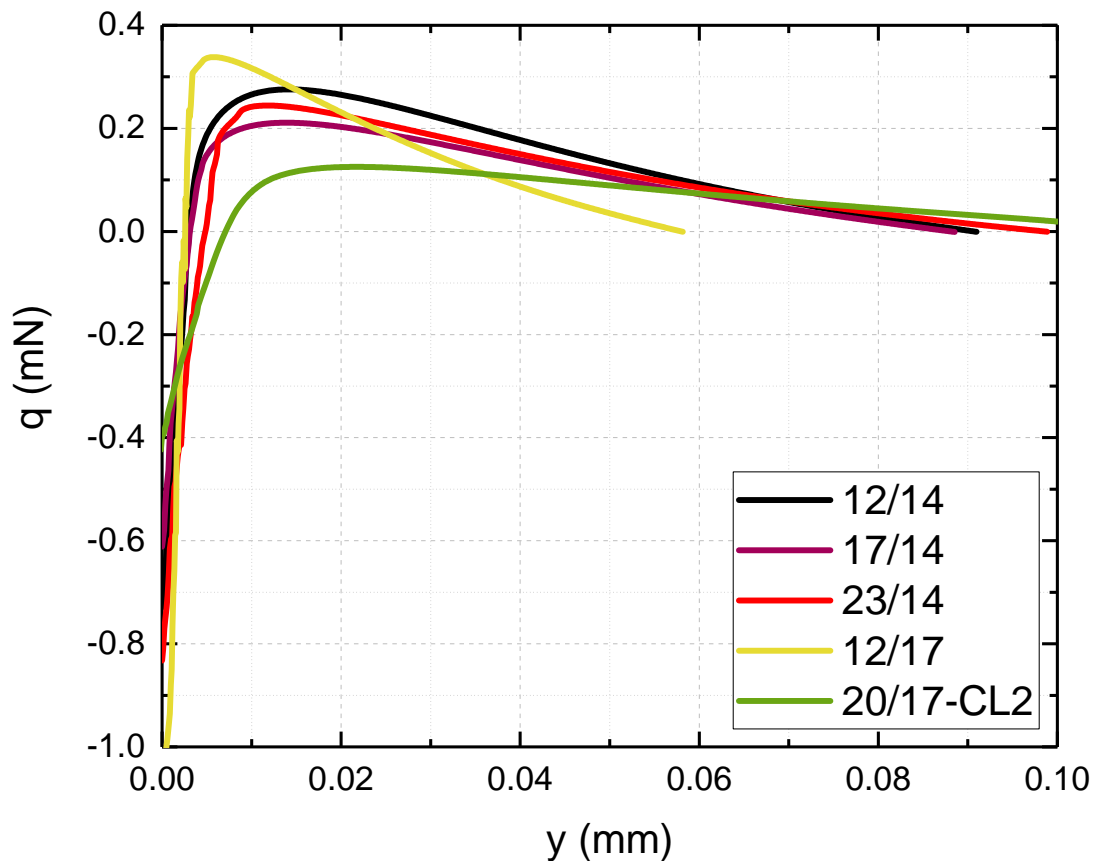
Figure 5.8: Average distributed adhesive force q of each sample vs. y coordinates identified by Complementary Energy Approach (CEA), which is known as traction–separation curves

anymore. Furthermore, The corresponding curves of the other three films ($12/14$, $17/14$ and $23/14$) are matching also in the average form and they don't vary from one sample to another that much.

The average tr-sp curve of film $20/17 - CL2$ in Fig. 5.8 has a similar behavior to the same curve from DA, which is illustrated in Fig. 5.4. Although slight differences are visible between them, their variation ranges of all the evaluated results were not so wide and different.

According to the values illustrated in Fig. 5.9 , the factors of q_{max}, y_{eq}, and y_* are compared once more for CEA results. The first three films of $12/14$, $17/14$ and $23/14$ have perfectly matching values and range of variations in all factors and satisfied the expectations. The less sensitivity of CEA method to the sharp bendings of the film $12/14$ configuration made it possible for the curves of this film to match the others, and provided the better results.

As explained earlier the tr-sp curves of film $12/17$ show similar behavior to the others in some individual configuration cases, this is also visible on Fig. 5.9. For instance, q_{max} values are spread pretty widely from 0.1 to 0.6 mN approximately for film $12/17$, while this factor varies for the other three films from 0.15 to 0.35 mN approximately. This gives us the variation range of q_{max} for film $12/17$ more than two times higher than the others.

On Fig. 5.9 it can be seen that, some of these values are exactly in the range of matching the others, but the majority and therefore the median line is much higher. More over, the same situation is observable for y_* too. The majority of the y_* values are below the average of the other films, which brings the median line lower than average of others and makes the average distributed area of the force q significantly lower than the others for film $12/17$.
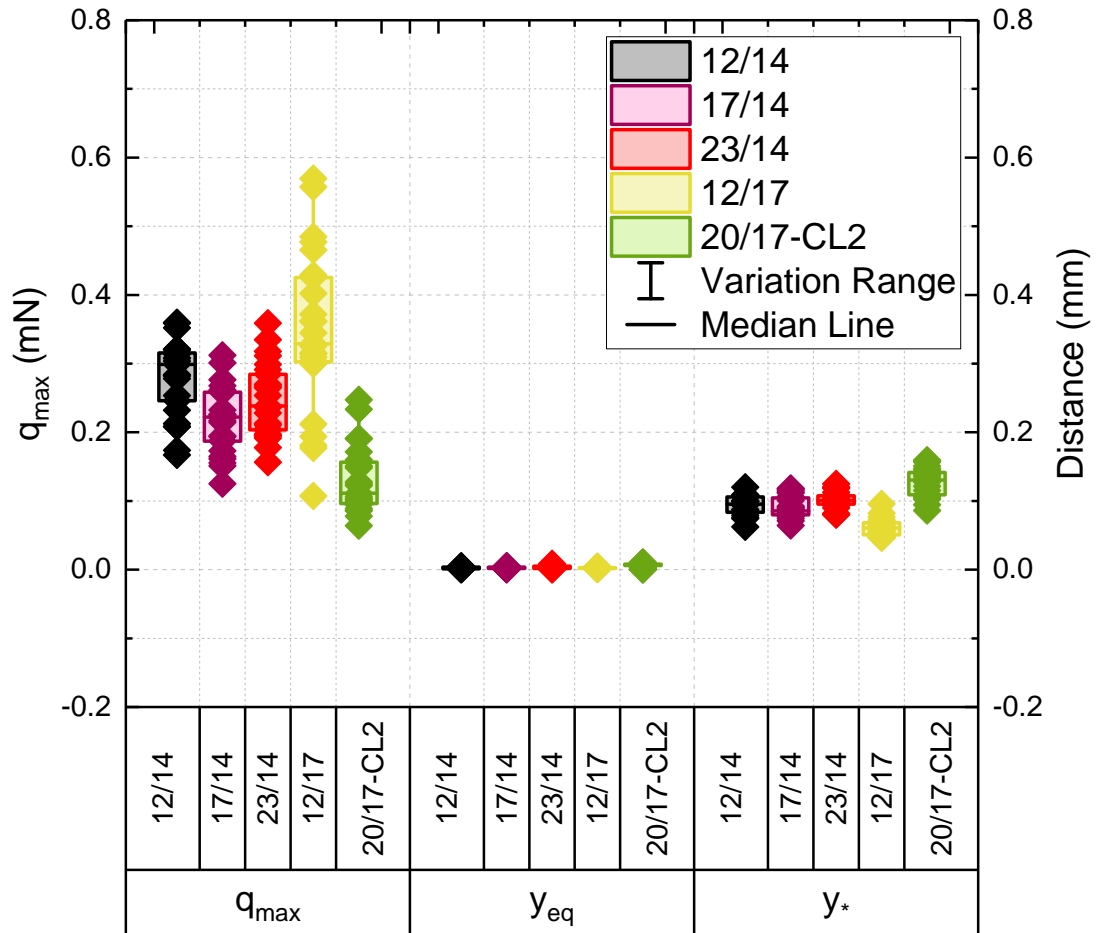
Figure 5.9: Comparison of q_{max}, y_{eq}, and y_* values, obtained from 25 evaluated pictures per sample, based on Complementary Energy Approach (CE)

The calculated values for film $20/17 - CL2$ from CEA and DA which are presented in Figs 5.9 and 5.5 respectively, are also in a good accordance with each other. Despite seeing some minor differences in distribution ranges of q_{max} and y_* factors, their corresponding median lines have very close values.

Now that tr-sp results are provided successfully based on CEA and they show satisfying behavior, it is time to perform the last step of method validation. In addition to the fact that CEA results could match that of the DA, their accuracy is checked by the comparison of peel force values in Fig. 5.10. There are two sets of box charts illustrated in Fig 5.10, the black ones represent the directly measured peel force values from the experiments of peel tests, which were 5 values per film type, and the red ones that are the values calculated from the identified distributed adhesive force q by CEA based on Eq. (4.36), which were 25 values per film type (according to the 25 evaluated film configuration pictures of each film).

According to the illustrated box charts of Fig. 5.10 both of the measured and calculated values of F_{peel} are in a good accordance to each other. By taking a look at every peel force value of each material individually which are illustrated in the red and black boxes it can be seen that, all films show matching values and they have some areas of variation ranges in common. However, we take the concentration of values (the median line) in to consideration. The comparison of the median lines of black an red boxes for each film provides us with the maximum and minimum amount of differences between them, which is approximately 3.5 and 0.5 mN respectively. These differences of the median lines might seem high in the
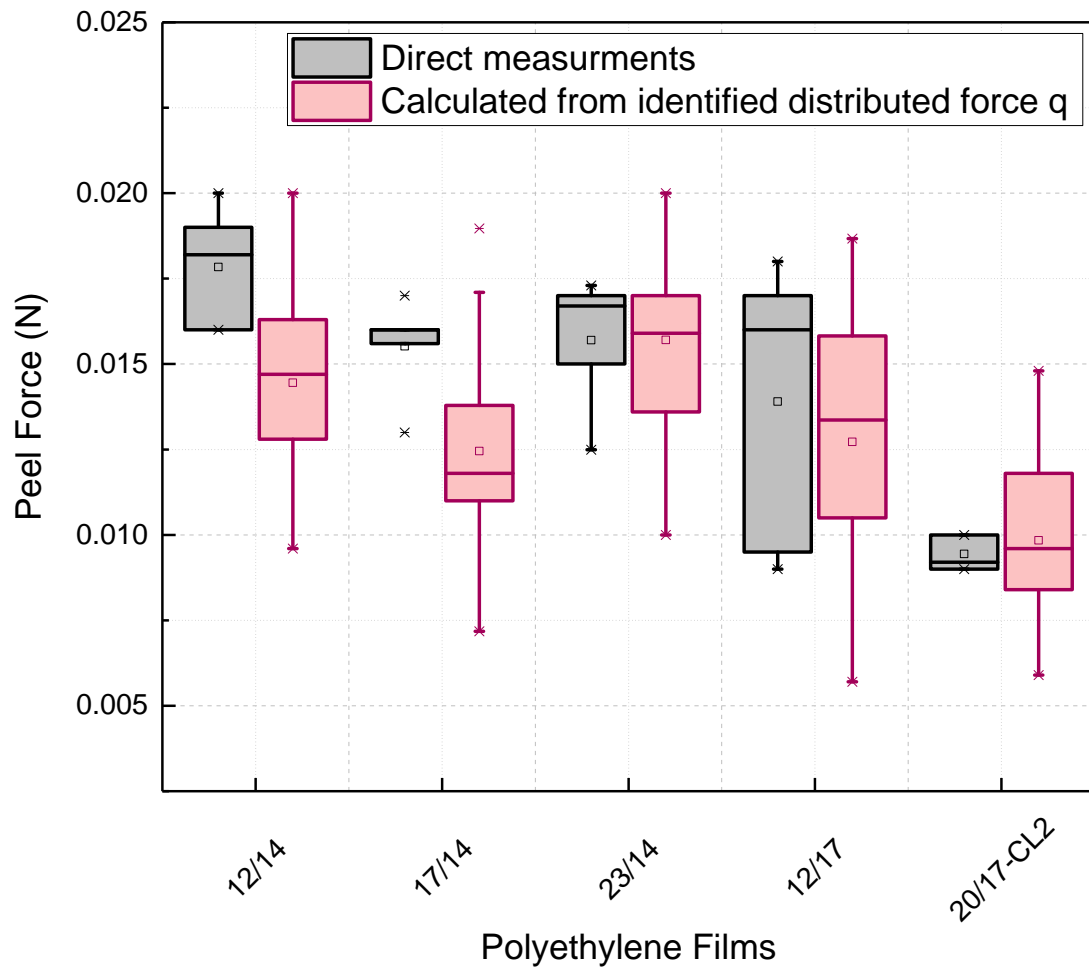
Figure 5.10: Peel force comparison obtained from direct measurements and calculated from the identified distributed force q based on Eqs (4.35) and more specifically (4.36)

graph but in reality they are super small values which can be neglected and considered as some minor errors in calculations or experiments.

Much like the values illustrated in Fig. 5.6, the least and the most dispersed F_{peel} values here also belong to film $17/14$ and $12/17$ respectively. This again confirms the idea of existence of manufacturing faults in film $12/17$. The wider configuration varies, the higher F_{peel} dispersion will be. However, the positive thing is that despite this dispersion in the values, the black and red boxes still match each other in all films.

In the case of film $20/17 - CL2$ the calculated values of F_{peel} show wide dispersion in comparison to that of the measured values. Although, the median line of both boxes have pretty close values and are in quiet good accordance. Such a harmony between the experimental and calculated results of this film reminds us that, despite not having another film with the same cling material as this film to compare the result with, both out come of DA and CEA model are correct and validated.

According to this graph it can be concluded that the validation step for CEA is done perfectly. This means the tr-sp curves corresponding to all films are provided correctly.

5.1.4 Exponential Approach

In this section the tr-sp curve generated by the Exponential Approach (explained in section 4.2.3) is presented. The idea behind all these approaches which is going in reverse path and generating the tr-sp curves of self-adhesive PE films based on their configurations durign the T-peel tests is tested and verified for 125 configuration pictures by each of CEA and DA approaches. Therefore, it was unnecessary to apply the time consuming procedure of evaluating this many configuration pictures by Exponential Approach too. Hence, in the EA approach the strategy of the calculations and validation is different than that of the others. In this model only one configuration picture from film $23/14$ was chosen randomly, then evaluated and its final result of tr-sp curve was compared with the equivalent one from CEA for validation.

As explained in section 4.2.3, in order to apply EA approach on the film configurations, their formerly extracted Cartesian-coordinates or the approximated polynomial series can not be used directly. Instead, the input data to the calculations in this approach, should be the angles extracted from the Cartesian-coordinates ready to provide the exponential approximations and the angle that could define the film position in each point is angel φ.
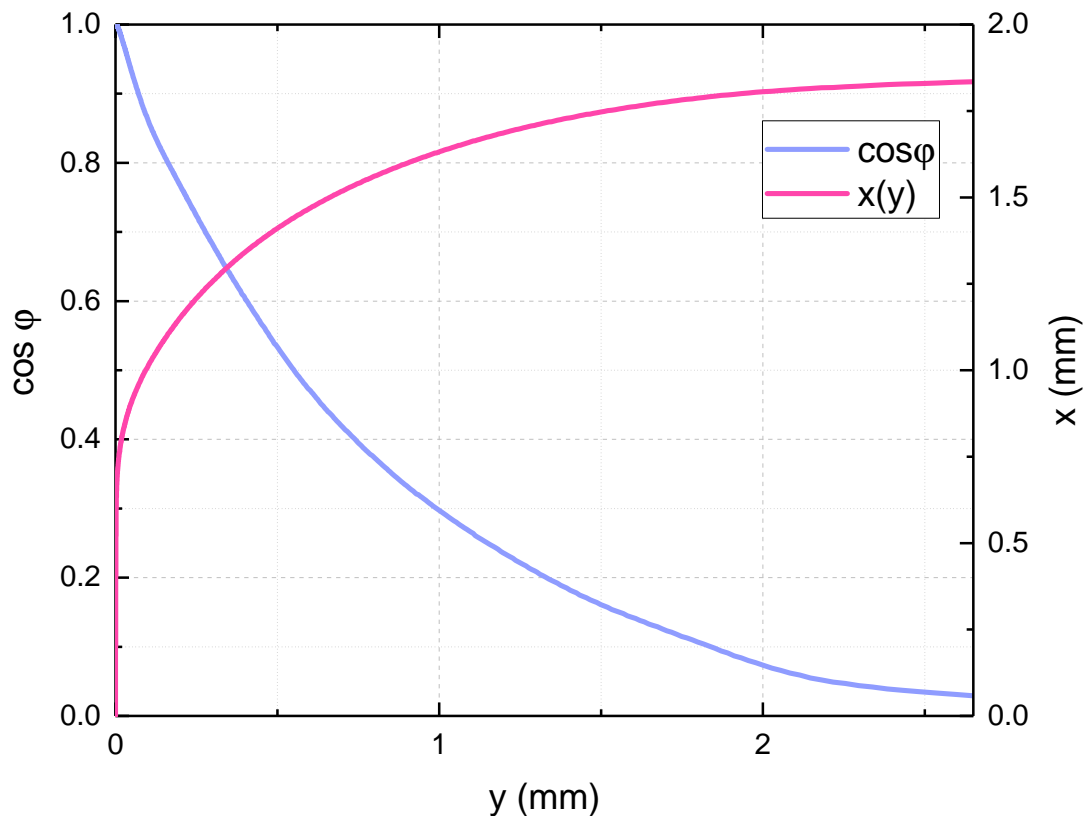

Figure 5.11: Digitized form of the film centerline configuration represented as functions of $x(y)$ and $\cos \varphi(y)$ identified from digital images, related to film $23/14$

Since the intended final result is the tr-sp curve and separation is defined as the y-coordinate, the x-coordinate was omitted and all the further calculations are related to y directly. To this end, the y-coordinates of digitized film configuration was used to provide its corresponding $\cos \varphi$, according to Eq. (4.52).

Figure. 5.11 illustrates the digitized data of film configurations in the form of x-coordinates and its corresponding $\cos \varphi$ (calculated from Eq. (4.52)) as a function of y by the pink and blue line respectively.
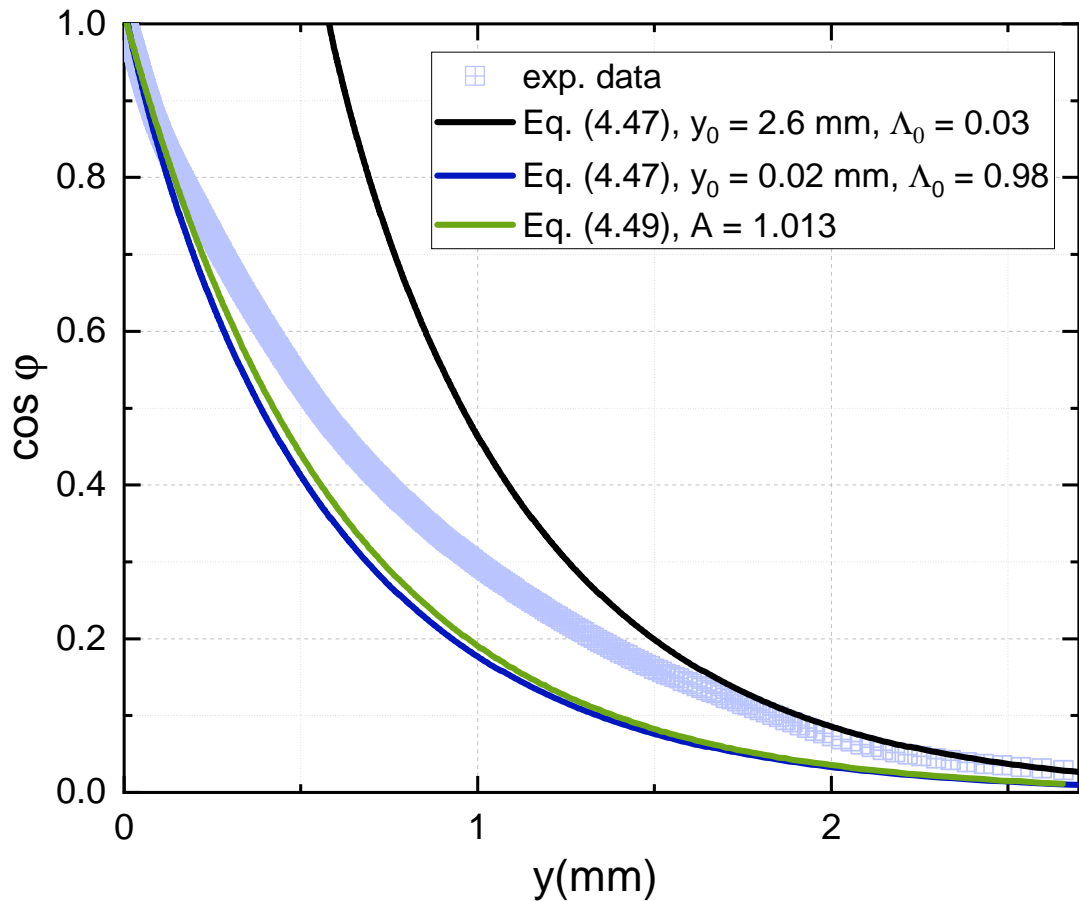
Figure 5.12: Experimental data as the function $\cos\varphi(y)$ identified from digital images of centerline, and its corresponding approximated lines by Eqs 4.47 and 4.49

This graph illustrates the coordinates for the whole film deformation. The adhesive interactions take place only in the delamination area. Therefore, it is not necessary to consider mathematically defining the whole deformed shape of the film. Hence, to provide the data regarding the area of interest for this study, as an input to the calculations, we need to zoom in to the area that $0\text{ mm} < y < 0.04\text{ mm}$ and define the configuration of that area properly. Figure 5.12 illustrates the approximations according to the closed-form analytical solution (4.47) for the beam part without the interaction forces, where Λ is assumed to be $\Lambda^2 \ll \Lambda < 1$. By defining the boundary values for a part of the beam which is out of the zone of interaction, and with the normalized peel force $\tilde{F}_{\text{peel}} = 3.23$ and by setting $y_0 = 2.6\text{ mm}, \Lambda_0 = 0.03$ the closed-form solution (4.47) agrees well with the experimental data (provided from centerline digitization by B-spline) for the right part of the beam having the opening within the range $1.6\text{ mm} < y < 2.6\text{ mm}$.

For the same closed-form solution (4.47) and the same peel force value if we set the boundary values this time as $y_0 = 0.02\text{ mm}, \Lambda_0 = 0.98$ the solution meets well the experimental data for the right edge of the beam as well as for the openings within the range $0.02\text{ mm} < y < 0.04\text{ mm}$, as it is illustrated in Fig. 5.13. Zooming into the zone of interaction (beginning of the delamination area) as shown in Fig. 5.13 provides us with the details of the approximated lines toward the experimental data. Plots of the exponential approximation based on Eq. (4.49) with the same peel force as the previous two approximated lines, and considering the coefficient $A = 1.013$ are also presented in both Figs 5.12 and 5.13. Equation (4.49) approximates the cross section rotation only for a part of the beam as a single-term

exponential. According to Fig. 5.12 it is observable that the exponential approximation almost coincides with the closed-form solution for $y_0 = 0.02$ mm and $W_0 = 0.98$. It should be noted that both the closed form solution and the single-term approximation are able to describe the function $\cos \varphi$ for a clamped cantilever beam which are without adhesive interaction. However, these approximations do not agree with experimental data for the left part of the beam as shown in Fig. 5.13, which is the tended area of approximation. Therefore, the approximation accuracy is increased by applying the two-terms exponential sum of Eq. (4.50), and the boundary conditions for the left edge of the beam are successfully satisfied. With $\beta = 127$ the function $\Lambda = \cos \varphi$ for a wide range of openings y is well approximated, the purple line in Fig. 5.13.
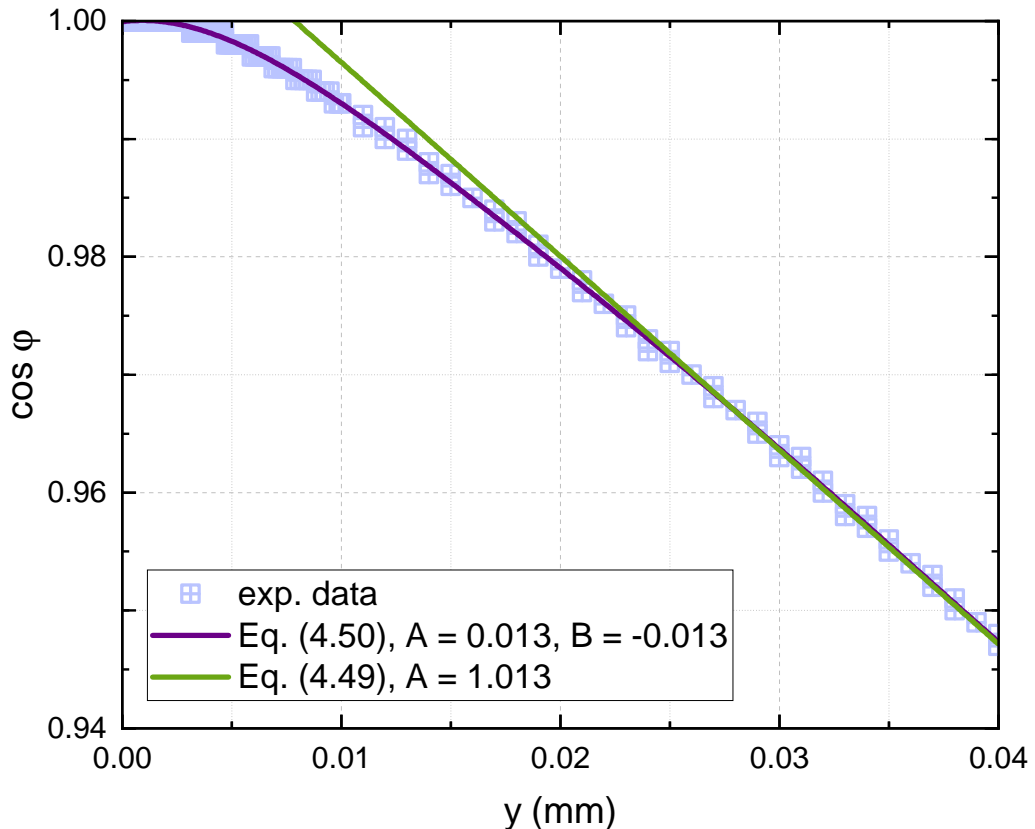

Figure 5.13: Experimental data as the function $\cos \varphi(y)$ identified from digital images of centerline in a close look visualizing the delamination are, and the approximated matching lines by Eqs 4.49 and 4.50

Now that the approximation based on Eqs (4.50) and (4.49) are done, it is time to insert them in EA model to see the tr-sp results. Figure 5.14 illustrates the results of identification applying the single-term and two-term exponential approximations. As expected, the single term approximation (4.49) leads to the negligible interaction forces for the whole beam and doesn't cover the interacting that are same as it didn't approximate the shape either. It matches the ending part of tr-sp curve though. In contrast the two-term exponential approximation of Eq. (4.50) provides the physically correct distribution of q vs. y or in other terms traction-separation curve which is of course in an exponential form too.

By going into the details of the results shown in Fig. 5.14, it can be seen that, both the maximum force $q_{\max}/B = 72$ 1/mm^3 (which is the normalized value divided by bending stiffness) and the critical opening $y_* \approx 0.075$ mm are identified by the purple line. The tr-sp
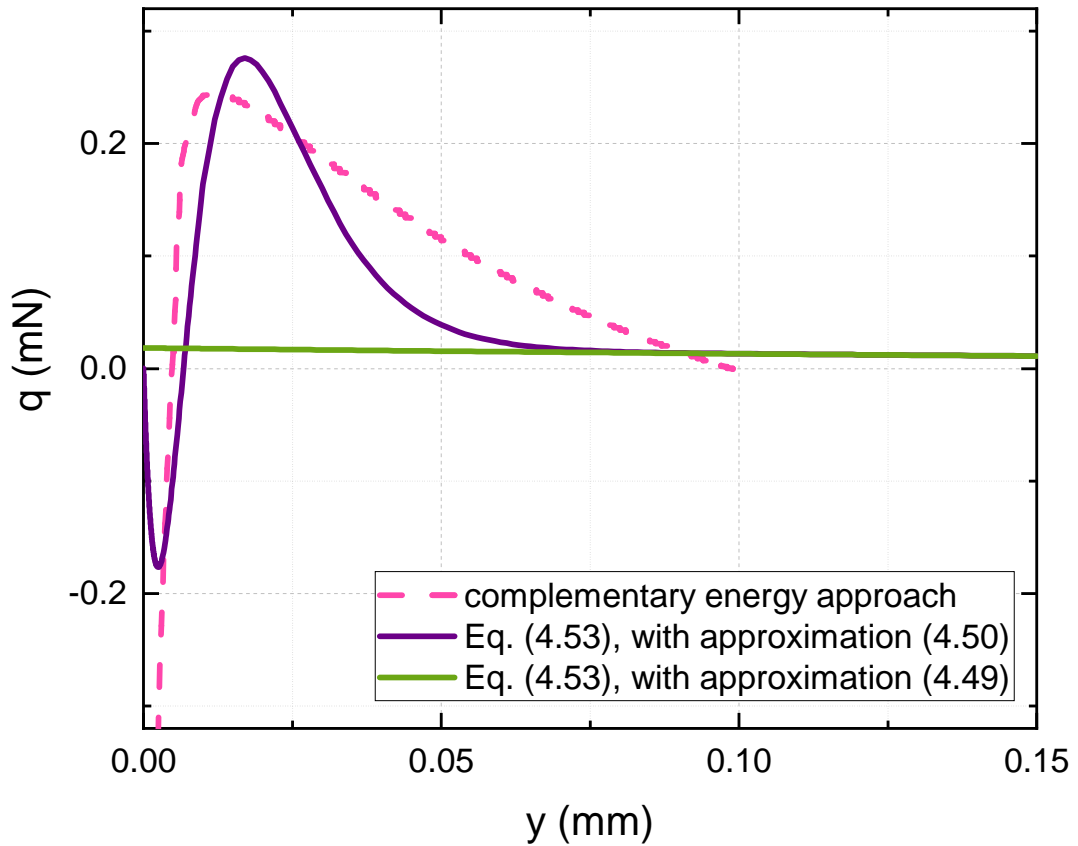
Figure 5.14: Interaction distributed forces q vs opening y evaluated different approaches

curve of the same configuration calculated by CEA is also provided with pink dashed line in this graph for comparison purpose. As explained before, in this method the distributed force q was approximated by the power series with respect to the x-coordinate and the coefficients in the series were computed from the complementary energy variational functional by the Ritz method. Considering that the tr-sp curves are calculated from different type of mathematical equations (one is polynomial and one exponential), they exhibit a pretty cloth match for all three parameters of the maximum force q_{max}, equilibrium y_{eq} and the critical opening y_*. The existence of the maximum value of the adhesive force q_{max} in such distance of separation value y achieved by both methods, indicates that self-adhesive polymeric films act by a relatively long range interaction forces. Long-range force interactions were also identified in [50, 146] for similar cling materials which is explained in detail by the next section.

5.2 Non-Local Modeling

In order to provide the non-local model for the notified long-range interactions which are present in adhesion system of our study, the principles of "bond-based" peridynamic theory were taken into account. As it was briefly explained in section 2.2.1, the original form of this theory was first presented by Silling [73] in 2000, the details of its basic theory was published az a book by Madenci, et al., [74] in 2013, and recently the related techniques to model materials were brought in a book by Bobaru et al., [63] which had Silling as a member of its editing group as well.

The suggested procedures in the "bond-based" peridynamic theory is to consider two separate and arbitrary points, each in a small element as part of a continuous body and assume there is a force denoted from one to the other point, called a pairwise bond force density. An integration on this force density, along the material length in our case, gives the force vector. However, the intention here is only the vertical components of the force vector to achieve the traction-separation curve of the film.
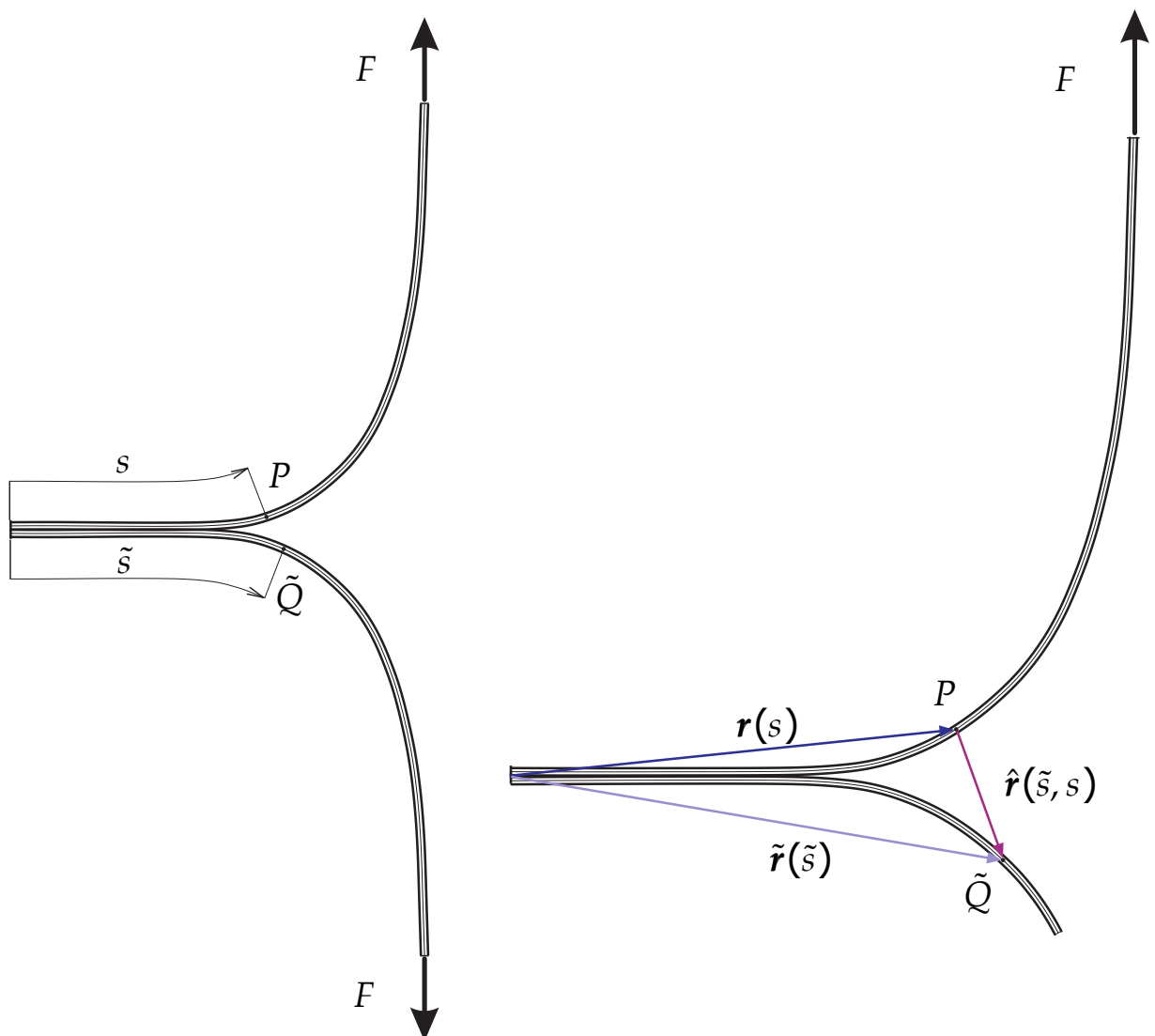

Figure 5.15: Schematics of deformed configuration of flexible films in a T-peel test, showing the coordinates and position vectors of points P and $\tilde{Q}$

The value of force density is supposed to be determined based on relations with the material properties. In this regards, general interatomic potentials of Morse [37] is taken into account to be the force density potential. To calculate the unknown parameters defining the material properties in this equation, the identified potential results from the previous section (complementary energy approach result) are used. By applying the least square method for these two potentials, the unknown parameters are identified and can be inserted in force density equation. The detaiels of this approach is provided in the followings.

$$q(s) = -\int_0^l \boldsymbol{e}_y \cdot \boldsymbol{f}(\tilde{s}, s)\mathrm{d}\tilde{s}$$
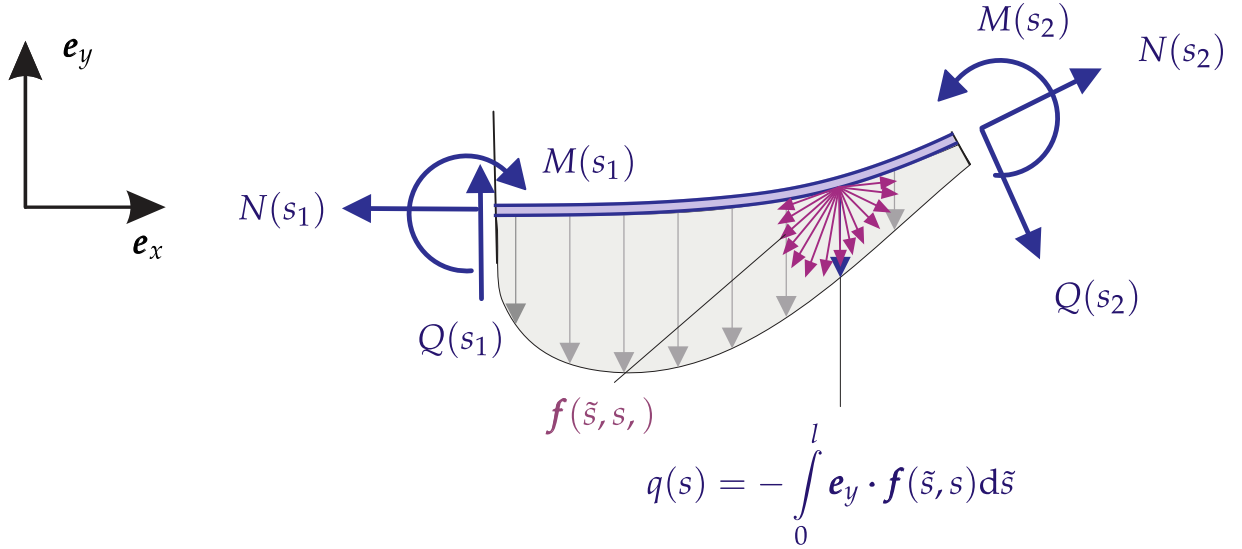
Figure 5.16: Free body diagram for an arbitrary part of the film within the delamination area illustrating non-local force density and its vertical projection as $q(s)$

Until this point of this study, it is indicated that the interaction forces between the adhesive layer of polymer films are of long-range and acting outside the contact zone. To this end, the modeling can be initiated by defining the film configuration. According to the schematics shown in Fig. 5.15, in order to define the film shape, s is the coordinate parameter and $\boldsymbol{r}(s)$ the position vector of an arbitrary point P on the top film. As the same way, the coordinate and the position vector of a arbitrary point $\tilde{Q}$ on the bottom film is specified by $\tilde{s}$ and $\tilde{\boldsymbol{r}}(\tilde{s})$, respectively. The vector connecting the points P and $\tilde{Q}$ is specified by $\hat{\boldsymbol{r}}(\tilde{s}, s) = \tilde{\boldsymbol{r}}(\tilde{s}) - \boldsymbol{r}(s)$. Figure 5.16 illustrates free-body diagram for a part of the film defined by the coordinate s in a range $s_1 \leq s \leq s_2$. The force vector acting on the point P from an element $\mathrm{d}\tilde{s}$ in the neighborhood of the point $\tilde{Q}$ is specified by $\boldsymbol{f}(\tilde{s}, s)\mathrm{d}\tilde{s}$. By analogy to peridynamics [63], the vector $\boldsymbol{f}$ can be termed as the mentioned bond force density.
The resultant force vector acting on the point P can be computed as follows

$$\boldsymbol{f}_\mathrm{R}(s) = \int_0^l \boldsymbol{f}(\tilde{s}, s)\mathrm{d}\tilde{s} \qquad (5.1)$$

Considering Eq. (5.1), the vertical projection $q(s) = -\boldsymbol{f}_\mathrm{R}(s) \cdot \boldsymbol{e}_y$ is shown in Fig. 5.16. We assume that the force density potential U_f exists such that the force density is defined as follows

$$f = \frac{\partial U_f}{\partial \hat{r}} = \frac{dU_f}{dr}\frac{\hat{r}}{r}, \quad r = |\hat{r}| \tag{5.2}$$

For the force potential the following exponential expression is assumed

$$U_f(r) = -a\exp\left(-\frac{r}{r_a}\right) + b\exp\left(-\frac{r}{r_b}\right), \tag{5.3}$$

where a, b, r_a and r_b are material parameters. Which can be calculated by applying the least square method on the identified equivalent force potential of the same configuration, using the complementary energy approach provided in the former section. Leading us the following values of the parameters.

$$r_a = 0.018\text{mm}, \quad r_b = 6.84 \cdot 10^{-3}\text{mm}, \quad a/B = 101.84\text{mm}^{-3}, \quad b/B = 116.56\text{mm}^{-3}$$

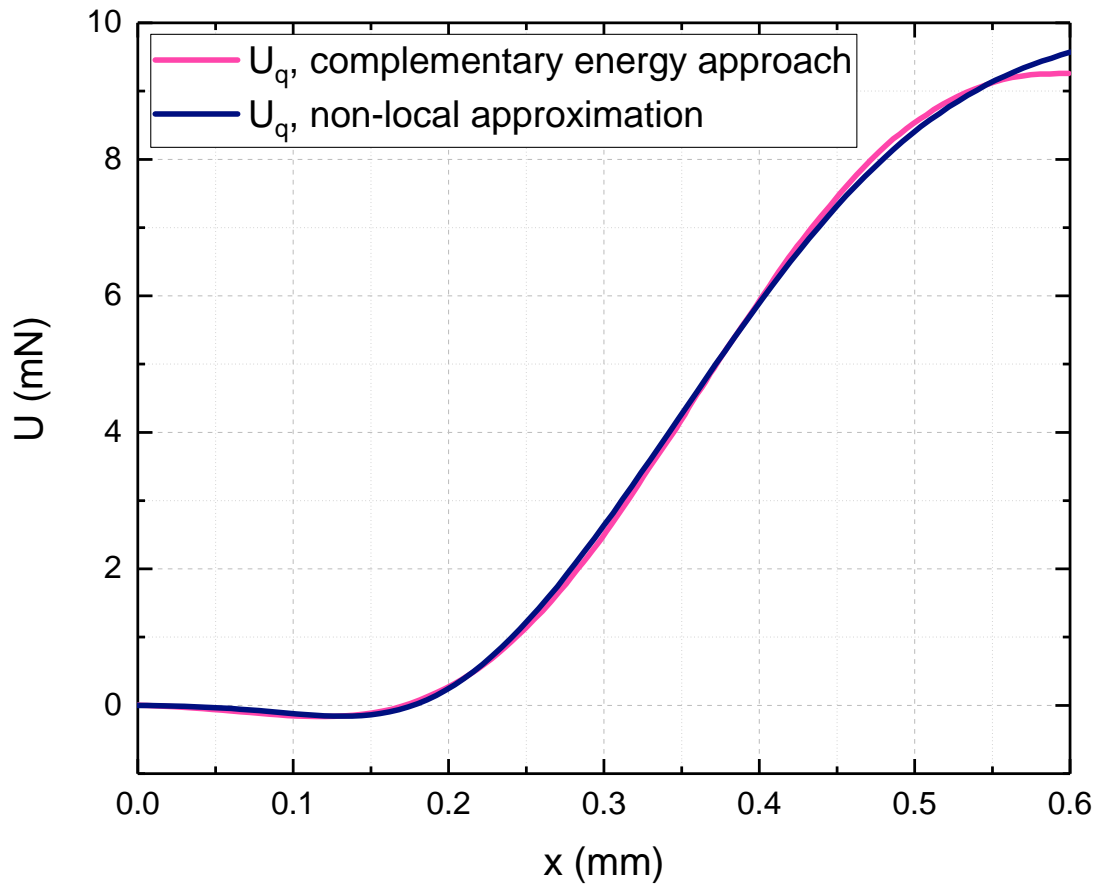
Figure 5.17: Force potential vs x-coordinate curves identified from experimental data based on former approach and non-local approximation

Figure 5.17 illustrates the matching values of the force potential from CEA and its equivalent value from non-local approximations, using the identified material parameters. The potential values show perfectly similar behavior to one another as expected.

With the force potential Eq. (5.3) the force density Eq. (5.2) is defined as follows

$$\boldsymbol{f}(r) = \left[\frac{a}{r_a} \exp\left(-\frac{r}{r_a}\right) - \frac{b}{r_b} \exp\left(-\frac{r}{r_b}\right) \right] \frac{\hat{\boldsymbol{r}}}{r} \tag{5.4}$$

Indeed, from Eq. (5.1) we obtain

$$q(s) = -\int_0^l \left[\frac{a}{r_a} \exp\left(-\frac{r}{r_a}\right) - \frac{b}{r_b} \exp\left(-\frac{r}{r_b}\right) \right] \frac{\tilde{y}(\tilde{s}) + y(s)}{r} \mathrm{d}\tilde{s} \tag{5.5}$$

By changing the integration variable to y, Eq. (5.5) can be rewritten as follows

$$q(y) = -\int_0^{y_{max}} \left[\frac{a}{r_a} \exp\left(-\frac{r}{r_a}\right) - \frac{b}{r_b} \exp\left(-\frac{r}{r_b}\right) \right] \frac{\tilde{y} + y}{r \sin \varphi(\tilde{y})} \mathrm{d}\tilde{y}, \tag{5.6}$$

$$r(y, \tilde{y}) = \sqrt{x(y) - x(\tilde{y})^2 + (y + \tilde{y})^2}$$
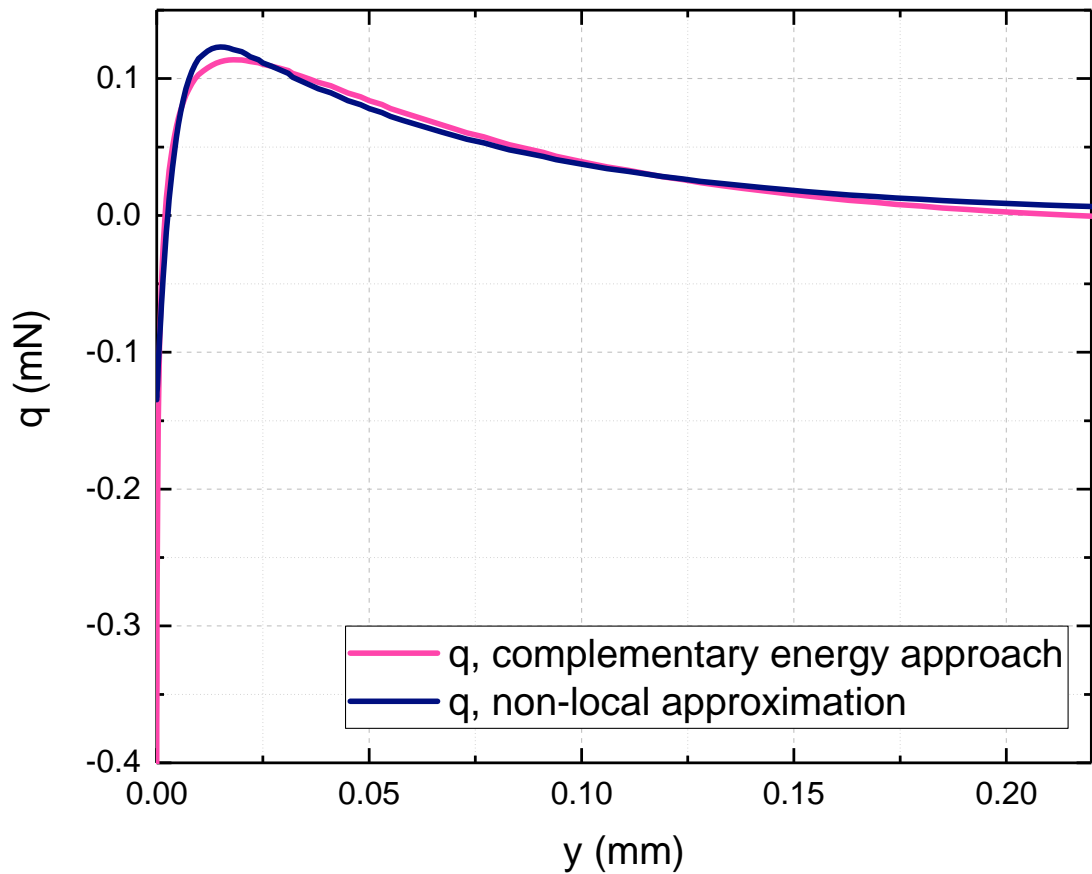
Figure 5.18: Traction-separation curves identified from experimental data based on former approach and non-local approximation

For the function $q(y)$ which is obtained from experimental data of the film configurations with Eq. (4.53) and approximation Eq. (4.50) as well as the deformed line $x(y)$, Eq. (5.6) is applied to match the values of material parameters in the non-local model. Figure 5.18 illustrates the results with the calculated material parameters.

As it is observable from Fig. 5.18 and 5.17, both values of force potential and traction-separation curve obtained by non-local model, behaved in a perfect accordance to their equivalent values of the same configuration from former approach.

6 Summary and Outlook

6.1 Summary

This thesis documents a novel idea to model the delamination of thin and flexible self-adhesive polyethylene films. The uniqueness of the idea behind this research, lies beneath going from a reverse path to solve the problem. In this study reverse means not following the usual path like using a CZM and FEM, for instance, to simulate the delamination path and configuration, but instead using the delamination configuration and trying to identify the matching traction-separation curve to the experiments.

To this end, experiments were done in the format of T-peel test, since this test is considered to be the most suitable test for flexible thin film adhered to one another like our choice of material for this study. As it can be realized from the naming, T-peel test is a test that peels two layers of material by vertically mounted clamps and if the testing specimen is provided from two layers of identical material it provides a symmetrical T shape. In this study, 5 types of differently manufactured polyethylene foils were tested and evaluated. The details about the individual properties of each foil is provided in Table 3.1, they were transparent, flexible, thin in μm scale for the thickness and because of coextrusion technology, possessing self-adhesive ability. The test specimens were provided from these films based on ASTM 1876 standard of T-peel tests. This standard contains the specimen size, procedures to make them and the T-peel test adjustments. The peel test was performed by a tensile testing machine made in Zwick-Roell company. For the purpose of providing statistically reliable experimental results, the T-peel test was repeated 5 times for each material which means 5 specimens were testes per material that comes to 25 specimens tested overall.

The usual output of such tests is the peel force measured by the load-cell attached to the upper clamp of the tensile machine which is used to calculate the work of adhesion. The measured peel force alone is not the only interest of this research since it is only the resultant value of the more important distributed forces between the films. The evaluation of these non-local forces directly from the peel test results is more challenging and , was the aim of this work. Hence, the important output of the tests which is also the input of the modeling procedure, would be configuration of the films during the peel test in the delamination zone. In order to provide this configurations a microscopic camera was installed perpendicularly to the transverse view of the films to record the whole peel test. By extracting the captured frames of the camera the intended configurations could be achieved in the form of pictures which are pixel based and what we needed was to convert them all to a smooth vector line only. In simpler words, these configurations were useful in case they were digitized and their mathematical information as the Cartesian-coordinates or the angles, defining the line orientation could be extracted. This need, leads us to process the images of peel tests. To this end, the extracted frames were inserted into a graphical software named CorelDRAW, by the help of B-spline drawing technique in this software, the vector line equivalent to the film configuration was provided. Once again to follow the statistical reliability of the results in modeling, 5 picture frames from each test video was chosen randomly to extract the vector image, now by considering that there was 5 times testing per material, and 5 different

materials, bring us to 125 pictures needing be processed overall. Now vector image itself doesn't have any mathematical data of our interest such as coordinates of the configuration. Therefore, the processing needs to go to the next step: vector images are imported into to Rhino software that has the ability to rebuild the configuration line with an actual B-spline curve and extract the required mathematical info to draw such a curve. Operating directly on a B-spline is a challenging and time consuming procedure, and all that was needed in this stage was Cartesian-coordinates corresponding to the film configurations. Hence, with using an algorithm in Matlab the Cartesian-coordinates of B-splines equivalent to film configuration were extracted. After testing plenty of softwares and methods of digitizing we found this procedure the most accurate to provide the digitized mathematical data presenting the film configurations. From this stage forward, this study entered the modeling stage.

Coordinate data are the input of identification step, however they were not inserted into the models directly. Three different approaches were introduced in this study, two of them operated on the polynomial equations fitted to the coordinates and the last one used the angles defining the configuration based the coordinates. Although, all these approaches followed the same goal and main idea. Therefore, they all shared the stages of basic kinematic characterization, free body diagram to define the governing equations parameters, and the constitutive equations. From these stages forward, each of the approaches went in different directions which is explained individually in the following.

- **Direct Approach (DA)** used the energy integral and the effective work of adhesion principles based on the defined constitutive equations. It started with defining a potential energy for the distributed force which is taken as the traction. Then it went forward by introducing the conservation law for the non-linear beam theory containing the strain energy density, force potential, bending moment, and the normal force. Since the strain energy density was only dependent on the local stretch, in the case of this study, and by an analogy to the J-integral in fracture mechanics, the relations between peel force and adhesion energy was derived. Which used later as a validation step by comparing the measured and calculated surface energy. As it is also clear from the naming this approach used the film configuration data defined as polynomial equation directly. Based on assumptions made specifically for the choice of material and defining some boundary conditions the constitutive equations were rewritten as a function of film configuration fitting polynomial. By the insertion of the polynomial in to these equations the intended force distributions were achieve. However, at the end the calculations had to go through four time derivations of the polynomial which leaded to some minor instabilities in the final results. Apart from this, the results achieved by this approach were qualitatively in a satisfying level.

- **Complementary Energy Approach (CEA)** introduced the complementary energy by the Legendre transformations to the strain energy density equation. By doing so, it provided a new form for the constitutive relations causing of which, containing complementary energy parameter in definition of the local stretch and curvature. The first variation of the complementary energy while applying integration over two arbitrary points defining the film configuration, resulted in the complementary energy type variational equation. Once again, the boundary conditions and assumption suitable to this study were applied to the calculations and the relations parameters were replaced to be as a function of film configuration polynomial based on the initial equilibrium conditions. In order to define three parameters of the bending moment, and the adhesive force distribution (traction) polynomial series were assumed according to

Ritz method. The so called polynomial series contained an unknown coefficient which could be determined by a linear algebraic equation on the transformed form of the formerly defined variational equation. But this time, the calculations only contained the first derivation of the polynomial, therefore, providing more accurate results. The accuracy of this method was estimated by the comparison between two peel force values, one being determined by an integration over the calculated adhesive force distribution, and the other being measured by the tensile testing machine. The final results of the traction-separation curves and the accuracy estimations were all done successfully. The outcome of this method showed more accuracy than that of DA, and because of containing only one derivation of the configuration polynomial, it was less sensitive to the minor polynomial fitting errors.

- **Exponential Approach (EA)** was the third applied option to obtain the traction-separation curve. This method was tried because both of the former methods, although working properly, had to pass a polynomial fitting procedures to the experimental data defining the film configuration. Going through such procedure increased the chance of accuracy reduction, simply by not providing the perfectly fitting equation to the actual experimental data. Which means, if the input data of the calculations is not accurate then the final result couldn't be perfectly accurate either. To prevent such problem from happening, the film configuration center line was defined by the angle between the tangent to the deformed line and the x-axis. Meaning, each of the Cartesian-coordinates defining the center line of the film were positioned in a specific angle toward the previous coordinate, the angles between these points leaded to the idea of an exponential approximation defining the film shape. In this regard, the boundary conditions of film configurations and the free body diagram illustrating the applied forces and moment resulted in two exponential approximations, which the first contained one constant and the second two constants needing to be calculated. Both approximations were able to match the experimental data partially, which was not a problem since the whole configurations was not necessary for the further calculations. However, the one with the two constant could match the correct and intended part of the film perfectly. The important issue was that they were a function of y-coordinate, or in other words the separations. It means, they could directly provide the traction as a function of separation with out any other variable in between such as the x-coordinate. In order to insert the approximations in the constitutions equations and further calculations, some transformations were done to make them adaptive with the inserted coordinate type. This approach resulted in a perfectly matching deformed line approximations for the intended area and providing a reliable and accurate result. The validation of this approach was performed by the comparison of equivalent traction-separation curve obtained from CEA, which showed a good accordance toward one another.

By this stage of the study, that the idea of going in a reverse path and providing the tr-sp curves of a sample using its configurations by mentioned former methods worked properly, the non-local modeling procedures were started. Since the interaction between the adhesive surfaces of the films were from Van der Waals type, they were considered to be as non-local interactions. One of the suggested methods to model non-local interactions which was discovered in the recent decades were peridynamic theory. This theory has developed until the present time and is consists of different directions fitting different material types or usages. By analogy to the "bond-based" peridynamic theory the bond force density vector was defined in section 5.2, which is the resultant force vector acting on an arbitrary point

on one layer from another arbitrary point on the other layer. The vertical projection of this bond force density along the film length provided us with the traction as a function of film shape coordinate parameter. Hence, by a change of parameter to separation the intended traction-separation could be computed if the force density equation was available. However, by taking the general interatomic potential of Morse, the force potential is assumed to be as an exponential function of material and configuration coordinate parameters. The material parameters were calculated by performing the least square procedure over the force potential equation and its equivalent calculated potential by the identification approaches. By having the force potential and the material parameters at hand, eventually the force density as well as vertical force distribution (tr-sp curve) were calculated. This curve was compared to its equivalent value from CEA to check the result accuracy and they matched perfectly.

6.2 Outlook

Future studies can be performed to take this study to some next levels from different aspects such as experimentally, mathematically and modeling.

- To **experimentally** improve this study, one may go in different directions. For instance, taking use of more advanced test devices (including the test machine or more sensitive load-cell), camera, or even test setup and environment. The reason that we used the existing test equipment or an ordinary microscopic camera for experiments, was to fit into the available project budget, and make sure if the idea of the study works before investing on high pricing devices. Now that the study reached up to this level of improvement, it is safe to say that the experiments could be done on a better level of accuracy. The test environment as well as the sample preparation environment could change to an highly equipped clean room to decrease the chance of any external particle or moist existence and provide an ideal like adhesion in the specimens and test procedure. An upgrade for the tensile testing machine can be applied to act smoother or provided with movable grips in both up and down direction in a symmetric situation to keep the delamination area constant and not moving, or otherwise, a movable arm attached to the machine clamp for the camera, to keep the view in a constant and direct position. The camera itself can be replaced by a higher resolution and shutter speed or even change to a digital image correlation system. The lightning or any other aspect can be adjusted to provide a more accurate film configuration. Even the peel test method can be changed to the other available ones although, different test requires different calculations.

- **Mathematical** improvements are partially related to the output data accuracy of the tests, so if the peel test results (i.e. images quality) gets better, it automatically helps the mathematical procedures. However, apart from the experimental results effect, any procedure that can help to improve defining the film configuration mathematically is recommended to be checked. Three different methods (numerical, polynomial, exponential) are applied until now, there are still plenty available. For instance, NURBS were only used to provide the numerical data here, but it is applicable on the whole identification and modeling steps, although can be complicated and time consuming.

- Regarding the **modeling** step, future studies can go further with the non-local formulations of the traction-separation law, describing the adhesive force interactions. Since, with a developed traction-separation law and the help of finite element method, the

peeling process can be simulated. The recently discussed examples, regarding the peridynamics modeling of layered systems, in [147] might be a helpful source in this procedure.

6.3 Conclusions

Traction-separation behavior identification in the layered systems, is considered as one of the important steps to analyze the adhesive performance in contact with tensions of the real life. To this end, a traction-separation law which is specific for the material of interest, identified from experimental data seems to be essential.

Based on the successful performance of the identification methods of DA, CEA, and EA and their final results, we can claim that the idea behind this study served the purpose properly, since each approach was validated individually and the procedures were repeated for statistical assurance. Although each approach faced specific challenges regarding its unique feature, each challenge directed the path to satisfying results. Now base on the achievements of this study, it can be concluded that:

two main conclusions can be made:

- The idea of going on a reverse path to provide the traction-separation curves, specific to the test material, worked properly under some conditions, such as the accurate approximation of the deformed peel-arm centerline. In order to do so, the function approximation the film configuration must be differentiable smoothly and as long as it satisfies kinematic and static boundary conditions as well as equilibrium conditions both for the forces and moments, useful results could be generated.

- Within the identified traction-separation curves of all the investigated approaches it is clearly showed that distributed force continues to outside of the contact zone. This indicates and supports the idea of non-local adhesive force interaction existence between the adhered layers of the film. Therefore, the non-local modeling was performed correctly and can be continued as further studies.

Bibliography

[1]   Gahleitner, M. and Paulik, C. "Polypropylene". In: *Ullmann's Encyclopedia of Industrial Chemistry*, 2014, pp. 1–44. DOI: `10.1002/14356007.o21{\_}o04.pub2`.

[2]   Bongaerts, H. *Flat Film Extrusion Using Chill-roll Casting*. 2nd. Munich: Hanser Publishers, 1997.

[3]   Izard, E. F. "Production of polyethylene terephthalate". Pat. 2534028. 1950.

[4]   Adams, J. F. E., Gerber, K. G., and Holmeswalker, W. A. "Process of the production of biaxially oriented polyethylene terephthalate film". Pat. 3177277. 1965.

[5]   DeMeuse, M. T., ed. *Biaxial Stretching of Film*. Woodhead Publishing, 2011. ISBN: 978-1-84569-675-7.

[6]   Goetz, W. *Polyamide for Flexible Packaging Film*. Rome, Italy, 12–14 May, 2003. URL: `https://www.tappi.org/content/enewsletters/eplace/2004/10-2goetz.pdf`.

[7]   Lew, D. *Theoretical Comparison Between Nylon and Silk: Global Warming*. 2021. URL: `https://www.drdarrinlew.us/global-warming/theoretical-comparison-between-nylon-and-silk.html`.

[8]   Vogler, H. "Competition for polyamid fibers". In: *CHEMIE* 47(1), 2013, pp. 62–63. DOI: `10.1002/ciuz.201390006`.

[9]   Kohan, M. I. *Nylon plastics handbook*. Munich and New York: Hanser Publishers, 1995. ISBN: 3446170480.

[10]   Chhabra, E. "Recycling nylon is good for the planet so why don't more companies do it?" In: *The Gaurdian*, 18 May 2016. URL: `https://www.theguardian.com/sustainable-business/2016/may/18/recycling-nylon-bureo-patagonia-sustainable-clothing`.

[11]   Beychok, M. R. "A data base of dioxin and furan emissions from municipal refuse incinerators". In: *Atmospheric Environment (1967)* 21(1), 1987, pp. 29–36. ISSN: 0004-6981. DOI: `10.1016/0004-6981(87)90267-8`.

[12]   Chanda, M. *Plastics Technology Handbook*. 5th. CRC Press, 2017. ISBN: 9781498786218.

[13]   Allsopp, M. W. and Vianello, G. "Poly(Vinyl Chloride), publisher = American Cancer Society, isbn = 9783527306732, booktitle = Ullmann's Encyclopedia of Industrial Chemistry, year = 2000, doi = 10.1002/14356007.a21_717". In:

[14]   Geyer, R., Jambeck, J. R., and Law, K. L. "Production, use, and fate of all plastics ever made". In: *Science Advances* 3(7), 2017. DOI: `10.1126/sciadv.1700782`.

[15]   Bamberger, E. and Tschirner, F. "Ueber die Einwirkung von Diazomethan auf b-Arylhydroxylamine". In: *Berichte der deutschen chemischen Gesellschaft* 33(1), 1900, pp. 955–959. DOI: `10.1002/cber.190003301166`.

[16]   Yang, Y., Wu, W. M., Zhao, J., and Jiang, L. "Evidence of Polyethylene Biodegradation by Bacterial Strains from the Guts of Plastic-Eating Waxworms". In: *Environmental Science & Technology* 48(23), 2014, pp. 13776–13784. ISSN: 0013-936X. DOI: `10.1021/es504038a`.

[17] Small, C. M., Mcnally, G. M., Garrett, G., and Murphy, W. R. "The Characteristics of Polyethylene Film for Stretch and Cling Film Applications". In: *Developments in Chemical Engineering and Mineral Processing* 12(1–2), 2008, pp. 5–20. DOI: 10.1002/apj.5500120102.

[18] Schulze, S. H., Pander, M., Naumenko, K., and Altenbach, H. "Analysis of laminated glass beams for photovoltaic applications". In: *International Journal of Solids and Structures* 49(15), 2012, pp. 2027–2036. ISSN: 0020-7683. DOI: 10.1016/j.ijsolstr.2012.03.028.

[19] Nase, M., Langer, B., Baumann, H. J., Grellmann, W., Geißler, G., and Kaliske, M. "Evaluation and simulation of the peel behavior of polyethylene/polybutene-1 peel systems". In: *Journal of Applied Polymer Science* 111(1), 2009, pp. 363–370. DOI: 10.1002/app.28999.

[20] Nase, M., Langer, B., and Grellmann, W. "Fracture mechanics on polyethylene/polybutene-1 peel films". In: *Polymer Testing* 27(8), 2008, pp. 1017–1025. ISSN: 0142-9418. DOI: 10.1016/j.polymertesting.2008.09.002.

[21] Naumenko, K. and Eremeyev, V. A. "A layer-wise theory of shallow shells with thin soft core for laminated glass and photovoltaic applications". In: *Composite Structures* 178, 2017, pp. 434–446. ISSN: 0263-8223. DOI: 10.1016/j.compstruct.2017.07.007.

[22] Weps, M., Naumenko, K., and Altenbach, H. "Unsymmetric three-layer laminate with soft core for photovoltaic modules". In: *Composite Structures* 105, 2013, pp. 332–339. ISSN: 0263-8223. DOI: 10.1016/j.compstruct.2013.05.029.

[23] Eisenträger, J., Naumenko, K., Altenbach, H., and Köppe, H. "Application of the first-order shear deformation theory to the analysis of laminated glasses and photovoltaic panels". In: *International Journal of Mechanical Sciences* 96-97, 2015, pp. 163–171. ISSN: 0020-7403. DOI: 10.1016/j.ijmecsci.2015.03.012.

[24] Dupont, S. R., Oliver, M., Krebs, F. C., and Dauskardt, R. H. "Interlayer adhesion in roll-to-roll processed flexible inverted polymer solar cells". In: *Solar Energy Materials and Solar Cells* 97, 2012, pp. 171–175. ISSN: 0927-0248. DOI: 10.1016/j.solmat.2011.10.012.

[25] Choi, J., Kim, D., Yoo, P. J., and Lee, H. H. "Simple Detachment Patterning of Organic Layers and Its Application to Organic Light-Emitting Diodes". In: *Advanced Materials* 17(2), 2005, pp. 166–171. DOI: 10.1002/adma.200400223.

[26] Yim, M. J. and Paik, K. W. "Recent advances on anisotropic conductive adhesives (ACAs) for flat panel displays and semiconductor packaging applications". In: *International Journal of Adhesion and Adhesives* 26(5), 2006, pp. 304–313. ISSN: 0143-7496. DOI: 10.1016/j.ijadhadh.2005.04.004.

[27] Chiang, C. J., Winscom, C., Bull, S., and Monkman, A. "Mechanical modeling of flexible OLED devices". In: *Organic Electronics* 10(7), 2009, pp. 1268–1274. ISSN: 1566-1199. DOI: 10.1016/j.orgel.2009.07.003.

[28] Kathe, K. and Kathpalia, H. "Film forming systems for topical and transdermal drug delivery". In: *Asian Journal of Pharmaceutical Sciences* 12(6), 2017, pp. 487–497. ISSN: 1818-0876. DOI: 10.1016/j.ajps.2017.07.004.

[29] Servati, A., Zou, L., Wang, Z. J., Ko, F., and Servati, P. "Novel Flexible Wearable Sensor Materials and Signal Processing for Vital Sign and Human Activity Monitoring". In: *Sensors (Basel, Switzerland)* 17(7), 2017. ISSN: 1424-8220. DOI: 10.3390/s17071622.

[30] Selke, S. E. "Packaging: Polymers in Flexible Packaging". In: *Reference Module in Materials Science and Materials Engineering*. Elsevier, 2019. ISBN: 978-0-12-803581-8. DOI: 10.1016/B978-0-12-803581-8.02168-8.

[31] Castro-Aguirre, E., Iñiguez-Franco, F., Samsudin, H., Fang, X., and Auras, R. "Poly(lactic acid) - Mass Production, Processing, Industrial Applications, and End of Life". In: *Advanced drug delivery reviews* 107, 2016. DOI: 10.1016/j.addr.2016.03.010.

Bibliography

[32]   *How polyethylene film is made*. 2015. URL: https://www.tri-cor.com/how-polyethylene-film-is-made/.

[33]   Brink, T. *Cast versus blown film: Technology*. Aug 2016. URL: https://www.slideshare.net/TedBrink/cast-versus-blown-film.

[34]   Li, H., Chang, J., Qin, Y., Wu, Y., Yuan, M., and Zhang, Y. "Poly(lactide-co-trimethylene carbonate) and Polylactide/Polytrimethylene Carbonate Blown Films". In: *International journal of molecular sciences* 15, 2014, pp. 2608–2621. DOI: 10.3390/ijms15022608.

[35]   Autumn, K. "Gecko Adhesion: Structure, Function, and Applications". In: *MRS Bulletin* 32(6), 2007, 473–478. DOI: 10.1557/mrs2007.80.

[36]   Gay, C. "Stickiness—Some Fundamentals of Adhesion". In: *Integrative and comparative biology* 42, 2002, pp. 1123–1126. DOI: 10.1093/icb/42.6.1123.

[37]   Israelachvili, J. N., ed. *Intermolecular and Surface Forces (Third Edition)*. Third Edition. San Diego: Academic Press, 2011. ISBN: 978-0-12-375182-9.

[38]   Cavallo, D. and Goossens, H. and Meijer, H. E. H. "Co-extruded Multilayer Polymer Films for Photonic Applications". In: *Organic and Hybrid Photonic Crystals*. Ed. by Comoretto, D. Cham: Springer International Publishing, 2015, pp. 145–166. ISBN: 978-3-319-16580-6. DOI: 10.1007/978-3-319-16580-6{_}7.

[39]   Jiri George Drobny, ed. *Applications of Fluoropolymer Films*. Plastics Design Library. William Andrew Publishing, 2020. ISBN: 978-0-12-816128-9.

[40]   Silva, L. F. M. da, Öchsner, A., and Adams, R. D., eds. *Handbook of Adhesion Technology*. Berlin, Heidelberg: Springer Berlin Heidelberg, 2011. ISBN: 978-3-642-01169-6.

[41]   Duncan, B. "14 - Developments in testing adhesive joints". In: *Advances in Structural Adhesive Bonding*. Ed. by Dillard, D. A. Woodhead Publishing Series in Welding and Other Joining Technologies. Woodhead Publishing, 2010, pp. 389–436. ISBN: 978-1-84569-435-7. DOI: 10.1533/9781845698058.3.389.

[42]   Broughton, W. "6 - Testing the mechanical, thermal and chemical properties of adhesives for marine environments". In: *Adhesives in Marine Engineering*. Ed. by Weitzenböck, J. R. Woodhead Publishing Series in Welding and Other Joining Technologies. Woodhead Publishing, 2012, pp. 99–154. ISBN: 978-1-84569-452-4. DOI: 10.1533/9780857096159.2.99.

[43]   PartoviShabestari, N., RashidianVaziri, M. R, Bakhshandeh, M., Alidokht, I., and Alizadeh, Y. "Fabrication of a simple and easy-to-make piezoelectric actuator and its use as phase shifter in digital speckle pattern interferometry". In: *Journal of Optics* 48(2), 2019, pp. 272–282. ISSN: 0974-6900. DOI: 10.1007/s12596-019-00522-4.

[44]   Wittrock, H. J. and Swanson, L. In: *Plating* 49, 1962, p. 880.

[45]   Ashter, S. A. "6 - Mechanics of Materials". In: *Thermoforming of Single and Multilayer Laminates*. Ed. by Ashter, S. A. Oxford: William Andrew Publishing, 2014, pp. 123–145. ISBN: 978-1-4557-3172-5. DOI: 10.1016/B978-1-4557-3172-5.00006-2.

[46]   Gerberich, W. and Yang, W. "8.01 - Interfacial and Nanoscale Failure". In: *Comprehensive Structural Integrity*. Ed. by Milne, I., Ritchie, R. O., and Karihaloo, B. Oxford: Pergamon, 2003, pp. 1–40. ISBN: 978-0-08-043749-1. DOI: 10.1016/B0-08-043749-4/08148-9.

[47]   Fedele, R., Raka, B., Hild, F., and Roux, S. "Identification of adhesive properties in GLARE laminates by digital image correlation". In: *Journal of the Mechanics and Physics of Solids* 57, 2009, pp. 1003–1016. ISSN: 0022-5096. DOI: 10.1016/j.jmps.2009.04.005.

[48]   Freund, L. and Suresh, S. "Thin film materials: Stress, defect formation and surface evolution". In: 2004. DOI: 10.1017/CBO9780511754715.

[49] Kinloch, A., Lau, C., and Williams, J. "The peeling of flexible laminates". In: *International Journal of Fracture* 66, 1994, pp. 45–70. ISSN: 1573-2673. DOI: `10.1007/BF00012635`.

[50] Nase, M., Rennert, M., Naumenko, K., and Eremeyev, V. A. "Identifying traction–separation behavior of self-adhesive polymeric films from in situ digital images under T-peeling". In: *Journal of the Mechanics and Physics of Solids* 91, 2016, pp. 40–55. ISSN: 0022-5096. DOI: `10.1016/j.jmps.2016.03.001`.

[51] Rennert, M., Fiedler, S., Nase, M., Menzel, M., Richter, S., Kressler, J., and Grellmann, W. "Investigation of the Migration Behavior of Polyisobutylene with Various Molecular Weights in Ethylene/ alpha- Olefin Copolymer Blown Stretch Films for Improved Cling Properties". In: *Journal of Applied Polymer Science* 131, 2014. DOI: `10.1002/app.40239`.

[52] Richefeu, V., Chrysochoos, A., Huon, V., Monerie, Y., Robert, P., and Wattrisse, B. "Toward local identification of cohesive zone models using digital image correlation". In: *European Journal of Mechanics - A/Solids* 34, 2012, pp. 38–51. DOI: `10.1016/j.euromechsol.2011.12.001`.

[53] Ruybalid, A. P., Hoefnagels, J. P. M., Sluis, O. van der, Maris, M. P. F. H. L. van, and Geers, M. G. D. "Mixed-mode cohesive zone parameters from integrated digital image correlation on micrographs only". In: *International Journal of Solids and Structures* 156-157, 2019, pp. 179–193. ISSN: 0020-7683. DOI: `10.1016/j.ijsolstr.2018.08.010`.

[54] KINLOCH, A. J. and WILLIAMS, J. G. "Chapter 8 - The mechanics of peel tests". In: *Adhesion Science and Engineering*. Ed. by Dillard, D. A., Pocius, A. V., and Chaudhury, M. Amsterdam: Elsevier Science B.V, 2002, pp. 273–301. ISBN: 978-0-444-51140-9. DOI: `10.1016/B978-0-444-51140-9.50035-4`.

[55] Such, T. E. and Wyszynski, A. E. "An Improvement in the Zincate Method for Plating on Aluminum". In: *Plating* 52(10), 1965, pp. 1027–1034. URL: `https://www.pfonline.com/articles/an-improvement-in-the-zincate-method-for-plating-on-aluminum`.

[56] Possart, W., ed. *Adhesion*. 2005 Wiley VCH Verlag GmbH & Co. KGaA, 2005. ISBN: 9783527607303. DOI: `10.1002/3527607307`.

[57] Kinloch, A. *Adhesion and Adhesives: Science and Technology*. 1st ed. Netherlands: Springer Netherlands, 1987. ISBN: 978-0-412-27440-4. DOI: `10.1007/978-94-015-7764-9`.

[58] Brinson, H. F., Dostal, C. A., Woods, M. S., Ronke, A., Henry, S. D., Daquila, J. L., and O'Keefe, K. L. "Engineered Materials Handbook Volume 3 Adhesives and Sealants". In: *ASM International*, 1990.

[59] Adams, R. D., Comyn, J., Wake, W. C., and Wake, W. C. *Structural adhesive joints in engineering*. Springer Science & Business Media, 1997.

[60] Petrie, E. M. *Handbook of adhesives and sealants*. McGraw-Hill Education, 2007.

[61] Ebnesajjad, S. and Landrock, A. H. *Adhesives technology handbook*. Plastics Design Library. William Andrew, 2014. ISBN: 9780323356022. URL: `https://books.google.de/books?id=V\_5PBAAAQBAJ`.

[62] Lacombe, R. *Adhesion measurement methods: theory and practice*. CRC Press, 2005. ISBN: 9781420028829. URL: `https://books.google.de/books?id=lTBUtvSwlPwC`.

[63] Bobaru, F., Foster, J. T., Geubelle, P. H., and Silling, S. A. *Handbook of Peridynamic Modeling*. 1st Edition. Engineering & Technology, Mathematics & Statistics. New York: Chapman and Hall/CRC, 2016. ISBN: 9781315373331. DOI: `10.1201/9781315373331`.

[64] Sidebottom, D. L. *Fundamentals of Condensed Matter and Crystalline Physics: An Introduction for Students of Physics and Materials Science*. Cambridge University Press, 2012. DOI: `10.1017/CBO9781139062077`.

[65] Koumpouras K. Larsson, J. A. "Distinguishing between chemical bonding and physical binding using electron localization function (ELF)". In: *Physics: Condensed Matter* 32(31), 2020, p. 5502.

[66] Needleman, A. "Micromechanical modelling of interfacial decohesion". In: *Ultramicroscopy* 40(3), 1992, pp. 203–214. ISSN: 0304-3991. DOI: 10.1016/0304-3991(92)90117-3.

[67] Gent, A. N. and Schultz, J. "Effect of Wetting Liquids on the Strength of Adhesion of Viscoelastic Material". In: *The Journal of Adhesion* 3(4), 1972, pp. 281–294. DOI: 10.1080/00218467208072199.

[68] Gutowski, W. "Thermodynamics of Adhesion". In: pringer US, isbn = 978-1-4899-2073-7, editor = Lee, Lieng-Huang, booktitle = Fundamentals of Adhesion, year = 1991, address = Boston, MA, doi = 10.1007/978-1-4899-2073-7_2, pp. 87–135.

[69] Good, R. J. and Chaudhury, M. K. "Theory of Adhesive Forces Across Interfaces". In: *Fundamentals of Adhesion*. Ed. by Lee, L.-H. Boston, MA: Springer US, 1991, pp. 137–151. ISBN: 978-1-4899-2073-7. DOI: 10.1007/978-1-4899-2073-7{_}3.

[70] Eringen, A., Speziale, C., and Kim, B. "Crack-tip problem in non-local elasticity". In: *Journal of the Mechanics and Physics of Solids* 25(5), 1977, pp. 339–355. ISSN: 0022-5096. DOI: 10.1016/0022-5096(77)90002-3.

[71] Eringen, A. "Linear theory of nonlocal elasticity and dispersion of plane waves". In: *International Journal of Engineering Science* 10(5), 1972, pp. 425–435. ISSN: 0020-7225. DOI: 10.1016/0020-7225(72)90050-X.

[72] Lee, L.-H. "The Chemistry and Physics of Solid Adhesion". In: *Fundamentals of Adhesion*. Ed. by Lee, L.-H. Boston, MA: Springer US, 1991, pp. 1–86. ISBN: 978-1-4899-2073-7. DOI: 10.1007/978-1-4899-2073-7{_}1.

[73] Silling, S. "Reformulation of elasticity theory for discontinuities and long-range forces". In: *Journal of the Mechanics and Physics of Solids* 48(1), 2000, pp. 175–209. ISSN: 0022-5096. DOI: 10.1016/S0022-5096(99)00029-0.

[74] Madenci, E. and Oterkus, E. "Peridynamic Theory and Its Applications". In: *Peridynamic Theory and Its Applications*, 2013. DOI: 10.1007/978-1-4614-8465-3.

[75] Gerstle, W., Sau, N., and Silling, S. "Peridynamic modeling of concrete structures". In: *Nuclear Engineering and Design* 237, 2007, pp. 1250–1258. DOI: 10.1016/j.nucengdes.2006.10.002.

[76] Silling, S., Epton, M., Weckner, O., Xu, J., and Askari, E. "Peridynamic States and Constitutive Modeling". In: *Journal of Elasticity* 88, 2007, pp. 151–184. DOI: 10.1007/s10659-007-9125-1.

[77] Silling, S. A. "Linearized Theory of Peridynamic States". In: *Journal of Elasticity* 99(1), 2010, pp. 85–111. DOI: 10.1007/s10659-009-9234-0.

[78] Lehoucq, R. B. and Sears, M. P. "Statistical mechanical foundation of the peridynamic nonlocal continuum theory: Energy and momentum conservation laws". In: *Phys. Rev. E* 84(3), 2011, p. 031112. DOI: 10.1103/PhysRevE.84.031112.

[79] Silling, S. A. "A COARSENING METHOD FOR LINEAR PERIDYNAMICS". In: *International Journal for Multiscale Computational Engineering* 9(6), 2011, pp. 609–622. ISSN: 1543-1649.

[80] Silling, S. A. and Bobaru, F. "Peridynamic modeling of membranes and fibers". In: *International Journal of Non-Linear Mechanics* 40, 2005, pp. 395–409. DOI: 10.1016/j.ijnonlinmec.2004.08.004.

[81] Kilic, B. *Peridynamic Theory for Progressive Failure Prediction in Homogeneous and Heterogeneous Materials*. 2008. URL: http://hdl.handle.net/10150/193658.

[82] Mitchell, J. A. "A non-local, ordinary-state-based viscoelasticity model for peridynamics." In: Oct. 2011. DOI: `10.2172/1029821`.

[83] Foster, J., Silling, S., and Chen, W. "Viscoplasticity using peridynamics". In: *International Journal for Numerical Methods in Engineering* 81, 2009, pp. 1242–1258. DOI: `10.1002/nme.2725`.

[84] Lancaster, J. "3 - The use of adhesives for making structural joints". In: *Metallurgy of Welding (Sixth Edition)*. Ed. by J.F., L. Woodhead Publishing Series in Welding and Other Joining Technologies. Woodhead Publishing, 1999, pp. 54–84. ISBN: 978-1-85573-428-9. DOI: `10.1533/9781845694869.54`.

[85] Rivlin, R. S. "The Effective Work of Adhesion". In: *Collected Papers of R.S. Rivlin: Volume I and II*. Ed. by Barenblatt, G. I. and Joseph, D. D. New York, NY: Springer New York, 1997, pp. 2611–2614. ISBN: 978-1-4612-2416-7. DOI: `10.1007/978-1-4612-2416-7{\textunderscore}179`.

[86] Kendall, K. "The adhesion and surface energy of elastic solids". In: *Journal of Physics D: Applied Physics* 4, May 2002, p. 1186. DOI: `10.1088/0022-3727/4/8/320`.

[87] Kendall, K. "Peel Adhesion of Solid Films-The Surface and Bulk Effects". In: *The Journal of Adhesion* 5, Dec. 2006, pp. 179–202. DOI: `10.1080/00218467308075019`.

[88] Kendall, K. "Thin-film peeling-the elastic term". In: *Journal of Physics D: Applied Physics* 8(13), 1975, pp. 1449–1452. DOI: `10.1088/0022-3727/8/13/005`.

[89] Griffith, A. A. "The Phenomena of Rupture and Flow in Solids". In: 221(A), 1920, pp. 163–198.

[90] Johnson, K. A., Kendal, K., and Roberts, A. D. "Surface energy and the contact of elastic solids". In: *Proceedings of the Royal Society of London. A. Mathematical and Physical Sciences* 324(1558), 1971, pp. 301–313. ISSN: 0080-4630. DOI: `10.1098/rspa.1971.0141`.

[91] Gent, A. N. and Hamed, G. R. "Peel mechanics of adhesive joints". In: *Polymer Engineering & Science* 17(7), 1977, pp. 462–466. DOI: `10.1002/pen.760170708`.

[92] Hadavinia, H., Kawashita, L., Kinloch, A., Moore, D. R., and Williams, J. G. "A numerical analysis of the elastic-plastic peel test". In: *Engineering Fracture Mechanics* 73, Nov. 2006, 2324–2335. DOI: `10.1016/j.engfracmech.2006.04.022`.

[93] Thouless, M. D. and Yang, Q. "A parametric study of the peel test". In: *International Journal of Adhesion and Adhesives* 28, June 2008, pp. 176–184. DOI: `10.1016/j.ijadhadh.2007.06.006`.

[94] Park, K. and Paulino, G. "Cohesive Zone Models: A Critical Review of Traction-Separation Relationships Across Fracture Surfaces". In: *Applied Mechanics Reviews* 64, 2011, pp. 1002–. DOI: `10.1115/1.4023110`.

[95] Andrés, A. de, Pérez, J. L., and Ortiz, M. "Elastoplastic finite element analysis of three-dimensional fatigue crack growth in aluminum shafts subjected to axial loading". In: *International Journal of Solids and Structures* 36(15), 1999, pp. 2231–2258. ISSN: 0020-7683. DOI: `10.1016/S0020-7683(98)00059-6`.

[96] Deshpande, V. S., Needleman, A., and Giessen, E. van der. "A discrete dislocation analysis of near-threshold fatigue crack growth". In: *Acta Materialia* 49, 2001, pp. 3189–3203. DOI: `10.1016/S1359-6454(01)00220-8`.

[97] Roe, K. L. and Siegmund, T. "An irreversible cohesive zone model for interface fatigue crack growth simulation". In: *Engineering Fracture Mechanics* 70, 2003, pp. 209–232. DOI: `10.1016/S0013-7944(02)00034-6`.

[98]   Maiti, S. and Geubelle, P. H. "A cohesive model for fatigue failure of polymers". In: *Engineering Fracture Mechanics* 72(5), 2005, pp. 691–708. ISSN: 0013-7944. DOI: `10.1016/j.engfracmech.2004.06.005`.

[99]   Ural, A., Krishnan, V. R., and Papoulia, K. D. "A cohesive zone model for fatigue crack growth allowing for crack retardation". In: *International Journal of Solids and Structures* 46(11), 2009, pp. 2453–2462. ISSN: 0020-7683. DOI: `10.1016/j.ijsolstr.2009.01.031`.

[100] Yang, Q. D. and Thouless, M. D. "Mixed-mode fracture analyses of plastically-deforming adhesive joints". In: *International Journal of Fracture* 110(2), 2001, pp. 175–187. ISSN: 1573-2673. DOI: `10.1023/A:1010869706996`.

[101] Xu, C., Siegmund, T., and Ramani, K. "Rate-dependent crack growth in adhesives: I. Modeling approach". In: *International Journal of Adhesion and Adhesives* 23, 2003, pp. 9–13. ISSN: 0143-7496. DOI: `10.1016/S0143-7496(02)00062-3`.

[102] Alfano, M., Furgiuele, F., Leonardi, A., Maletta, C., and Paulino, G. "Mode I fracture of adhesive joints using tailored cohesive zone models". In: *International Journal of Fracture* 157, 2009, pp. 193–204. ISSN: 1573-2673. DOI: `10.1007/s10704-008-9293-4`.

[103] Khoramishad, H., Crocombe, A. D., Katnam, K. B, and Ashcroft, I. A. "Predicting fatigue damage in adhesively bonded joints using a cohesive zone model". In: *International Journal of Fatigue* 32(7), 2010, pp. 1146–1158. ISSN: 0142-1123. DOI: `10.1016/j.ijfatigue.2009.12.013`.

[104] Chandra, N., Li, H., Shet, C., and Ghonem, H. "Some issues in the application of cohesive zone models for metal–ceramic interfaces". In: *International Journal of Solids and Structures* 39(10), 2002, pp. 2827–2855. ISSN: 0020-7683. DOI: `10.1016/S0020-7683(02)00149-X`.

[105] Shahverdi, M., Vassilopoulos, A., and Keller, T. "12 - Simulating the effect of fiber bridging and asymmetry on the fracture behavior of adhesively-bonded composite joints". In: *Fatigue and Fracture of Adhesively-Bonded Composite Joints*. Ed. by Vassilopoulos, A. Woodhead Publishing, 2015, pp. 345–367. ISBN: 978-0-85709-806-1. DOI: `10.1016/B978-0-85709-806-1.00012-4`.

[106] Tvergaard, V. "Effect of fibre debonding in a whisker-reinforced metal". In: *Materials Science and Engineering: A* 125(2), 1990, pp. 203–213. ISSN: 0921-5093. DOI: `10.1016/0921-5093(90)90170-8`.

[107] Needleman, A. "A Continuum Model for Void Nucleation by Inclusion Debonding". In: *Journal of Applied Mechanics-transactions of The Asme - J APPL MECH* 54, 1987. DOI: `10.1115/1.3173064`.

[108] Tvergaard, V. and Hutchinson, J. W. "The influence of plasticity on mixed mode interface toughness". In: *Journal of the Mechanics and Physics of Solids* 41(6), 1993, pp. 1119–1135. ISSN: 0022-5096. DOI: `10.1016/0022-5096(93)90057-M`.

[109] Needleman, A. "Damage Evolution, Instability and Fracture in Ductile Solids". In: *Disorder and Fracture*. Ed. by Charmet, J. C., Roux, S., and Guyon, E. Boston, MA: Springer US, 1990, pp. 219–238. ISBN: 978-1-4615-6864-3. DOI: `10.1007/978-1-4615-6864-3{\_}13`.

[110] Geubelle, P. and Baylor, J. "Impact-induced delamination of composites: A 2D simulation". In: *Composites Part B: Engineering* 29, 1998, pp. 589–602. DOI: `10.1016/S1359-8368(98)00013-4`.

[111] Needleman, A. "Some Issues in Cohesive Surface Modeling". In: *Procedia IUTAM* 10, 2014, pp. 221–246. ISSN: 2210-9838. DOI: `10.1016/j.piutam.2014.01.020`.

[112] Barenblatt, G. I. "Equilibrium cracks forming during brittle fracture". In: *Prikl Mat Mekh (PMM)* 23, 1959, pp. 434–444.

[113] Barenblatt, G. I. "Mathematical theory of equilibrium cracks". In: *Adv Appl Mech* 7, 1962, pp. 56–129.

[114] Dugdale, D. "Yielding of steel sheets containing slits". In: *Journal of the Mechanics and Physics of Solids* 8(2), 1960, pp. 100–104. ISSN: 0022-5096. DOI: `10.1016/0022-5096(60)90013-2`.

[115] Xu, X.-P. and Needleman, A. "Numerical simulations of fast crack growth in brittle solids". In: *Journal of the Mechanics and Physics of Solids* 42(9), 1994, pp. 1397–1434. ISSN: 0022-5096. DOI: `10.1016/0022-5096(94)90003-5`.

[116] Rice, J. R. and Wang, J. S. "Embrittlement of interfaces by solute segregation". In: *Materials Science and Engineering: A* 107, 1989, pp. 23–40. ISSN: 0921-5093. DOI: `10.1016/0921-5093(89)90372-9`.

[117] Tvergaard, V. and Hutchinson, J. W. "The relation between crack growth resistance and fracture process parameters in elastic-plastic solids". In: *Journal of the Mechanics and Physics of Solids* 40(6), 1992, pp. 1377–1397. ISSN: 0022-5096. DOI: `10.1016/0022-5096(92)90020-3`.

[118] Camacho, G. and Ortiz, M. "Computational modelling of impact damage in brittle materials". In: *International Journal of Solids and Structures* 33(20), 1996, pp. 2899–2938. ISSN: 0020-7683. DOI: `10.1016/0020-7683(95)00255-3`.

[119] Sorensen, B. F. and Jacobsen, T. K. "Determination of cohesive laws by the J integral approach". In: *Engineering Fracture Mechanics* 70(14), 2003, pp. 1841–1858. DOI: `10.1016/S0013-7944(03)00127-9`.

[120] Peng, Z. and Chen, S. "Effect of bending stiffness on the peeling behavior of an elastic thin film on a rigid substrate". In: *Physical Review E* 91, Apr. 2015. DOI: `10.1103/PhysRevE.91.042401`.

[121] Oyharcabal, X. and Frisch, T. "Peeling off an elastica from a smooth attractive substrate". In: *Physical review. E, Statistical, nonlinear, and soft matter physics* 71, Apr. 2005, p. 036611. DOI: `10.1103/PhysRevE.71.036611`.

[122] Schneider, P. "NURBS Curves: A Guid for the Uninitiated". In: *MACTECH*, 2014. URL: `http://preserve.mactech.com/articles/develop/issue_25/schneider.html`.

[123] Schoenberg, I. J. "Spline Functions and the Problem of Graduation". In: *National Academy of Sciences* 4(54), 1964, pp. 947–950. DOI: `10.1073/pnas.52.4.947`.

[124] Rogers, D. F., ed. *An Introduction to NURBS*. The Morgan Kaufmann Series in Computer Graphics. San Francisco: Morgan Kaufmann, 2001. ISBN: 978-1-55860-669-2.

[125] Curry, H. B. and Schoenberg, I. J. "On Pólya Frequency Functions IV: The Fundamental Spline Functions and their Limits". In: *I. J. Schoenberg Selected Papers*. Ed. by Boor, C. de. Boston, MA: Birkhäuser Boston, 1988, pp. 347–383. ISBN: 978-1-4899-0433-1. DOI: `10.1007/978-1-4899-0433-1{\_}17`.

[126] Schoenberg I, J. "Contribution to the problem of approximation of equidistant data by analytic functions". In: *Quart. Appl. Math.* 4, 1946, pp. 45–99. URL: `https://www.ams.org/journals/qam/1946-04-01/S0033-569X-1946-15914-5/S0033-569X-1946-15914-5.pdf`.

[127] Ramshaw, L. H. and Digital Equipment Corporation. Systems Research Center. *Blossoming: A Connect-the-dots Approach to Splines*. Digital. Digital SRC. Palo Alto, CA: Digital Systems Research Center, 1987. URL: `https://books.google.de/books?id=bOVZPgAACAAJ`.

[128] COX, M. G. "The Numerical Evaluation of B-Splines". In: *IMA Journal of Applied Mathematics* 10(2), 1972, pp. 134–149. ISSN: 0272-4960. DOI: `10.1093/imamat/10.2.134`.

[129]   Boor, C. de. "On calculating with B-splines". In: *Journal of Approximation Theory* 6(1), 1972, pp. 50–62. ISSN: 0021-9045. DOI: `10.1016/0021-9045(72)90080-9`.

[130]   Boor, C. de. "A Practical Guide to Spline". In: *Applied Mathematical Sciences, New York: Springer, 1978* Volume 27, 1978. DOI: `10.2307/2006241`.

[131]   Cottrell, J., Hughes, T., and Bazilevs, Y. "Isogeometric Analysis: Toward integration of CAD and FEA". In: 2009. ISBN: 0470748737. DOI: `10.1002/9780470749081.ch7`.

[132]   Piegl, L. and Tiller, W. *The NURBS Book*. 2nd ed. Berlin, Heidelberg: Springer, Berlin, Heidelberg, 1997. ISBN: 978-3-540-61545-3. DOI: `10.1007/978-3-642-59223-2`.

[133]   *200x USB Digital Microscope, Electronics Microscope with Microscope Camera Capture photo/video*. URL: `https://www.globalsources.com/si/AS/Mustech-Electro-nics/6008849250611/pdtl/USB-Digital-Microscope/1166830942.htm`.

[134]   *Zwick/Roell company: Zwick*. URL: `https://www.zwickroell.com/en/unive-rsal-testing-machines/allroundline-test-machine`.

[135]   Altenbach, H., Naumenko, K., and Zhilin, P. A. "A direct approach to the formulation of constitutive equations for rods and shells". In: 2006, pp. 87–90. ISBN: 0415383900.

[136]   Antman, S. S. *Nonlinear problems of elasticity*. Applied Mathematical Sciences. Springer New York, 1995. DOI: `10.1007/978-1-4757-4147-6`.

[137]   Green, A., Naghdi, P., and Wenner, M. "On the Theory of Rods. I. Derivations from the Three-Dimensional Equations". In: *Royal Society of London Proceedings Series A* 337, 1974, pp. 451–483. DOI: `10.1098/rspa.1974.0061`.

[138]   Kienzler, R. and Herrmann, G. *Mechanics in Material Space: With Applications to Defect and Fracture Mechanics*. Vol. 55. 2002. DOI: `10.1115/1.1451102`.

[139]   Maugin, G. A. *Material Inhomogeneties in Elasticity*. Sept. 1993. ISBN: 9781000110012. DOI: `10.1007/978-1-4899-4481-8`.

[140]   Eremeyev, V. A. and Naumenko, K. "A relationship between effective work of adhesion and peel force for thin hyperelastic films undergoing large deformation". In: *Mechanics Research Communications* 69, 2015, pp. 24–26. ISSN: 0093-6413. DOI: `10.1016/j.mechrescom.2015.06.001`. URL: `http://www.sciencedirect.com/science/article/pii/S009364131500097X`.

[141]   Dimitri, R., Cornetti, P., Mantič, V., Trullo, M., and De Lorenzis, L. "Mode-I debonding of a double cantilever beam: A comparison between cohesive crack modeling and Finite Fracture Mechanics". In: *International Journal of Solids and Structures* 124, 2017, pp. 57–72. ISSN: 0020-7683. DOI: `10.1016/j.ijsolstr.2017.06.007`.

[142]   Blackman, B. R. K., Hadavinia, H., Kinloch, A. J., and Williams, J. G. "The use of a cohesive zone model to study the fracture of fibre composites and adhesively-bonded joints". In: *International Journal of Fracture* 119(1), 2003, pp. 25–46. ISSN: 1573-2673. DOI: `10.1023/A:1023998013255`.

[143]   Beylkin, G. and Monzón, L. "Approximation by exponential sums revisited". In: *Applied and Computational Harmonic Analysis* 28(2), 2010, pp. 131–149. ISSN: 1063-5203. DOI: `10.1016/j.acha.2009.08.011`.

[144]   Holmström, K. and Petersson, J. "A Review of the Parameter Estimation Problem of Fitting Positive Exponential Sums to Empirical Data". In: *Appl. Math. Comput.* 126(1), 2002, pp. 31–61. ISSN: 0096-3003. DOI: `10.1016/S0096-3003(00)00138-7`.

[145]   Potts, D. and Tasche, M. "Nonlinear approximation by sums of nonincreasing exponentials". In: *Applicable Analysis* 90(3-4), 2011, pp. 609–626. DOI: `10.1080/00036810903569499`.

[146] Bagheri, B., Schulze, S. H., Naumenko, K., and Altenbach, H. "Identification of traction-separation curves for self-adhesive polymeric films based on non-linear theory of beams and digital images of T-peeling". In: *Composite Structures* 216, 2019, pp. 222–227. ISSN: 0263-8223. DOI: `10.1016/j.compstruct.2019.02.060`.

[147] Yan, G. and Oterkus, S. "Fully coupled thermomechanical analysis of laminated composites by using ordinary state based peridynamic theory". In: *Composite Structures* 207, 2018. ISSN: 0263-8223. DOI: `10.1016/j.compstruct.2018.09.034`.

[148] Dunning, D. J. "Blown Film Production". In: *Developments in Plastics Technology—1: Extrusion*. Ed. by Whelan, A. and Dunning, D. J. Dordrecht: Springer Netherlands, 1982, pp. 75–153. ISBN: 978-94-009-6622-2. DOI: `10.1007/978-94-009-6622-2{\_}3`.

[149] Blackman, B. R. K. "Fracture Tests". In: *Handbook of Adhesion Technology*. Ed. by Silva, L. F. M. da, Öchsner, A., and Adams, R. D. Berlin, Heidelberg: Springer Berlin Heidelberg, 2011, pp. 473–501. ISBN: 978-3-642-01169-6. DOI: `10.1007/978-3-642-01169-6{\_}20`.

[150] Dogan, F., H.adavinia, H., Donchev, T., and PS, B. "Delamination of impacted composite structures by cohesive zone interface elements and tiebreak contact". In: *Central European Journal of Engineering* 2, 2012, pp. 612–626. DOI: `10.2478/s13531-012-0018-0`.

[151] Gurtin, M. E. *An Introduction to Continuum Mechanics*. ISSN. Elsevier Science, 1982. ISBN: 9780080918495. URL: `https://books.google.de/books?id=W-0b09yIgq4C`.

[152] Park, K., Paulino, G. H., and R., R. J. "A unified potential-based cohesive model of mixed-mode fracture". In: *Journal of the Mechanics and Physics of Solids* 57(6), 2009, pp. 891–908. ISSN: 0022-5096. DOI: `10.1016/j.jmps.2008.10.003`.

[153] Van Krevelen, D. W. and Te Nijenhuis, K. "Chapter 13 - Mechanical Properties of Solid Polymers". In: *Properties of Polymers (Fourth Edition)*. Amsterdam: Elsevier, 2009, pp. 383–503. ISBN: 978-0-08-054819-7. DOI: `10.1016/B978-0-08-054819-7.00013-3`.

[154] Hui, C. Y., Ruina, A., Long, R., and Jagota, A. "Cohesive Zone Models and Fracture". In: *The Journal of Adhesion* 87(1), 2011, pp. 1–52. DOI: `10.1080/00218464.2011.538315`.

[155] Kausch, H. H., ed. *Crazing in Polymers*. 1st ed. Vol. 52-53. Advances in Polymer Science. Berlin, Heidelberg: Springer, 1983. ISBN: 978-3-662-15952-1. DOI: `10.1007/BFb0024054`.

[156] Wu, S. *Polymer Interface and Adhesion*. 2017. ISBN: 9780203742860. DOI: `10.1201/9780203742860`.

[157] Becaro, A. A., Puti, F. C., Correa, D. S., Paris, E. C., Marconcini, J. M., and Ferreira, M. D. "Polyethylene Films Containing Silver Nanoparticles for Applications in Food Packaging: Characterization of Physico-Chemical and Anti-Microbial Properties". In: *Journal of nanoscience and nanotechnology* 15(3), 2015, pp. 2148–2156. ISSN: 1533-4880. DOI: `10.1166/jnn.2015.9721`.

[158] Clint, J. H. "Adhesion and components of solid surface energies". In: *Current Opinion in Colloid & Interface Science* 6(1), 2001, pp. 28–33. ISSN: 1359-0294. DOI: `10.1016/S1359-0294(00)00084-4`.

[159] Marsh, K. and Bugusu, B. "Food Packaging—Roles, Materials, and Environmental Issues". In: *Journal of Food Science* 72(3), R39–R55. DOI: `10.1111/j.1750-3841.2007.00301.x`.

Publications

Refereed Articles

1. Bagheri, B., Schulze, S. H., Naumenko, K. and Altenbach, H.: „Identification of traction-separation curves for self-adhesive polymeric films based on non-linear theory of beams and digital images of T-peeling ". In: *Composite Structures*, 2019. DOI: `10.1016/j.compstruct.2019.02.060`

2. Naumenko, K. and Bagheri, B.: „A direct approach to evaluate interaction forces between self-adhesive polymeric films subjected to T-peeling". In: *Archive of Applied Mechanics*, 2021. DOI: `10.1007/s00419-020-01834-9`